A THEORETICAL AND EXPERIMENTAL INVESTIGATION OF THE LEIDENFROST PHENOMENON FOR SMALL DROPLETS

By

CHAU JEN LEE

Bachelor of Science in Chemical Engineering
National Taiwan University
Taipei, Taiwan
June, 1957

Master of Science in Chemical Engineering
Kansas State University
Manhattan, Kansas
May, 1961

Submitted to the Faculty of the Graduate School of
the Oklahoma State University
in partial fulfillment of the requirements
for the degree of
DOCTOR OF PHILOSOPHY
May, 1965

A THEORETICAL AND EXPERIMENTAL INVESTIGATION OF THE LEIDENFROST PHENOMENON FOR SMALL DROPLETS

Thesis Approved:

Kenneth J. Bell
Thesis Adviser

John B. Wert

Wayne C. Edmister

Jerald D. Parker

J. J. Boggs
Dean of the Graduate School

PREFACE

The physical mechanisms of heat transfer and phase change processes involved in the Leidenfrost phenomenon for small droplets were studied. Experimental data on droplet evaporation time and on instantaneous droplet size were obtained and analysed in order to support the model and to verify the assumptions made in the development of the theory. The liquids used for the experimental work were water, ethyl alcohol, benzene, carbon tetrachloride and n-octane.

I am very much indebted to Dr. Kenneth J. Bell for his inspiring advice during the course of my thesis work and also for his patience and friendship inguiding me through the entire graduate study at Oklahoma State University. I wish to express my gratitude to the members of my graduate committee: Professor W. C. Edmister, Professor of Chemical Engineering; Dr. J. D. Parker, Associate Professor of Mechanical Engineering; Dr. J. B. West, Associate Professor of Chemical Engineering.

Discussions with my fellow graduate students, particularly Messrs. Dale Bush, Edward Godleski, David Knoebel, B. M. Patel, and Dr. James Webster, were of considerable help during this study.

Financial support and equipment funds for the initial phases of this work were gratefully received from the Office of Engineering Research of Oklahoma State University; The U. S. Army Research

Office (Durham, North Carolina) supported the research during the last two years of this work. The Wollensack Xenon Lamp used as the light source in the photographic study was purchased with a grant from the National Science Foundation.

Phillips Petroleum Company supplied n-octane for this work and also generously donated time on their IBM 7094 computer for part of the computation in this work. I also owe a great debt of gratitude to Mr. and Mrs. J. E. Robinson for their willingness to play host family and American parentship during our stay in Stillwater, Oklahoma.

I wish to acknowledge and epxress my indebtness to my wife, Huey-li, for her endurance and constant encouragement, and to my parents for their aid and spiritual support. Without their stimulation and encouragement, my entire graduate studies would have not been possible.

TABLE OF CONTENTS

LIST OF TABLES

LIST OF FIGURES

LIST OF PLATES

CHAPTER I

INTRODUCTION

What is the Leidenfrost Phenomenon?

The behavior of liquid droplets on hot surfaces has long been of interest to scientists. It was Johann G. Leidenfrost, a German doctor, who first made a careful observation and an objective study of water droplets on a hot, well-polished iron spoon (17). This quiescent, slow evaporation of water droplets on a very hot surface has since been named after Leidenfrost and is known as the Leidenfrost Phenomenon or the Spheroidal State.

The similarity between the typical pool boiling curve and the Leidenfrost phenomenon was first pointed out by Drew and Mueller (7). Figure 1 illustrates this similarity; the solid curve represents a typical pool boiling curve found by Nukiyama (20). As the pool boiling curve is discussed in detail elsewhere (4, 7, 8), it will suffice here to indicate the regions only by their accepted names with a brief identification of their distinct mechanisms.

Region A is the free convection regime governed by natural convection heat transfer with no change in phase occurring at the solid-liquid interface. Region B is the nucleate boiling regime, characterized by the formation of bubbles from favored spots on the heating surface. Region C is the transitional film boiling regime in which nucleate boiling coexists with an unstable

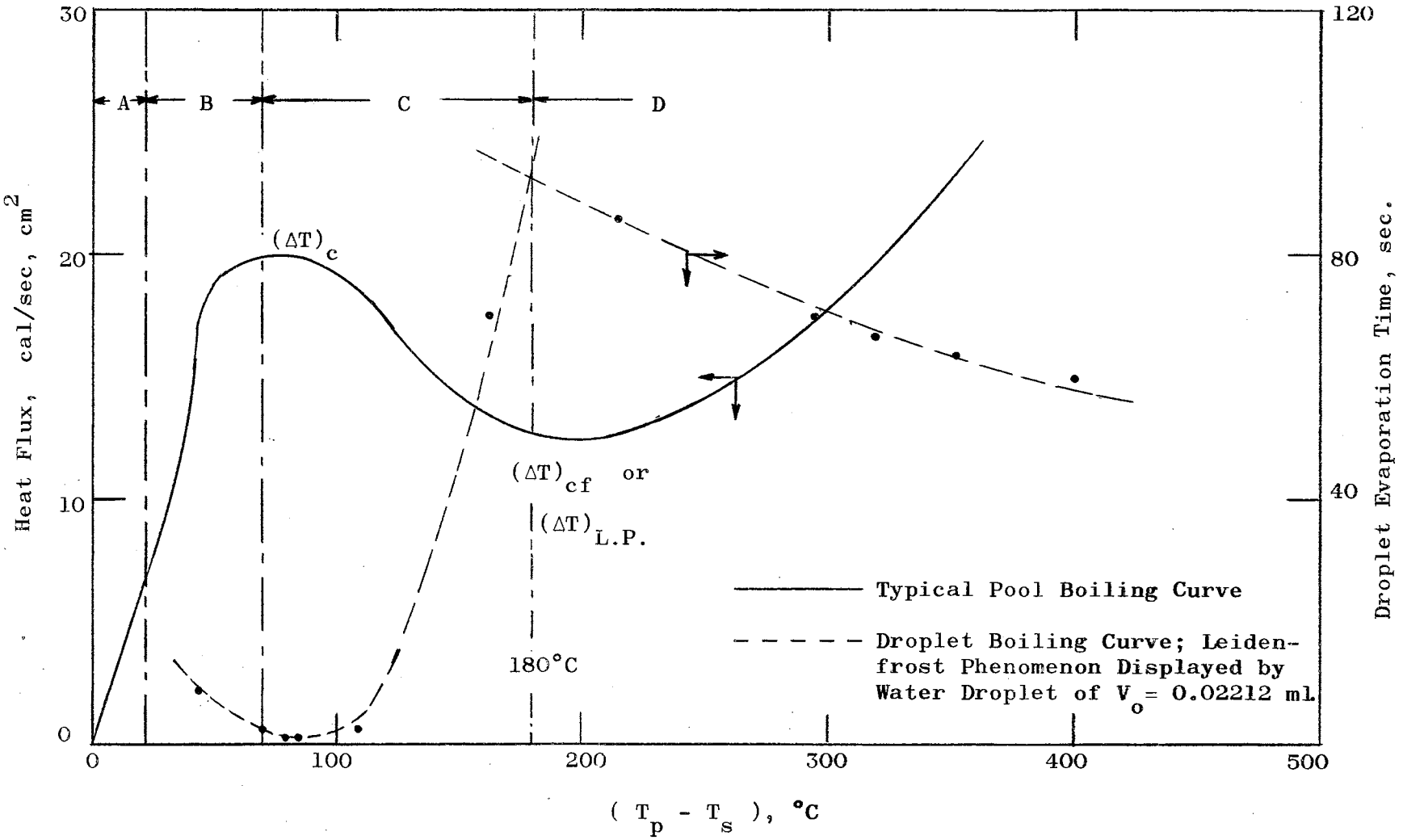

Figure 1 Typical Boiling Curve

vapor film partially masking the heating surface. Region D is the stable film boiling regime characterized by a more or less uniform vapor film surrounding the heated surface.

There are two critical points appearing on the pool boiling curve; the first critical point indicated by $(\Delta T)_c$ is the critical temperature difference corresponding to the maximum heat flux and is the upper limit to nucleate boiling. The second critical point, $(\Delta T)_{cf}$ is the point at which stable film boiling first takes place and is known as the minimum heat flux point in pool boiling.

The dotted curve in Figure 1 is a plot of droplet life time for a liquid droplet laying on a heated surface. In the nucleate boiling regime, the droplet receives comparatively higher heat flux through the solid-liquid interface; therefore, the droplet takes less time to vaporize and to disappear visually. At the point of maximum heat flux, a liquid droplet will disappear almost instantaneously after it contacts the heating surface.

As the temperature of the heating surface is further increased, the rate of vapor generation at the liquid-solid interface increases. But at the same time, the generated vapor partially masks off the solid-liquid interface. As a result, the droplet would take longer to evaporate completely. When the surface temperature reaches the critical temperature difference corresponding to the minimum heat flux, the solid-liquid interface is completely blanketed by the generated vapor. Heat transfer is henceforth by conduction through the vapor film instead of phase change at the solid-liquid interface. This is the surface temperature at which

droplets have the maximum evaporation time and is termed as the Leidenfrost point. This is also recognized as the minimum surface temperature at which the stable spheroidal state exists.

It seems that modern physicists have relegated spheroidal state boiling to their limbo for exceedingly curious but not particularly important phenomena. This is unfortunate because this phenomenon is technically important, and furthermore, the literature on the subject is very considerable, quite old, obscurely located, and somewhat confused.

Importance of Film Boiling

Film boiling has been defined as that type of boiling which occurs when a continuous vapor film separates the heated surface from the boiling liquid. It is a well-known fact that the coefficients of heat transfer in film-boiling are much smaller than those in nucleate boiling. The study of film boiling heat transfer has, nevertheless, its own merit other than purely scientific curiosity. The research on film-boiling is becoming more important as this type of boiling process is observed in many modern technological problems such as in mercury vapor Rankine-cycle systems and in cryogenic liquid systems.

The Leidenfrost phenomenon is a special case of the film boiling process. If the liquid on the hot surface is not sufficient to cover the surface, then the liquid exists in droplets or discontinuous masses. They are supported by vapor which is continuously generated on the bottom of the droplets. This phenomenon has been identified as a controlling heat transfer

mechanism associated with diverse situations, e.g., rain drop erosion on high-speed vehicles, flash boilers, and fuel atomizers.

Objectives

The principal objective of this work was to study the physical mechanisms of the heat transfer and phase change processes involved in the Leidenfrost phenomenon for small droplets. From this, an analytical model was developed for the numerical computation of instantaneous droplet size, instantaneous evaporation rate and droplet total evaporation time. Experimental data on droplet total evaporation time and sequenced high-speed still photographs were to be obtained to support the theoretical model.

CHAPTER II

LITERATURE SURVEY

In 1934 Nukiyama (20) published his experimental work establishing the complete pool boiling curve (see Figure 1). This boiling curve has since been accepted as typical of all pool boiling systems.

The celebrated work of Drew and Mueller (7) constitues a very complete review of literature on "Boiling" up to 1937. It contains an extensive survey on the boiling process in general, from nucleate to stable film boiling. Bromley (14) developed a theory of pool film boiling from a heated cylinder with some fundamental assumptions and a series of experimental data. This theory enables us to predict the coefficients of heat transfer to be expected in the stable film boiling regime from a horizontal tube submerged in a pool of liquid. Chang (5,6) and Zuber (34, 35) introduced the wave theory into the study of the transition mechanism from nucleate to meta-stable and stable film boiling. They aimed to investigate the critical values of the boiling curve by means of wave stability criterion. From further study of the hydrodynamic stability of film boiling, Berenson (2) derived a set of equations which predict the heat transfer coefficients, the minimum heat flux, and minimum temperature at which film boiling occurs. An up-to-date survey of the published work on

"boiling" was outlined by Westwater (33).

A chronological tracing of historical interest on the Leidenfrost phenomenon can be found in Gorton's Ph.D. thesis published in 1953 (8). According to the literature (8), the Leidenfrost phenomenon was actually first reported by Eller in 1746. Leidenfrost then investigated this phenomenon objectively on a well-polished iron spoon which was heated over glowing coals until the spoon was glowing bright red. Under a subtitle "On the Fixation of Water In Diverse Fire" of his treatise (17), Leidenfrost describes the phenomenon:

> 1. An iron spoon of any size, well polished within and free from rust and dirt, is heated over glowing coals until it glows with light. Send through a glass tube of suitable length of which the other end finishes in a very narrow capillary canal one drop of very pure distilled water to this glowing spoon, removed from the coals. ..... Moreover, the water which I mostly used runs into a protected pool, now and for six and some odd years. No disturbance was noticed in all this time.... This drop which first fell upon the glowing iron is divided into a few little globes, which after a little while are collected in one big globe again. At the instant when the drop touches the glowing iron, it is spherical. It does not adhere to the spoon, as water which touches colder iron is accustomed to do....
>
> 2. If then the spoon remains motionless, this water globe will lie quiet and without any visible motion, without any bubbling very clear like a crystalline globe, always spherical, adhering nowhere to the spoon, but to be near it in one point. However, although motion is not visible in the pure drop, nevertheless it delights in a very swift motion of turning which is seen when a small colored speck adheres to the drop. For this is turned around the drop with a marvelous velocity..... It runs at least 34 or 35 seconds before the whole drop disappears. Which drop at last exceedingly diminished so that it can hardly anymore be seen, finishes its existence with an audible crack which one easily hears with the ears, and it leaves a small particle of earth in the spoon.
>
> 3. While these things are done, the glowing spoon ceases to glow and becomes cooler. Therefore, as soon as the first drop disappears, send another drop similar to the first through the same glass tube to that same spoon, which drop with similar phenomena will disappear in 9 or 10 seconds. But there is this

difference: This second drop in this case is divided into more golbules than the first, which globules return into one globe with more difficulty. They are moved to and fro and as if dancing, they produce a hiss with their motion in the spoon.

4. Meantime while the iron is cooled more, after the second drop has evaporated, then let go a third, which, with a great motion of globules, greater certainly than can be called boiling, will disappear with a period of three seconds. I observed nothing remaining of solid, earthy matter from the second and third drop, as from the first drop, unless there was an obvious impurity in the spoon.

5. If, then, you put in the fourth drop with the same precaution, this is no longer rolled into a globe, but adheres to the spoon and makes a damp spot in it and with a hiss surges into the true motion of boiling, and thus foaming into vapors it will depart very swiftly within the period of one second or even swifter, and leaves nothing which is in anyway sensible of earth or of solid matter.

6. If after this you send down successively the fifth, sixth, seventh, and more drops to the same spoon now cooled enough so that it can be touched with the fingers with no harm, it will be evident to the eyes that because the spoon is cooler, the drop falling imparts a greater moist spot to the spoon, and adheres to it a longer time before it is evaporated.

Research on spheroidal-state film boiling has been scarce in this country. There are, however, quite a few Russian studies on the Leidenfrost phenomenon. Some of them are now available in English translations. Pleteneva and Rebinder (23) studied water and some organic liquids of various polarities (benzene, chloroform, methyl alcohol, propyl alcohol, isoamyl alcohol, nitrobenzol, ortho toluidine, and ethyleneglycol), on a stainless steel plate placed in the air with electrical heating. They timed the total evaporation time of various liquid droplets on the heated metal plate. From the experimental data, they concluded that at plate temperature 250°C, water droplets started to show the characteristics of spheroidal state, not disintegrating, and the evaporation time rises sharply to a maximum value at 275°C. Above this point the

evaporation time decreases as the plate temperature further increases (see Figure 1). Similar phenomena were also observed with organic liquids. They found that the plate temperature which gave the maximum evaporation time for organic liquids was proportional to the absolute boiling point of the liquid.

In another article published by Plenteneva and Rebinder (25), they studied the effect of surface active substances on the evaporation of water drops in the spheroidal state. The surface tension of liquids was found to have an appreciable effect on the droplet evaporation time and the initiation of the spheroidal state.

The experimental results of Borishansky (3) further confirms the fact that there are two critical temperatures in the vaporization of liquid droplets on an open heating surface. The first one, $(\Delta T)_c$ corresponding to the maximum heat flux in pool boiling curve is the temperature at which the droplet has the minimum evaporation time. The second is $(\Delta T)_{cf}$, at which the pure spheroidal state of the liquid droplet is established. This is the temperature of the heating surface at which evaporation of the droplet takes the longest time. Borishansky also extended his work to larger masses of water. He observed that for larger masses, the thickness of the liquid mass reached a constant value (about 7 mm.). If more water is added, the mass flatten out on the hot surface. For these larger masses in the spheroidal state, part of the vapor leaves in the form of large vapor bubbles through the thickness of the spheroid from time to time. The study of the Leidenfrost phenomenon for extended liquid

masses is being carried on by Patel (21). His objective is to explore the hydrodynamics and the heat transfer mechanism of bubbly spheroids.

Gorton in his Ph.D. thesis (8) attempted to measure photographically the film thickness which separates the spheroid from the hot plate. The experimental technique which he used did not give him a satisfactory degree of accuracy, and he thought that his measurements for film thickness were in error. In another attempt to investigate the heat transfer coefficients for heat transfer from a heating surface to droplet, he used both stainless steel and platinum for the test surfaces. He concluded that the type of surface affected only the contribution due to radiation caused by the different metal emissivities, though he was unable to make a definite statement concerning the contribution due to conduction through the vapor film because of the inaccurate measurements for the film thickness.

There is some work in the literature which approaches the problem of drop phenomenon analytically. Savic (28, 29) with a view to obtaining information about the mechanism of turbine blade cooling by means of impinging drops has developed a theory based on an approximate treatment of potential theory of ideal fluids. It seems that an analogy may be drawn between Savic's analysis for impinging drops and the analysis for the Leidenfrost phenomenon, though it may be seen that the physical model for a liquid droplet vaporizing quietly on a hot surface is less involved than for the case where a fluid sphere impacts on a solid plane surface.

Among the other important fields in drop phenomena is the evaporation of liquid droplets in high temperature gaseous surroundings, which is important in a number of processes such as cyclone evaporation, spray drying, and atomized liquid fuel combustion. Hoffman and Gauvin (12) in their recent published work, attempted a theoretical analysis on the heat transfer and mass transfer mechanism of the above-mentioned processes.

The most recent work which contributes directly to the study of the Leidenfrost phenomenon is by Kistemaker (15). He studied the historical development of the Leidenfrost phenomenon and performed some experiments to determine heat-flow, drop to surface distance, and evaporation rate for a water droplet above a highly polished brass block, at a hot surface temperature ranging from 100°C to 500°C. The vapor film thicknesses reported vary from 30 to 60 microns. The measurements for film thickness were made on X-ray photographs. By dissolving some sodium acetate in the water droplet, Kistemaker obtained a good contrast on the X-ray pictures. It may be noted that the introduction of a foreign material in a water droplet might have changed the physical properties and thus affected the transport phenomena of a pure water droplet. In another recent work, Gross-Gronomski (10) studied the droplet evaporation problems of nitric acid and aniline. He reported that the evaporation times were exponential functions of the temperature of the hot surface.

Perhaps, Gottfried (9) was the first one who actually initiated a complete analytical approach to the study of the Leidenfrost phenomenon for small droplets. He hypothesized that

the evaporating droplets were spherical and postulated a physical mechanism based on simultaneous conduction, convection, diffusion and radiation effects. The semi-empirical numerical solution on a digital computer gave the predicted vaporization times which agreed with his experimental data for water, ethyl alcohol, benzene, and carbon tetrachloride evaporating into air within a maximum error of 25 percent.

CHAPTER III

EXPERIMENTAL APPARATUS

The experimental apparatus used in this study is shown in Plate I while a schematic sketch is presented in Figure 2.

The main part of the apparatus consisted of a stainless steel plate sitting on a flat electric heating unit. The plate was made of Type 304 stainless steel, and was four inches in diameter and 1/4 inch thick in the center of test area. The complete dimensions of the plate are shown in Figure 3.

One of the five chromel-alumel thermocouples (24 gauge) was installed at the center and the rest were symmetrically installed beneath the circumference of the center test area. Each of these thermocouples was fastened to the plate with Sauereisen high temperature cement in a slot 1/16 inch from the surface of the plate.

The test plate was centered upon a 14 inch x 8 3/4 inch Hevi-Duty #56-TS, flat electric heating unit. The plate together with heating unit was then supported by two asbestos insulating plates which were constructed such that the horizontal level of the heating unit was adjustable. The Hevi-Duty heating unit was connected to a 10 ampere, 120 volt Variac, which was in turn connected to the 120 volt 60 cycle line.

The five thermocouples embedded underneath the test area were

Plate I

Experimental Apparatus

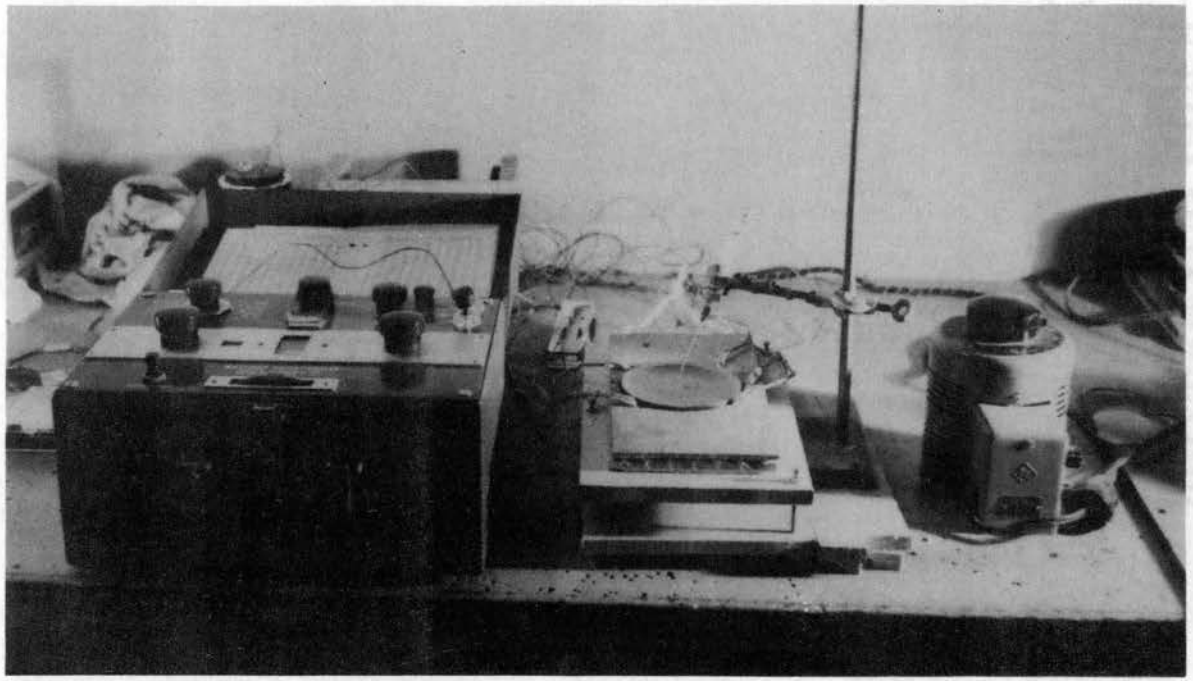

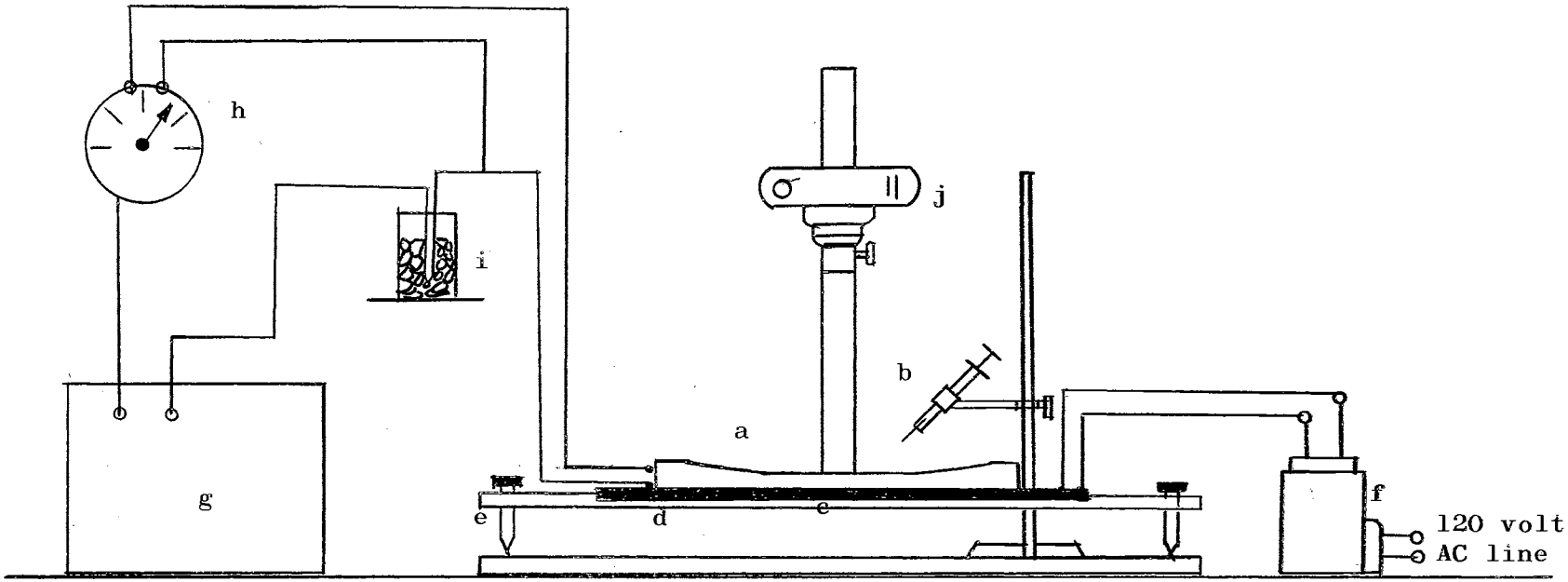

a	Stainless Steel Plate	b	Hypodermic Syringe	c	Heating Unit
d	Asbestos Plate (Insulator)	e	Horizontal Level Adjuster	f	Variac
g	Potentiometer	h	Selector Switch	i	Ice Junction
j	Still Camera				

Figure 2 Schematic Sketch of Apparatus

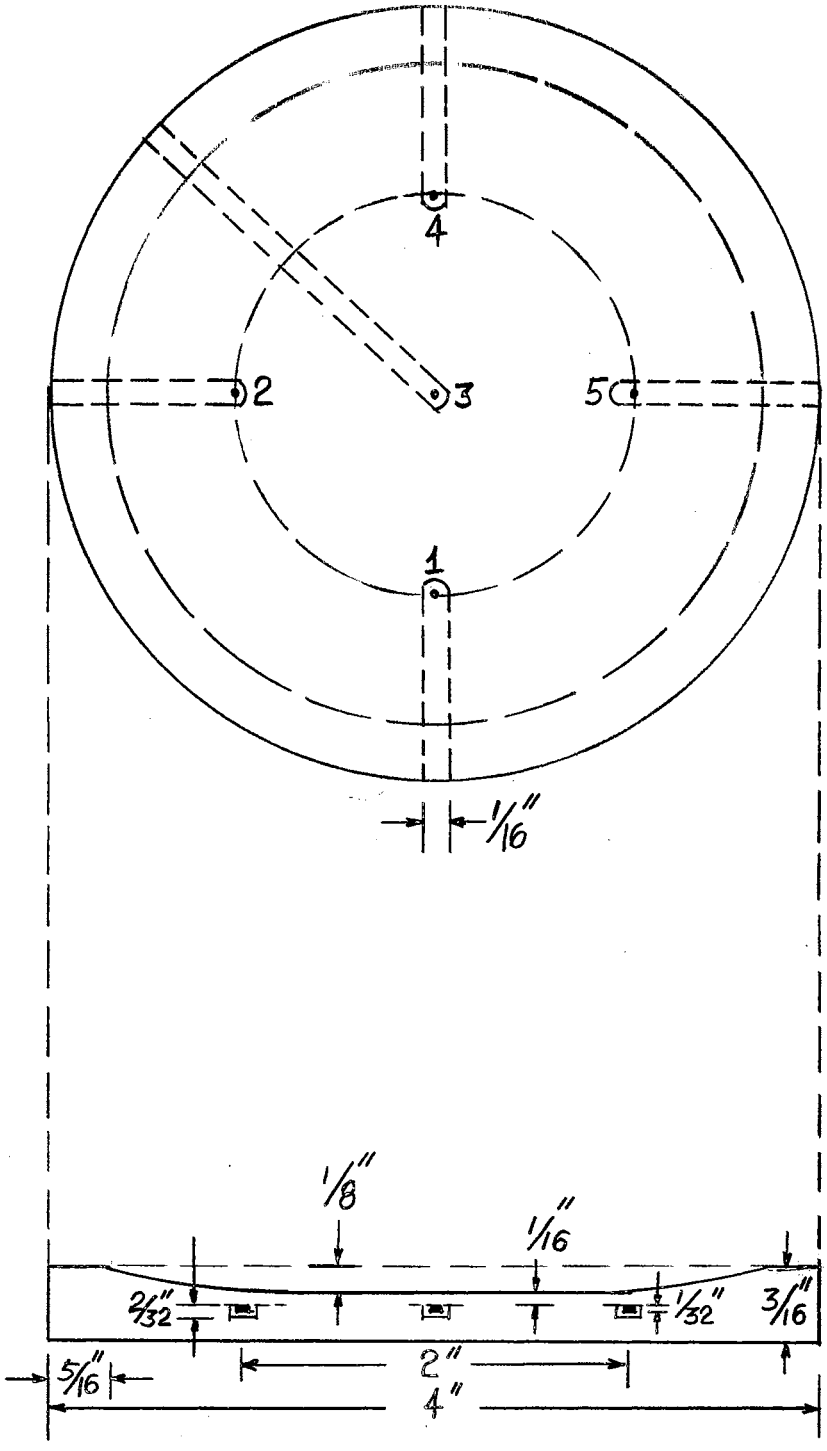

Figure 3 Schematic Diagram of Stainless Steel Plate; Chromel-Alumel Thermocouple Locations Designated by "."

connected to a selector switch and an ice-bath cold junction and then to a Leeds and Northrup #8690 millivolt potentiometer.

For the purpose of studying the instantaneous droplet size during evaporation, a Konica FS 35 mm still camera was mounted on a photographic copying stand. The stand was set on the top of the hot plate only when such photographic runs were necessary. The camera was attached with an Ednalite +3 close-up lens so that the boiling droplets could be magnified and clearly focused.

The hypodermic syringe and needle used to produce liquid droplets were fixed on a stand. When making the liquid droplets, the needle tip was held about 1/2 inch above the test area, and the hypodermic syringe was placed at a 45 degree angle to the plate. Needles of 13, 16, 17, and 21 gauge were used to produce the various droplet sizes.

CHAPTER IV

EXPERIMENTAL PROCEDURE

Hypodermic Needle Calibrations

The initial volumes of liquid droplets used in this experiment were produced by means of a hypodermic syringe and several stainless steel needles of 13, 16, 17, and 21 gauges. The needles were filed down to a smooth flat tip. The hypodermic syringe and the attached needle were set at a 45 degree angle to the horizontal and fixed on a stand. Then, if one carefully screwed the delivery plunger of the syringe, the droplet was slowly formed on the needle tip until the weight of droplet became sufficient to detach from the tip of the needle. All needles were calibrated for drop size using distilled water, ethyl alcohol, benzene, carbon tetrachloride, and n-octane. The calibration was made with a precise balance and several narrow-necked weighing bottles. Ten droplets were individually formed and weighed for each needle for each liquid. Although less consistency was observed with the more volatile liquids, the reproducibility of making uniform size droplets appeared to be very satisfactory. The average deviation was less than $\pm$ 3 percent from the arithmetic mean value in every case. The technique of placing the hypodermic syringe at a 45 degree angle was an improvement over the vertical

positioning used by Gottfried (9) where he reported an average deviation of ± 7 percent. A table for the needle calibration and the deviations is given in Appendix B.

Hot Plate Setting

Prior to each series of runs, the variac was set at a fixed value and the test plate then heated up. Under normal conditions, the test area would take about two to four hours to reach a steady-state temperature. Figure 4 shows a typical curve for the heating process. Upon reaching steady-state, the five thermocouples indicated a maximum plate temperature variation of ± 2°C.

Droplet Evaporation Time

After the stainless steel was heated to a steady state temperature, the hypodermic syringe was filled with liquid and brought into position. The liquid droplets were formed by the same technique as used in the needle calibrations. The total evaporation time of a particular liquid droplet was measured visually with a stopwatch (Meylan #218) which can be read to 0.01 second. The experimental data for five different liquids and four droplet sizes collected in this manner (usually five determinations for each size of droplet of a particular liquid) are given in Appendix F and are plotted in Figure 6 through 25. The consistency and the significance of these results will be discussed in a separate section.

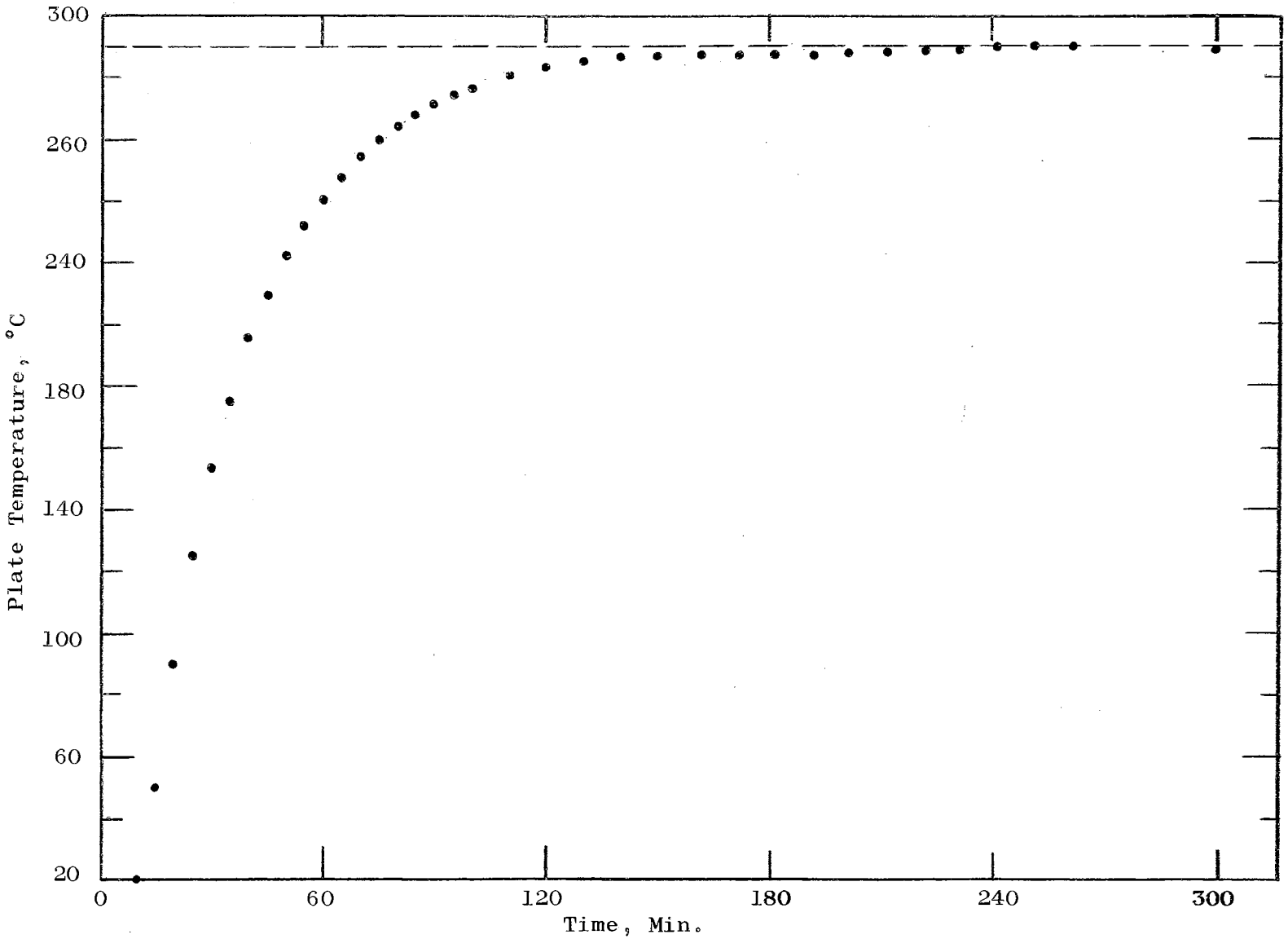

Figure 4 Typical Curve for Hot Plate Heating Process

Photographic History of the Rate of Droplet Evaporation

In order to study the instantaneous droplet size during the process of droplet evaporation, several runs were taken with the photographic arrangement which has been described in the previous chapter. The procedure for these experimental runs was exactly the same as for the experiments on droplet evaporation time, except that at each five or ten second interval, a photograph was taken from above of the droplet evaporating on the hot plate. Kodak Tri-X emulsion rolls which have a film speed of ASA 400 were consistently used with the 35 mm Konica FS still camera. To avoid the blurring effect which might be introduced by the vigorous vortex observable inside the boiling droplet, the shutter speed was set on 1/1,000 of a second with the aperture opening at 2. Lighting was by means of a Wollensak WF-36 Xenon Lamp, which was able to supply a good light source without transferring significant heat to the droplet by radiation.

In each photographic run, two small (4 inches long) stainless steel rulers were put on the edges of the hot plate to indicate the proportionality factor of the actual object size to that appearing on the exposed film. Two typical photographs for the instantaneous droplet size are shown in Plate II.

Each frame of the developed films was mounted onto a slide. These slides were then measured for the droplet size under a precision metallurgical microscope having X320 magnification power. The microscope reading was calibrated within 0.001 cm precision with a micro-scale. Plate III is a photograph of the

Plate II

Typical Photograph for

Instantaneous Droplet Size

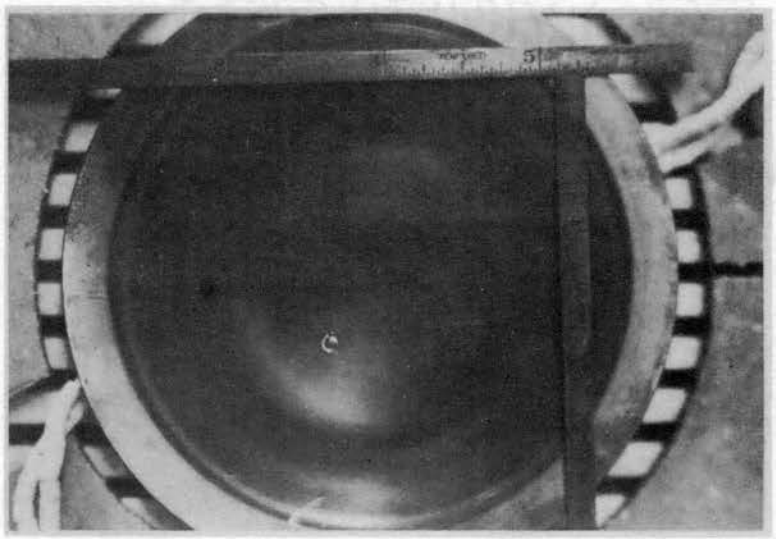

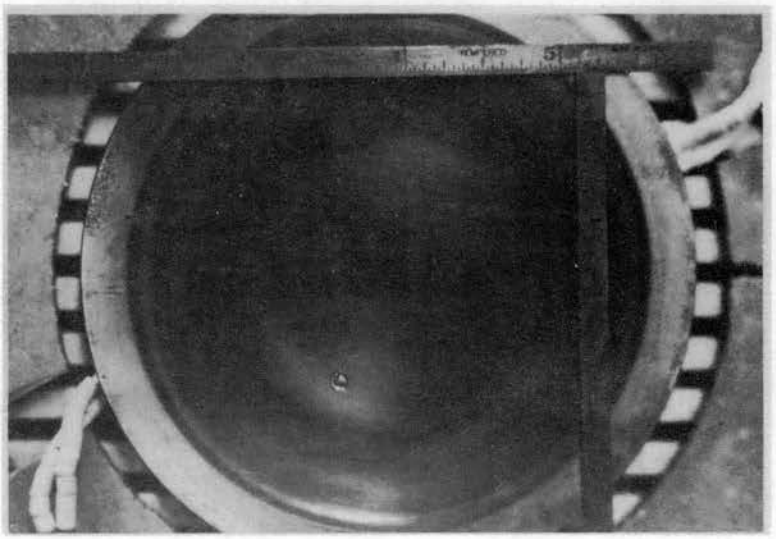

Plate III

Microscope Set-up

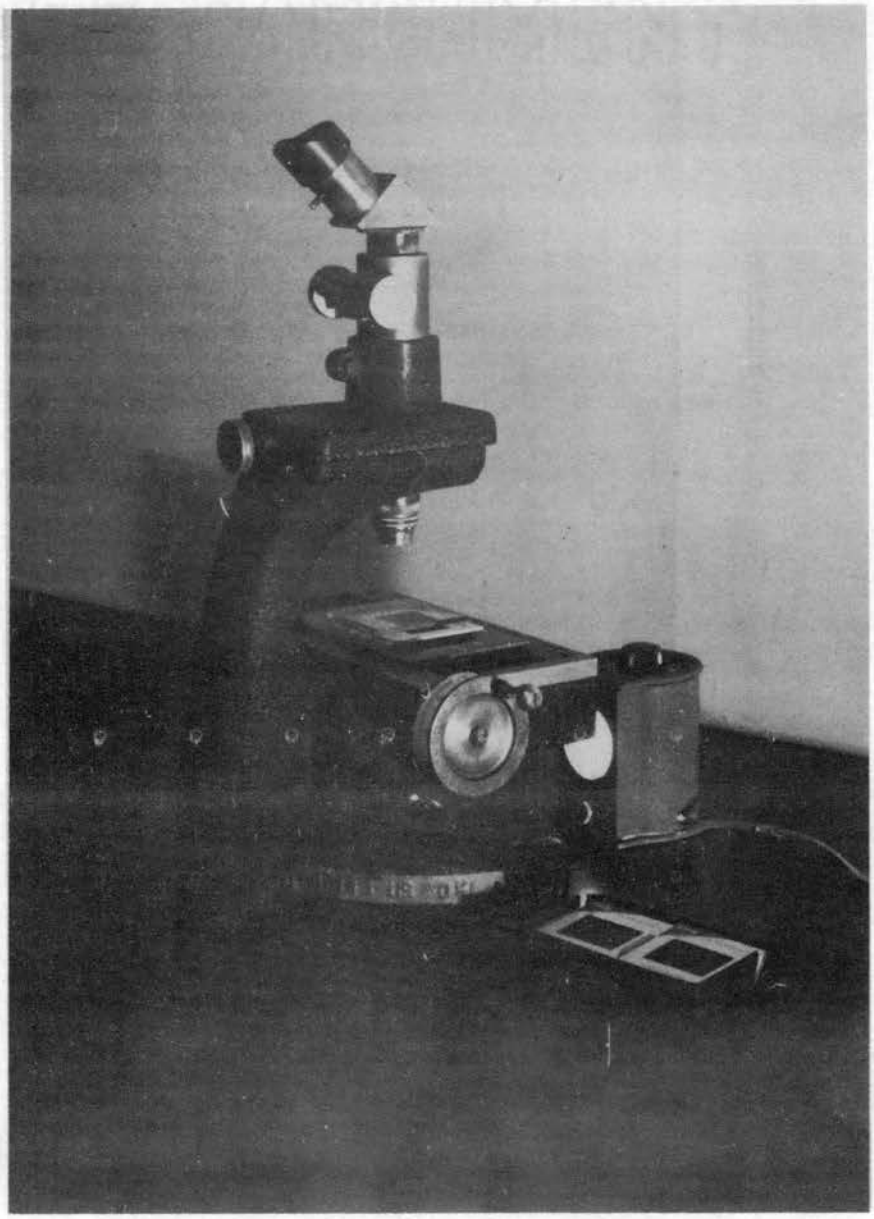

microscope and the illuminating lamp. The small wheel shown on the right of the microscope is a micrometer drive for the object deck. Thus the diameter of the image on slide could be measured on the micrometer scale.

The projected radii of droplets measured in this manner are summarized in Table F-2. Figure 26 through 33 show the comparisons between these data and the theoretically computed values. These results will be discussed more extensively in a later section.

CHAPTER V

THEORETICAL DEVELOPMENT

This theoretical development consists of two major parts. The first part is the formulation of a set of equations from a postulated physical mechanism in order to describe closely the transport phenomena. The second part develops a computer solution to the established equations.

Transport Mechanism

The logic and the philosophy for an analytical approach to the Leidenfrost phenomenon for small droplets were first developed by Gottfried (9). He made a series of physical and mathematical assumptions in the formulation of the physical model. The first assumption was that the droplet was a perfect sphere throughout the process of evaporation. The liquid droplet was assumed to be quiescent relative to the surface and to be at its saturation temperature. The liquid droplet was fully supported by the vapor continuously being generated on the bottom of the droplet.

It is further postulated that several physical phenomena occur simultaneously over the upper and lower surface of the droplet. On the upper surface, molecular diffusion (from the droplet-air interface to the atmosphere) and radiative heat transfer

(from the heating surface to the liquid droplet) are assumed to take place. On the lower portion of liquid droplet, vaporization occurs as a result of convective-conductive and radiative heat transfer from the heating surface to the droplet (Fig. 5-b).

Based on these assumptions together with the geometrical configuration shown in Figure 5, the following equations may be written:

MASS BALANCE EQUATION

$$\rho_L \frac{dV}{dt} = - (W_1 + W_2) \qquad (1)$$

where W_1 and W_2 designate the overall rate at which vapor leaves the lower and upper half of the droplet respectively. Both W_1 and W_2 are implicit functions and must be mathematically resolved.

HEAT BALANCE EQUATION

$$Q_c + Q_{R1} + Q_{R2} = W_1 \left[\lambda + C_p (T_r - T_s) \right] + W_2 \lambda = Q_1 + Q_2 \qquad (2)$$

This equation can be readily written from the heat transfer mechanism shown in Figure 5-b, where T_v is the mean temperature of the vapor being generated which flows between the hot surface and the bottom of droplet. This is assumed to be the arithmetic mean of the plate temperature, T_p and the droplet temperature, T_s. Q_c is the quantity of heat conducted from the heating surface to the liquid droplet through the vapor film existing between the heating surface and the liquid droplet.

Q_{R1} and Q_{R2} are the heat input by thermal radiation from the hot surface to the lower and upper halves of the liquid droplet respectively. These functions Q_c, Q_{R1} and Q_{R2} will be obtained

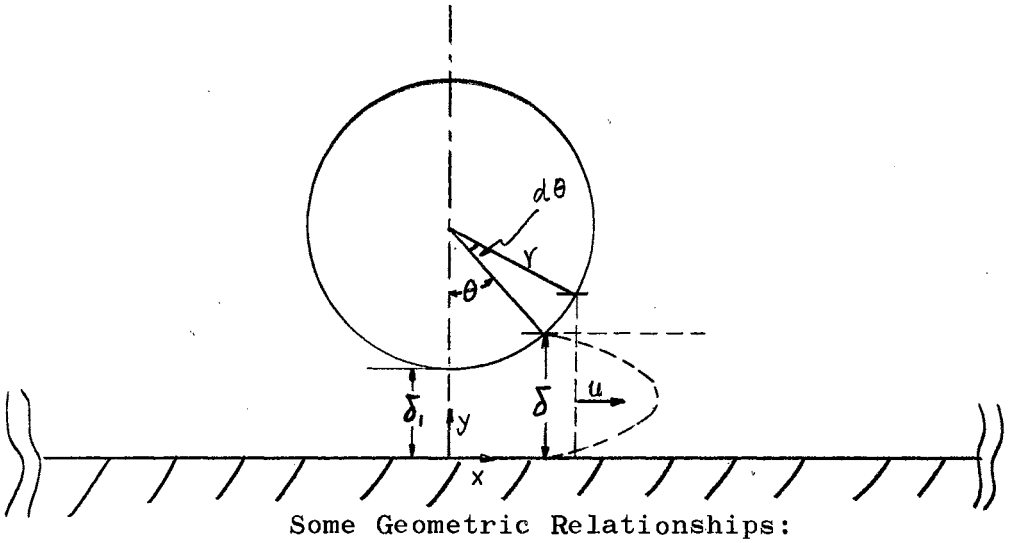

Some Geometric Relationships:

$$\delta = \delta_1 + r(1-\cos\theta)$$

$$x = r\sin\theta$$

$$dx = r\cos\theta\, d\theta$$

$$dA_p = 2\pi x dx = 2\pi r^2 \sin\theta\cos\theta\, d\theta$$

Figure 5-a Geometric Configuration for the Spherical Droplet Model

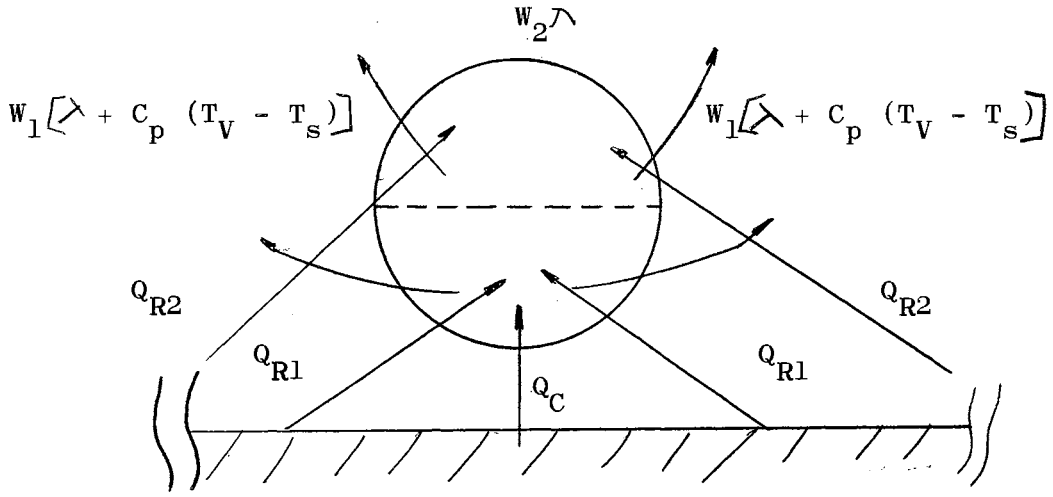

Figure 5-b Heat Transfer Mechanism for the Spherical Droplet Model

explicitly in a later section.

MOMENTUM BALANCE EQUATION

Since the liquid droplet is assumed to be quiescent on the hot plate, the only place where the momentum transfer may take place in this system is in the vapor stream between the plate and the bottom of the droplet. The one-dimensional Navier-Stokes equation for momentum transfer in cylindrical coordinates is (30)

$$\frac{\partial u}{\partial t} + u\frac{\partial u}{\partial x} = -\frac{g_c}{\rho_v}\frac{\partial P}{\partial x} - \frac{\partial \Omega}{\partial x} + \frac{\mu}{\rho_v}\left(\frac{\partial^2 u}{\partial x^2} + \frac{1}{x}\frac{\partial u}{\partial x} + \frac{\partial^2 u}{\partial y^2}\right) \quad (3)$$

$$0 \leqslant x \leqslant r, \quad 0 \leqslant y \leqslant \delta$$

where u is the pointwise radial vapor velocity and is dependent upon x, y, and t.

For the first approximation, assuming that the variation of u with respect to time is small compared to the variation of u with respect to spatial coordinates, i.e., $\partial u/\partial t \approx 0$.

For a relatively slow moving fluid, the inertial terms and field forces may be neglected. In a narrow channel, i .e., $\delta << r$, it may be further assumed that

$$\frac{\partial^2 u}{\partial x^2} + \frac{1}{x}\frac{\partial u}{\partial x} << \frac{\partial^2 u}{\partial y^2} \quad (4)$$

Under such conditions, Equation (3) simplifies to

$$g_c \frac{\partial P}{\partial x} = \mu \frac{\partial^2 u}{\partial y^2} \quad (5)$$

Integrating Equation (5) with respect to y, with the assumed boundary conditions: (a) u = 0 at y = 0, and (b) u = 0 at y = δ, the vapor velocity profile along the y-axis may be given

$$u = \frac{g_c}{2\mu} \frac{\partial P}{\partial x} (y - \delta) y \qquad (6)$$

These simplifications and assumptions will be justified later by comparison with the results of the analysis.

We are now ready to find analytical expression for the implicit functions W_1 and W_2 which appear in Equation (1).

In developing an equation for the evaporation rate from the upper half of droplet, W_2, use is made of the following expression given by Froessling (9):

$$\left(\frac{k_c r}{D}\right) = 1.0 + 0.3 \, Re^{1/2} Sc^{1/3} \qquad (7)$$

for mass transfer from spheres. If the relative air velocity, for flow past the sphere is zero, then the Reynolds number, Re vanishes, and Equation (7) simplifies to

$$k_c = \frac{D}{r} \qquad (8)$$

which physically corresponds to pure molecular diffusion.

From the general theory of mass transfer,

$$W_2 = k_c M (C_s - C_\infty) A_2 \qquad (9)$$

where C is the concentration of the diffusing substance. Assuming that the diffusing medium is an ideal gas and that $C_\infty = 0$, Equation (9) simplifies to

$$W_2 = \frac{k_c M P_s}{R T_s} A_2 \qquad (10)$$

where P_s, the partial pressure of the diffusing vapor is equal to the system pressure for a boiling liquid at pressure equilibrium withits surroundings, i.e., P_s = 1 atm. for the present study.

Equations (8) and (10) may now be combined to give

$$W_2 = \frac{MD\ P_s}{R\ T_s r}\ A_2 \tag{11}$$

which is the desired result for the evaporation rate over the upper half of the droplet surface A_2.

Turning now to the lower half of the droplet, consider an annulus of height δ, radius x, and thickness dx, $0 \leqslant x \leqslant r$, for an incompressible fluid (see Figure 5-a). A material balance may be written as

$$W_1(\Theta') = \rho_v\ 2\pi\ x\ \delta\ \bar{u} \tag{12}$$

where $\bar{u}$ is the average radial velocity of the vapor at Θ' and is obtained by substituting Equation (6) into the following equation

$$\bar{u} = \frac{1}{\delta} \int_o^{\delta} u\ d\ y \tag{13}$$

or

$$\bar{u} = \frac{g_c \delta^2}{12\mu}\ \left(-\frac{\partial P}{\partial x}\right) \tag{14}$$

Substituting Equation (14) as well as the geometric relationships from Figure 5-a into Equation (12)

$$W_1(\Theta') = \frac{2\pi \rho_v g_c x}{12\mu}\ \left(-\frac{\partial P}{\partial x}\right)\ \left[\delta_1 + r - r\ \mathrm{Cos}\ \Theta'\right]^3 \tag{15}$$

The pressure distribution in the vapor stream is obtained by introducing $dx = r\ \mathrm{Cos}\ \Theta\ d\ \Theta$ and rewriting Equation (15) in integral form

$$\int_{P(o)}^{P(\Theta'')} (-dP) = \frac{6\ \mu}{\pi g_c \rho_v} \int_o^{\Theta''} \frac{W_1(\Theta')\mathrm{Cos}\Theta' d\Theta'}{\mathrm{Sin}\ \Theta' \left[\delta_1 + r - r\mathrm{Cos}\Theta'\right]^3} \tag{16}$$

where $P(\theta'')$ is defined as the excess pressure existing beneath the droplet and $P(0)$ is the excess pressure exerted at the bottom center of the droplet. $P(\theta'')$ vanishes at $\theta'' = \pi/2$, i.e., $P(\pi/2) = 0$, and therefore

$$P(0) = \frac{6\mu}{g_c \rho_v} \int_0^{\pi/2} \frac{W_1(\theta') \cos \theta' \, d\theta'}{\sin \theta' \left[\delta_1 + r - r\cos\theta'\right]^3} \qquad (17)$$

The pressure at any given point of the lower droplet from Equations (16) and (17) is

$$P(\theta'') = \frac{6\mu}{g_c \rho_v} \int_{\theta''}^{\pi/2} \frac{W_1(\theta') \cos \theta' \, d\theta'}{\sin \theta' \left[\delta_1 + r - r\cos\theta'\right]^3} \qquad (18)$$

The total upward force which is exerted on the droplet is

$$F = \int_{Ap} P(\theta'') \, dAp = 2\pi r^2 \int_0^{\pi/2} P(\theta'') \sin \theta'' \cos\theta'' d\theta'' \qquad (19)$$

Since the liquid droplet is assumed quiescent on the hot plate, this excess force acting on the droplet from underneath must be counter-balanced by the weight of the droplet, i.e.,

$$4/3 \, \pi r^3 (\rho_L - \rho_V) \frac{g}{g_c} = 2\pi r^2 \int_0^{\pi/2} P(\theta'') \sin\theta'' \cos\theta'' d\theta'' \qquad (20)$$

Introducing Equation (18) into Equation (20) and rearranging

$$r = \frac{9}{\pi} \frac{\mu}{g \rho_V (\rho_L - \rho_V)} \int_0^{\pi/2} \sin\theta'' \cos\theta'' d\theta'' \int_0^{\pi/2} \frac{W_1(\theta') \cos\theta' d\theta d\theta'}{\sin\theta' \left[\delta_1 + r - r\cos\theta'\right]^3} \qquad (21)$$

It should be noticed that the rate of vapor generation over the

lower surface of the droplet, $W_1(\Theta')$ appears implicitly in Equation (21). The solution of this equation is therefore, impossible without recourse to an analysis for the hypothetical mechanisms of the heat and mass transfer taking place on the lower portion of the droplet.

Let us first hypothesize that the vapor generation from the bottom of the droplet up to a position Θ', $W_1(\Theta')$ is due to an <u>effective</u> heat conduction in y-direction from the heating plate to the droplet, i.e.,

$$d\left[W_1(\Theta')\right] = \frac{1}{\lambda'}\left[\frac{k_e\,\Delta T}{\delta}\right] dA_p \qquad (22)$$

or

$$W_1(\Theta') = \frac{2\pi r}{\lambda'}\int_o^{\Theta'} \frac{k_e\,\Delta T}{\left[\delta_1/r + 1-\mathrm{Cos}\Theta\right]} \mathrm{Sin}\,\Theta\mathrm{Cos}\,\Theta\, d\,\Theta$$

$$= \frac{2\pi r\, k_e \Delta T}{\lambda'}\int_o^{\Theta'} \frac{\mathrm{Sin}\Theta\ \mathrm{Cos}\Theta\ d\Theta}{\left[\delta_1/r + 1 - \mathrm{Cos}\,\Theta\right]} \qquad (23)$$

where λ' is the heat of vaporization with the superheating being taken into consideration, i.e.,

$$\lambda' = \lambda + C_p\,(T_v - T_s) = \lambda + 1/2\ C_p \Delta T \qquad (24)$$

The symbol k_e in Equation (23) denotes the effective thermal conductivity for the hypothetical heat conduction mechanism; Its value shall be determined by the overall heat balance of Equation (2).

By introducing Equation (23) into Equation (21) and simplifying, the following equation may be obtained

$$r^3 = \frac{18\ \mu\ k_e\ \Delta T}{g\ \rho_V(\rho_L-\rho_V)\lambda'}\ I_3\ (\delta_1/r) \qquad (25)$$

where

$$I_3(\delta_1/r) = \int_o^{\pi/2} \text{Sin}\ \theta''\ \text{Cos}\theta''\ I_2\ (\delta_1/r,\theta'')d\theta'' \qquad (26)$$

where

$$I_2(\delta_1/r,\theta'') = \int_o^{\theta''} \frac{\text{Cos}\theta'\ I_1(\delta_1/r,\theta')d\theta''}{\text{Sin}\theta'\left[\delta_1/r + 1-\text{Cos}\theta'\right]^3} \qquad (27)$$

and where

$$I_1\ (\delta_1/r,\ \theta') = \int_o^{\theta'} \frac{\text{Sin}\theta\ \text{Cos}\theta\ d\theta}{\delta_1/r + 1 - \text{Cos}\theta} \qquad (28)$$

Evaluation of Integrals

The numerical evaluations for the above integrals, I_1 through I_3 are found in Appendix C. The results of the numerical integration were curve-fitted and presented in the following forms (see Appendix C):

for $0.0198 \leqslant I_3\ (\delta_1/r) \leqslant 11{,}213{,}855$

$$\ln(\delta_1/r) = -1.3832 - 0.3980\ \ln\left[I_3(\delta_1/r)\right] - 0.0104\left\{\ln\left[I_3(\delta_1/r)\right]\right\}^2 + 0.000355\left\{\ln\left[I_3\ (\delta_1/r)\right]\right\}^3 \qquad (C1)$$

for $0 \leqslant \delta_1/r \leqslant 0.01$

$$I_1(\delta_1/r,\ \pi/2) = -0.8321 - 0.9746\left[\ln\ (\delta_1/r)\right] \qquad (C2)$$

for $0.01 \leq \delta_1/r$

$$I_1(\delta_1/r, \pi/2) = 0.3874 - 0.2835 \left[\ln(\delta_1/r)\right] + 0.1328 \left[\ln (\delta_1/r)\right]^2 + 0.0087 \left[\ln (\delta_1/r)\right]^3 \quad (C3)$$

Therefore, the total evaporation rate from the lower half of the droplet may be obtained as

$$W_1 = W_1 \ (\theta' = \pi/2) = \frac{2\pi r \, k_e \, \Delta T}{\lambda'} \ I_1(\delta_1/r, \pi/2) \quad (29)$$

The Analysis for Conductive and Radiative Heat Transfer

The rate of heat transfer from a heated surface to a liquid under film-boiling conditions is due to convective-conductive transport and to radiative transport. The functions Q_c, Q_{R1}, Q_{R2} and Q_1 of Equation (2) are to be analysed in this section.

Let q_c be the heat transfer rate per unit area due to thermal conduction through the vapor film existing between the plate and bottom of the droplet. If we assume that conduction is in the y-direction only, the Fourier equation gives

$$q_c = \frac{k\Delta T}{\delta}$$

or

$$Q_c = \int_{Ap} \frac{k\Delta T}{\delta} \, dA_p = \frac{k\Delta T}{\bar{\delta}} \, A_p \quad (30)$$

where $\bar{\delta}$ is the mean film thickness through which heat is conducted from the heating surface to the liquid droplet. By substituting

the geometrical relationships of Figure 5-a into Equation (30), $\bar{\delta}$ is obtained as follows:

$$\bar{\delta} = \left[\frac{2\,(\delta_1 + r)}{r^2} \ln \frac{\delta_1 + r}{\delta_1} - \frac{2}{r} \right]^{-1} \qquad (31)$$

The heat transfer rate due to thermal conduction from the heating surface to the droplet, therefore, can be expressed by Equations (30) and (31).

In general, the effect of radiative heat transport becomes increasingly more important as the plate temperature increases. The radiative heat transport proceeds by two mechanisms, The first is a direct transfer between the heated plate and the liquid. The second is the absorption and the emission of radiation in the vapor film which lies between the plate and the liquid droplet.

The effect of the second radiative heat transfer mechanism, however, is negligible in most practical cases (31). By assuming that the plate and the lower half of the droplet are separated by a non-absorbing, non-emitting medium, the rate of radiative heat transfer between these two bodies is given (19)

$$Q_{R1} = A_1 \mathcal{F}_1 \sigma (T_p^4 - T_s^4) \qquad (32)$$

where $\mathcal{F}_1$ is the overall configuration factor for radiation between hot plate and the lower half of the liquid droplet. $\mathcal{F}_1$ is given for a system of two-zone, source-sink surfaces in Reference (19):

$$\frac{1}{\mathcal{F}_1} = \left(\frac{1}{\epsilon_L} - 1 \right) + \frac{A_1}{A_s} \left(\frac{1}{\epsilon_s} - 1 \right) + \frac{1}{\bar{F}_1} \qquad (33)$$

Since $A_1 << A_s$, Equation (33) can be further simplified

$$\frac{1}{\mathcal{F}_1} = \left(\frac{1}{\epsilon_L} - 1\right) + \frac{1}{\bar{F}_1} \tag{34}$$

Similarly, the overall configuration factor for radiation from hot plate to the upper half of the liquid droplet can be expressed

$$\frac{1}{\mathcal{F}_2} = \left(\frac{1}{\epsilon_L} - 1\right) + \frac{1}{\bar{F}_2} \tag{35}$$

The problem now is to obtain expressions for $\bar{F}_1$ and $\bar{F}_2$, the average configuration factors for radiation from hot plate to the lower and upper halves of spherical droplets respectively. This can be done by considering the fraction of solid angle which actually sees the infinite plate. If we define the pointwise configuration factor as $F(\theta_1) = (2\pi - 2\theta_1)/2\pi$ then, the average configuration factor becomes (see Figure 6)

$$\bar{F}_1 = \frac{\int_{A_1} F(\theta_1)\, dA_1}{A_1} = \frac{\int_0^{\pi/2} \left(\frac{2\pi - 2\theta_1}{2\pi}\right)(2\pi r \sin\theta_1)\, r d\theta_1}{2\pi r^2} \tag{36}$$

Integrating Equation (36) and simplifying, we obtain

$$\bar{F}_1 = \frac{1}{\pi}\left[\pi - 1\right] = 0.682 \tag{37}$$

Similarly, by the geometrical configuration presented in Figure 6-b, the value for $\bar{F}_2$ is obtained as follows

$$\bar{F}_2 = \frac{\int_{A_2} \frac{2(\pi/2 - \theta_2)}{2\pi}\, dA_2}{A_2} = \frac{\int_0^{\pi/2} \frac{(\pi/2 - \theta_2)}{\pi} (2\pi r \cos\theta_2) r d\theta_2}{2\pi r^2} \tag{38}$$

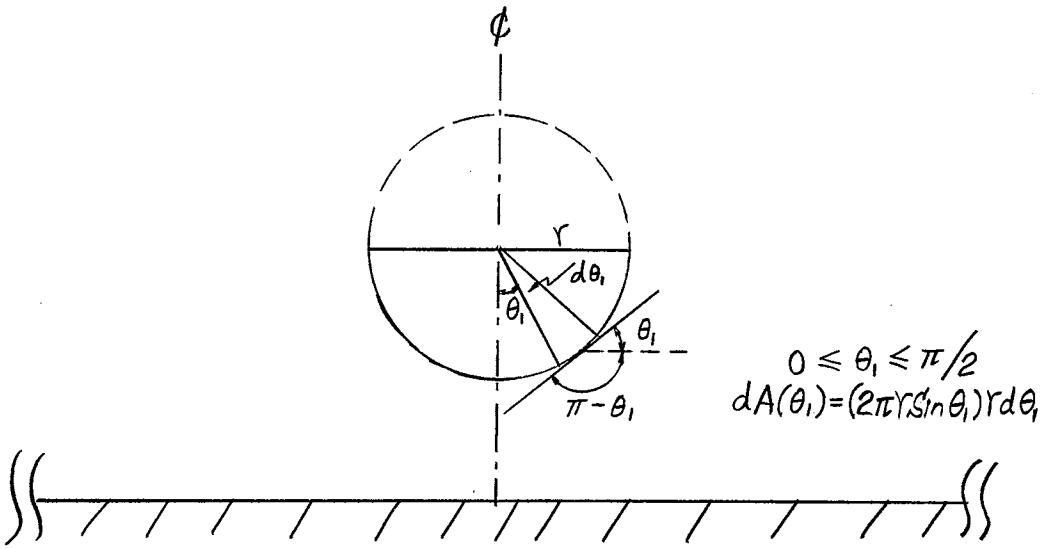

Figure 6-a Configuration Factor for Thermal Radiation from Infinite Surface to a Lower Hemisphere

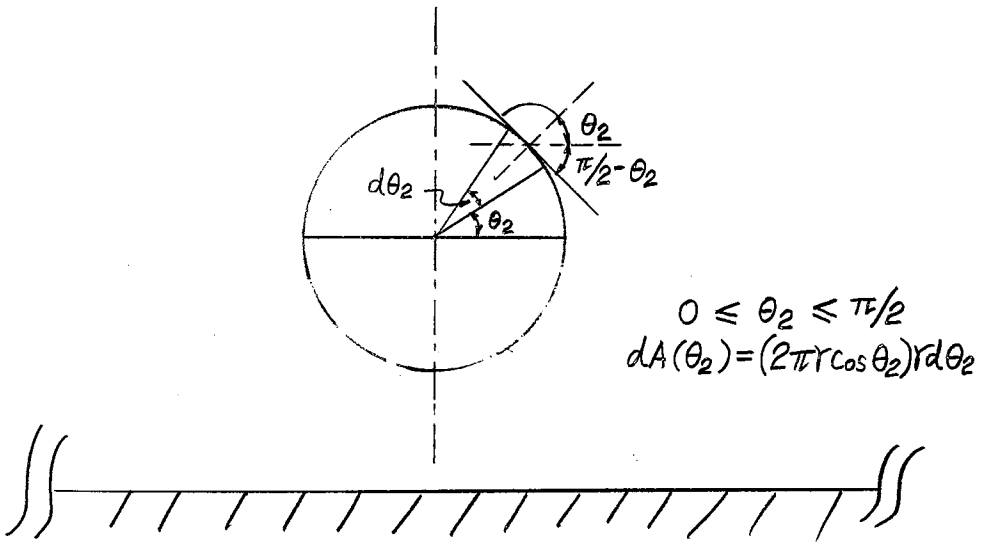

Figure 6-b Configuration Factor for Thermal Radiation from Infinite Surface to an Upper Hemisphere

Therefore,

$$\bar{F}_2 = 1/\pi = 0.318 \tag{39}$$

Substituting Equation (37) into Equation (34) and again to Equation (32), the radiation heat transfer from the heating plate to the lower half of spherical droplet becomes

$$Q_{R1} = \frac{A_1\sigma(T_p^4 - T_s^4)}{(1/\epsilon_L - 1) + 1/0.682} \tag{40}$$

By a similar procedure, the radiative heat transfer from the heating plate to the upper half of spherical droplet may be obtained

$$Q_{R2} = \frac{A_2\sigma(T_p^4 - T_s^4)}{(1/\epsilon_L - 1) + 1/0.318} \tag{41}$$

With Equations (30), (31), (40), and (41), it is seen that the effective heat transfer from the heating plate to the bottom half of droplet, Q_1, can be readily obtained from Equation (2).

$$Q_1 = \frac{k_e \Delta T}{\bar{\delta}} A_p = (Q_c + Q_{R1} + Q_{R2}) - W_2\lambda \tag{42}$$

where $k_e = (1 + K)k$.

K is defined as the correction factor between the actual thermal conductivity of vapor, k and the effective thermal conductivity for the heat transfer taking place between the heating plate and the lower half of droplet, k_e.

In the following computational scheme, the factor K is consecutively approximated by K = 0 and

$$K = Q_{R1}/Q_c \tag{43}$$

The convergence of K is then checked by the heat balance of Equation (42).

Overall Computational Scheme

It may be seen from the above analysis that the final form of Equation (1) is very nonlinear. This non-linearity precludes an analytical solution for the total evaporation time and evaporation rate of droplets in the Leidenfrost regime. Therefore, a numerical analysis must be developed.

A functional analysis gives the following equation

$$\frac{dV}{dt} = - \frac{1}{\rho_L} (W_1 + W_2) = f\ (V,t) \tag{44}$$

This type of first order, ordinary differential equation may be appropriately solved by using the modified Euler's method (16).

Let V_i be the droplet volume at time t_i, and V_{i+1} the droplet volume after a time increment Δt. Our intial approximation for V_{i+1} is then,

$$V_{i+1} = V_i + \Delta t\ f\ (V_i, t_i) \tag{45}$$

This value of V_{i+1} is then modified using an average evaporation rate for the interval Δt, i.e.,

$$V_{i+1}^{(1)} = V_i + \frac{\Delta t}{2} \left[f\ (V_i, t_i) + f\ (V_{i+1}, t_{i+1}) \right] \tag{46}$$

— — — — — — — — — — — — — —

$$V_{i+1}^{(j-1)} = V_i + \frac{\Delta t}{2} \left[f\ (V_i, t_i) + f\ (V_{i+1}^{(j-2)}, t_{i+1}) \right] \tag{47}$$

$$V_{i+1}^{(j)} = V_i + \frac{\Delta t}{2} \left[f\ (V_i, t_i) + f\ (V_{i+1}^{(j-1)}, t_{i+1}) \right] \tag{48}$$

These equations are solved by the method of iteration until the following convergence is obtained:

$$\left| \frac{V_{i+1}^{(j)} - V_{i+1}^{(j-1)}}{V_{i+1}^{(j)}} \right| \leqslant 10^{-5} \qquad (49)$$

With this outline for the numerical method, the computation then proceeds as follows:

A. First-stage Computation

(1) The radius and the surface area of the spherical droplet are first obtained from V_i.

(2) Ignoring the radiative heat transfer for the first-stage iteration by taking K = 0, the integral I_3 (δ_1/r) may be determined from Equations (25) and $k_e = k$. This $I_3(\delta_1/r)$ is then substituted in Equation (C1) from Appendix C to obtained the dimensionless vapor film thickness corresponding to V_i. Then from Equation (C2) or (C3) of Appendix C, the integral $I_1(\delta_1/r, \pi/2)$ is determined.

(3) The total evaporation rate on the lower half of the droplet (without correction factor), $(W_1)_{K=0}$ is obtained by direct substitution of $I_1(\delta_1/r, \pi/2)$ in Equation (29).

(4) The value for W_2 is computed from Equation (11) and the surface area of the droplet obtained in step (1).

(5) The initial guess for V_{i+1} is made by substituting $(W_1)_{k_e=k}$ and W_2 into Equation (44) and then to Equation (45).

(6) Steps (1) through (5) are successively repreated until the required convergence of Equation (49) is obtained.

(7) The values for r, δ_1/r and $\bar{\delta}$ corresponding to the converged value of V_{i+1} are then used in the second-stage

computation, where the effect of radiative heat transfer is considered.

B. Second-stage Computation

(1) The heat transfer due to radiation, Q_{Rl} is computed from Equation (40).

(2) The first estimate for K is then determined from Equations (30), (40), and (43).

(3) With the first estimate of K, the computation then goes back to Equations (25), (C1), (C2), (C3), and (29) to obtain the value of W_1.

(4) The convergence of K is tested by Equation (42), the heat balance equation where the value for $\overline{\delta}$ is to be obtained from Equation (31), and Q_c from Equation (30).

(5) If Equation (42) is not satisfied, the iteration goes back to A. using the value for K obtained as

$$K = \frac{k_e}{k} - 1 \tag{50}$$

where k_e is obtained from Equation (42).

(6) If Equation (42) is satisfied to within an allowable error, the solutions for instantaneous droplet volume, droplet radius, evaporation rate are obtained. The computation then moves on to the next time interval.

The whole process goes on and on until the droplet volume, V approaches zero. The complete flow diagram and the Fortran program for the digital machine computation are presented in Appendix D.

An extensive discussion on the computed results compared to

the experimental values will be found in Chapter VII.

CHAPTER VI

ENGINEERING CORRELATION OF EXPERIMENTAL DATA

The theoretical development in the previous chapter is purely analytical. It does not require any experimental data (except physical properties) in the prediction for droplet evaporation time; however, it involves complicated iterational computations before it converges to the correct values for droplet evaporation time. Thus, a digital computer is a necessary tool to perform these numerical computations. For the engineering calculation, it is desirable to obtain a relatively simple equation which would imply the correct functional dependence upon variables and allow a prediction for droplet evaporation time without recourse to a computer. In order to obtain such an empirical correlation of the experimental data, a functional equation between the dependent variable and the independent variables must be obtained.

The overall evaporation rate per unit area of liquid droplet on a hot surface $\rho_L V_o/\tau A$ may simply be expressed as follows

$$\rho_L V_o/\tau A \propto \frac{1}{\lambda'} \left[q_c + q_R \right] \tag{51}$$

For a spherical droplet, it becomes

$$\rho_L \gamma_o/\tau \propto \frac{1}{\lambda'} \left[q_c + q_R \right] \tag{52}$$

By taking the emissivity of liquid, $\epsilon_L = 1.0$ McAdams (19) gives

$$q_R \approx \sigma \epsilon_s (T_p^4 - T_s^4) \tag{53}$$

and from the one-dimensional Fourier equation, the conductive heat transfer term may be written

$$q_c \approx \frac{k \Delta T}{\delta_1 (t=0)} \tag{54}$$

where $\delta_1(t=0)$ is the vertical distance from plate to bottom of the intial liquid droplet. The values for (δ_1/r) are always less than 0.02 for the range of droplet volumes shown in the computational results. For this range of (δ_1/r), the curve fit with the values given in Appendix C may be obtained as

$$\delta_1/r = \text{Exp}\ (-0.475) \left[I_3(\delta_1/r) \right]^{-0.496} \tag{55}$$

where $I_3(\delta_1/r)$ is the triple integral and is given in the following form from equation (25)

$$I_3\ (\delta_1/r) = \frac{r^3\ g\ \rho_L\ (\rho_L - \rho_V)\ \lambda'}{18\ \mu\ \rho_v\ \Delta T} \tag{56}$$

Substituting Equation (56) into Equation (55) and rearranging

$$\delta_1/r = (\text{Constant}) \left[\frac{\mu\ k\ \Delta T}{r^3\ g\ \rho_V (\rho_L - \rho_V)\ \lambda'} \right]^{1/2} \tag{57}$$

Thus,

$$\delta_1(t=0) = (\text{Constant}) \left[\frac{\mu\ k\ \Delta T}{r_o\ g\ \rho_V (\rho_L - \rho_V) \lambda'} \right]^{1/2} \tag{58}$$

Therefore Equation (54) may now be written

$$q_c = \frac{k\ \Delta T}{\delta_1(t=0)} = (\text{Constant})\left[k\ \Delta T\right]\left[\frac{\mu\ k\ \Delta T}{r_o\ g\ \rho_V(\rho_L - \rho_V)\lambda'}\right]^{-1/2}$$

$$= (\text{Constant})\left[\frac{k\ \Delta T\ r_o\ g\ \rho_V(\rho_L - \rho_V)\lambda'}{\mu}\right]^{1/2} \tag{59}$$

Substituting Equation (53) and (59) into Equation (52), the following equation is obtained:

$$\frac{\rho_L r_o}{\tau} = C_1\left[\frac{k\ \Delta T\ r_o\ g\ \rho_V(\rho_L - \rho_V)}{\mu\lambda'}\right]^{1/2} + C_2\left[\frac{p\ (T_p^4 - T_s^4)}{\lambda'}\right] \tag{60}$$

C_1 and C_2 are the correlational constants to be evaluated from the experimental data. This may be carried out by the method of least squares.

If we denote

$$Y = \rho_L r_o/\tau \tag{61}$$

$$X_1 = \left[\frac{k\ \Delta T\ r_o\ g\ \rho_V(\rho_L - \rho_V)}{\mu\lambda'}\right]^{1/2} \tag{62}$$

$$X_2 = \frac{\sigma \epsilon_p\ (T_p^4 - T_s^4)}{\lambda'} \tag{63}$$

Equation (60) then may be compactly written

$$Y = C_1X_1 + C_2X_2 \tag{64}$$

By the general regression analysis with the experimental data, Equation (64) may be easily solved for C_1 and C_2. The result is given in the following form:

$$\frac{\rho_L r_o}{\tau} = 1.1703 \times 10^{-2} \left[\frac{k \, \Delta T \, r_o \, g \, \rho_V (\rho_L - \rho_V)}{\mu \lambda'} \right]^{1/2}$$

$$+ 2.3815 \left[\frac{\sigma \epsilon_p (T_p^4 - T_s^4)}{\lambda'} \right] \qquad (65)$$

The results of this correlation are presented in Figure 39 and will be discussed in the next chapter.

CHAPTER VII

DISCUSSION OF RESULTS

The justification of the analytical model developed in Chapter V is by the comparison between experimental data and the theoretically computed values. The total droplet evaporation time and the instantaneous droplet diameters are two types of experimental data which can be directly compared against the theoretical values.

At plate temperatures beyond the Leidenfrost point where the spheroidal state film boiling is very well defined, the experimental data on droplet evaporation time were reproducible to within a maximum variation of $\pm$ 5 percent. The experimental results together with the theoretically computed values are shown in Figures 6 through 25.

The technique of making liquid droplets with the hypodermic syringe set at a 45 degree angle to the heating plate may be considered an improvement over holding the syringe normal to the plate. One significant advantage is that it shortens the duration between the droplet formation and droplet departure from the tip of the needles; thus it minimizes the liquid-temperature effect on the formation of droplet sizes. As the radiation from the hot plate may cause a droplet to heat up while it is being formed, thus lowering its surface tension and consequently producing a

smaller droplet, the liquid in the hypodermic needle should be kept as close to room temperature as possible. Gottfried (9) in his thesis discussed the liquid-temperature effect on the formation of droplet size, and reported that water droplets have the largest change in size as a function of liquid temperature. The average size of water droplets at saturation temperature is about 10 percent smaller than the average size of water droplets obtained at room temperature. Gottfried, nevertheless, concluded that the needle calibrations obtained with liquids at room temperature were correct, since there was not enough time for the droplet temperature to increase and the surface tension to decrease significantly before the droplet came into contact with the plate. His statement was supported by a few sets of droplet evaporation time data obtained with boiling water rather than water at room temperature. The resulting evaporation times were only 2 to 3 percent less than the corresponding evaporation times for water at room temperature.

The solid curves in Figures 6 through 25 represent the droplet evaporation time predicted by the theoretical model. The solid dots are the arithmetic average of five individual determinations of the droplet evaporation time at a constant plate temperature. The range of the variation is shown by two bars which indicate the maximum and the minimum values among these five determinations. The best agreement between theory and the experiment is found in the cases of water and carbon tetrachloride which have relatively high liquid density at their boiling point; Figures 7, 8, and 20 present the best coincidence between theoretically

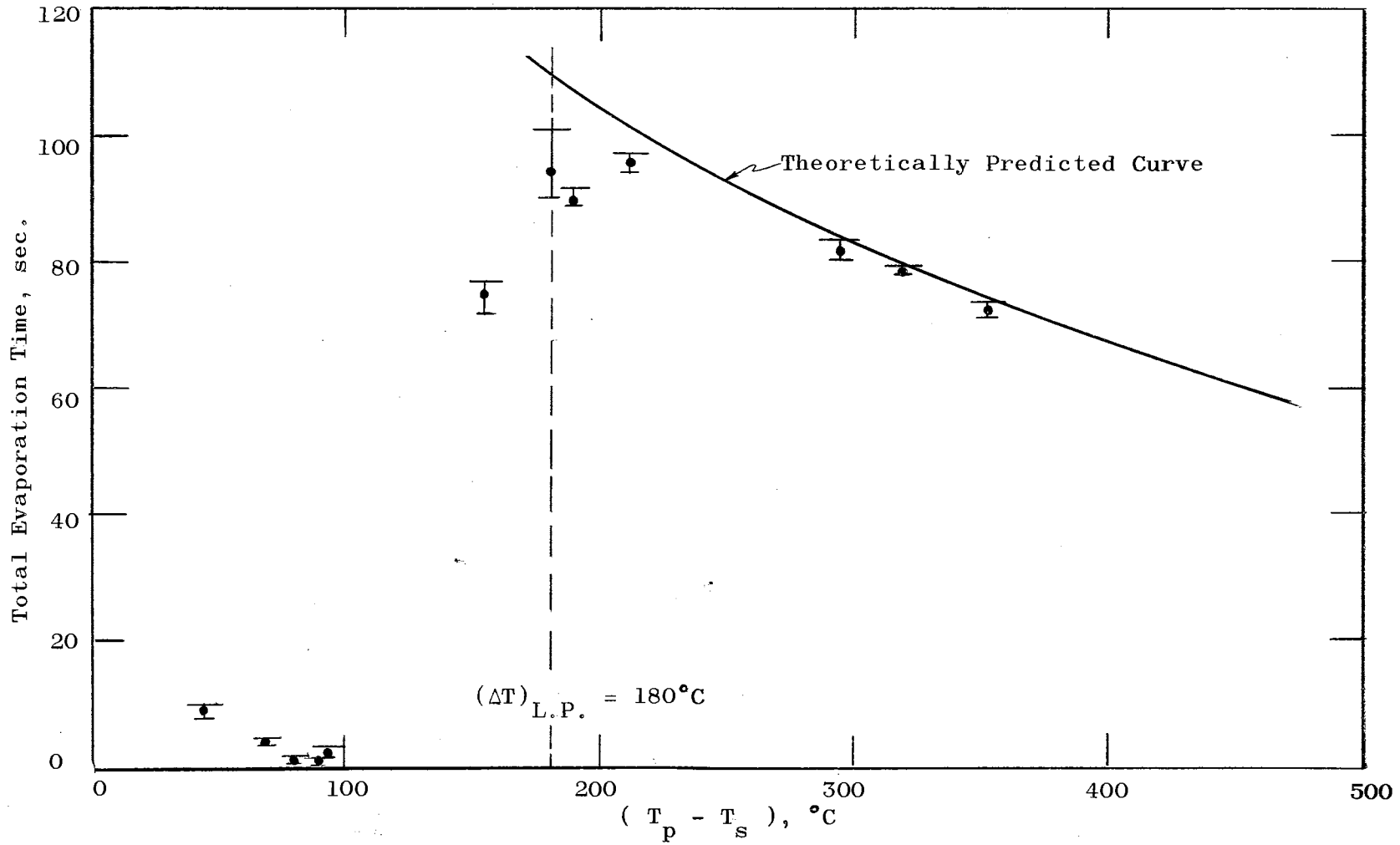

Figure 6 Droplet Evaporation Time vs. ΔT for Water Droplets; V_o = 0.03196 ml.

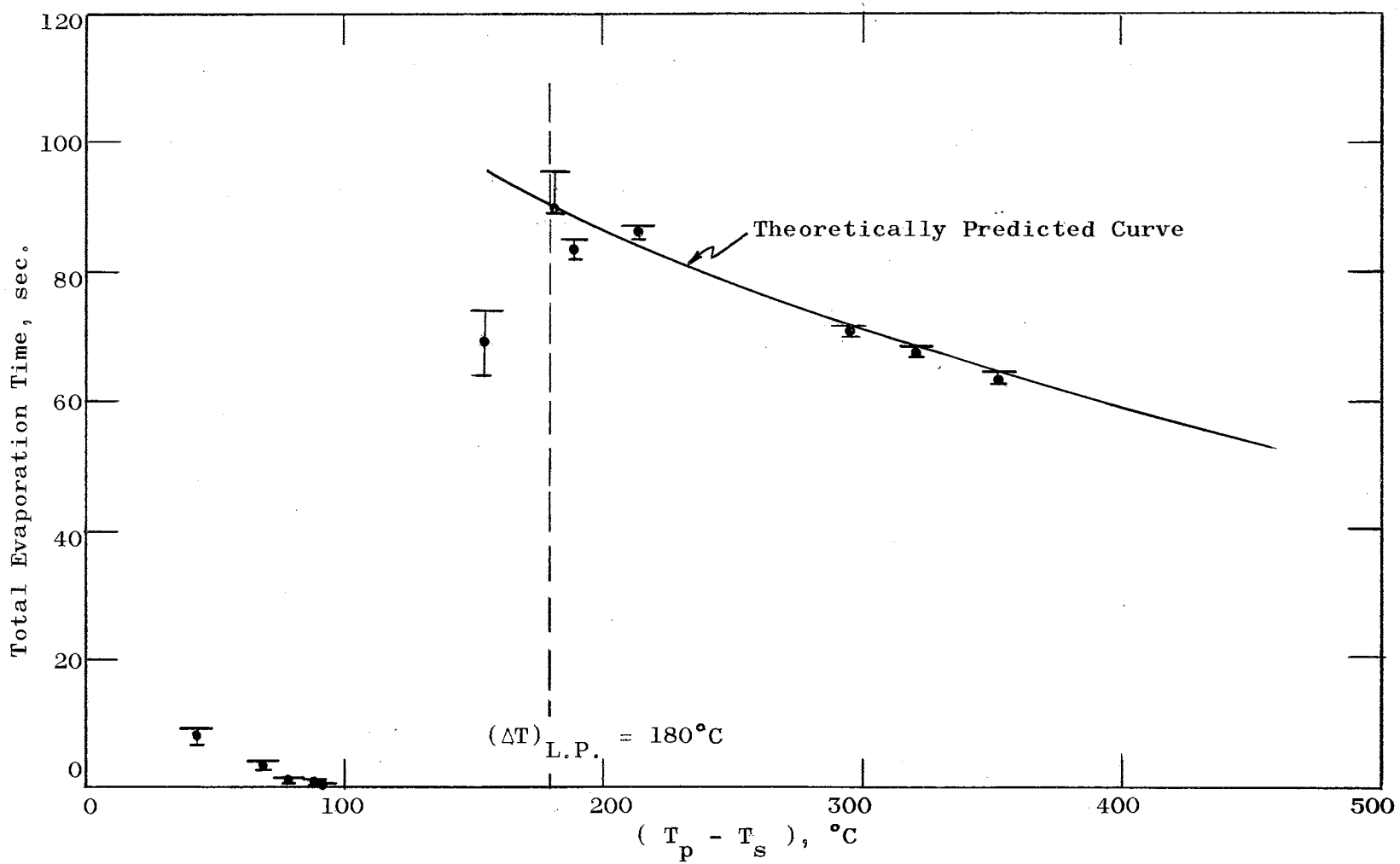

Figure 7 Droplet Evaporation Time vs. ΔT for Water Droplets; V_o = 0.02212 ml.

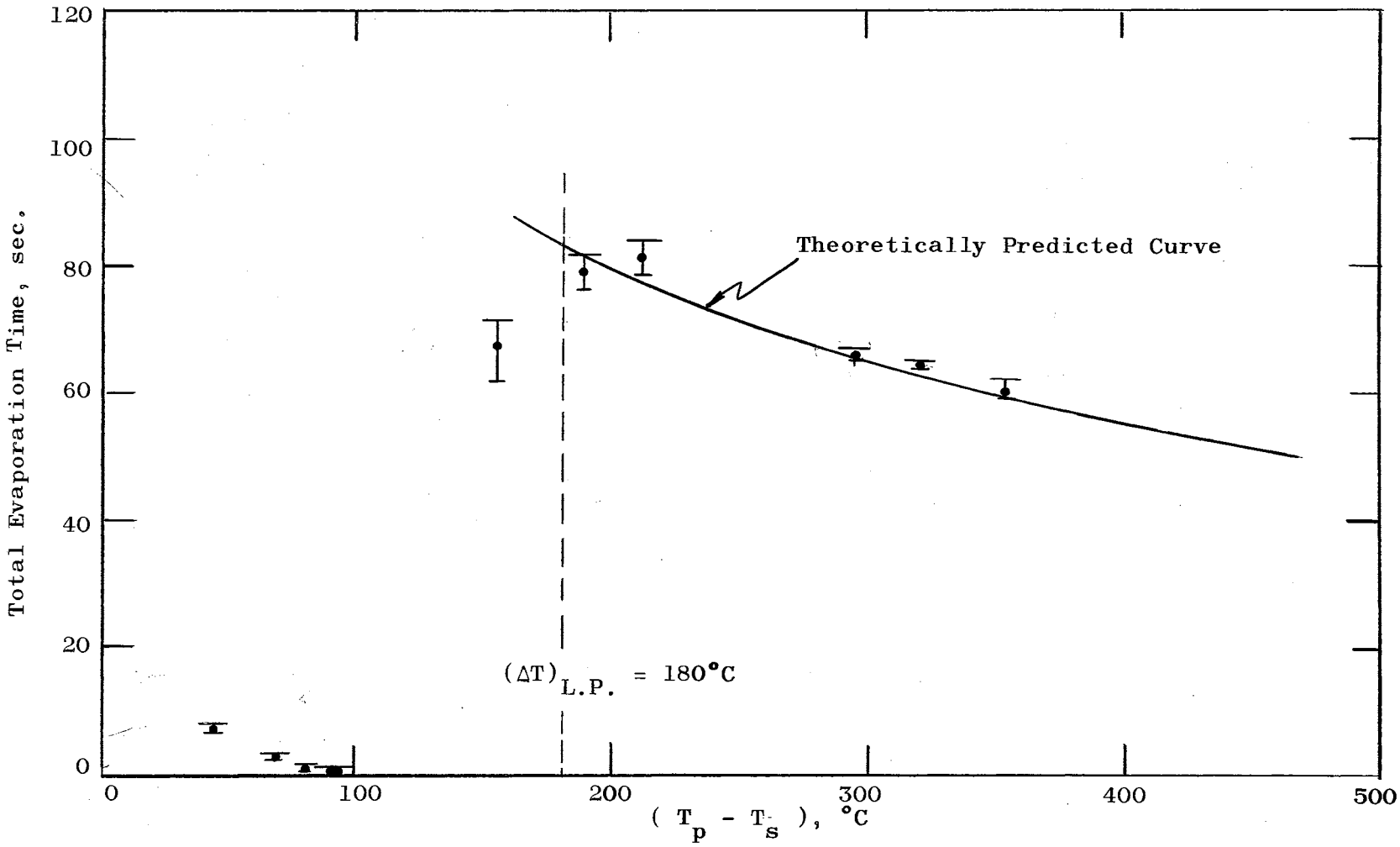

Figure 8 Droplet Evaporation Time vs. ΔT for Water Droplets; V_o = 0.01920 ml.

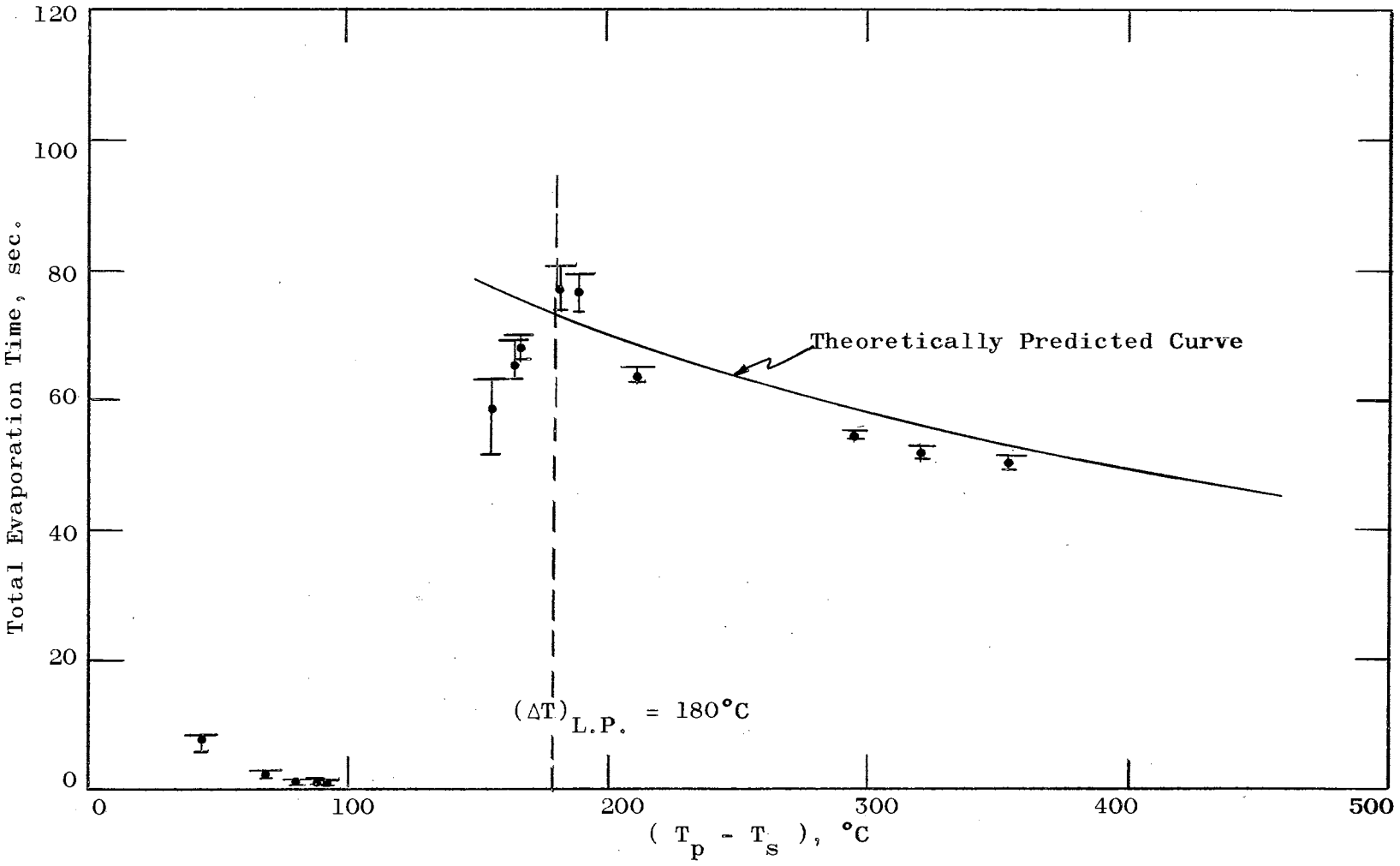

Figure 9 Droplet Evaporation Time vs. ΔT for Water Droplets; V_o = 0.0154 ml.

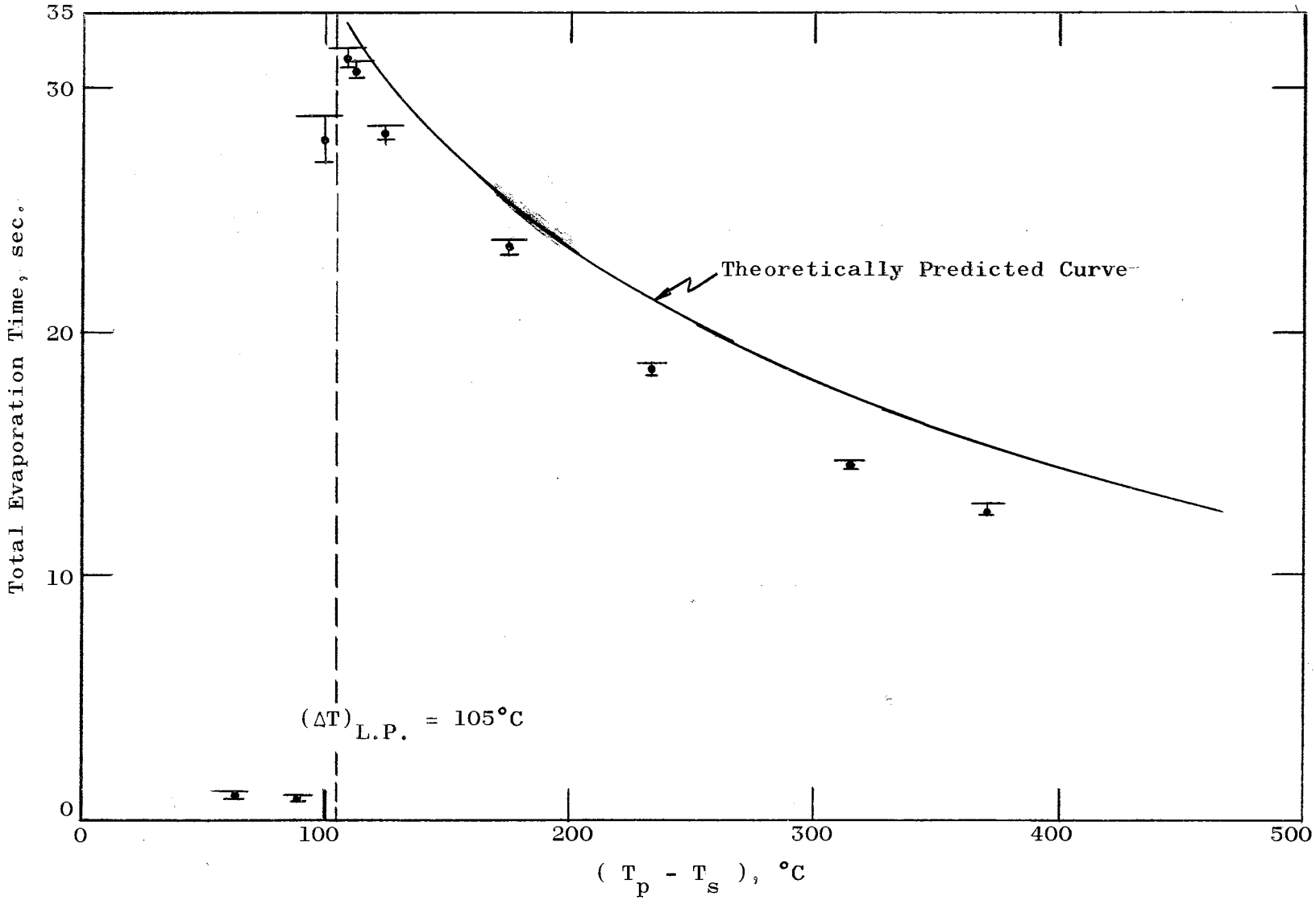

Figure 10 Droplet Evaporation Time vs. ΔT for Benzene Droplets; V_o = 0.01618 ml.

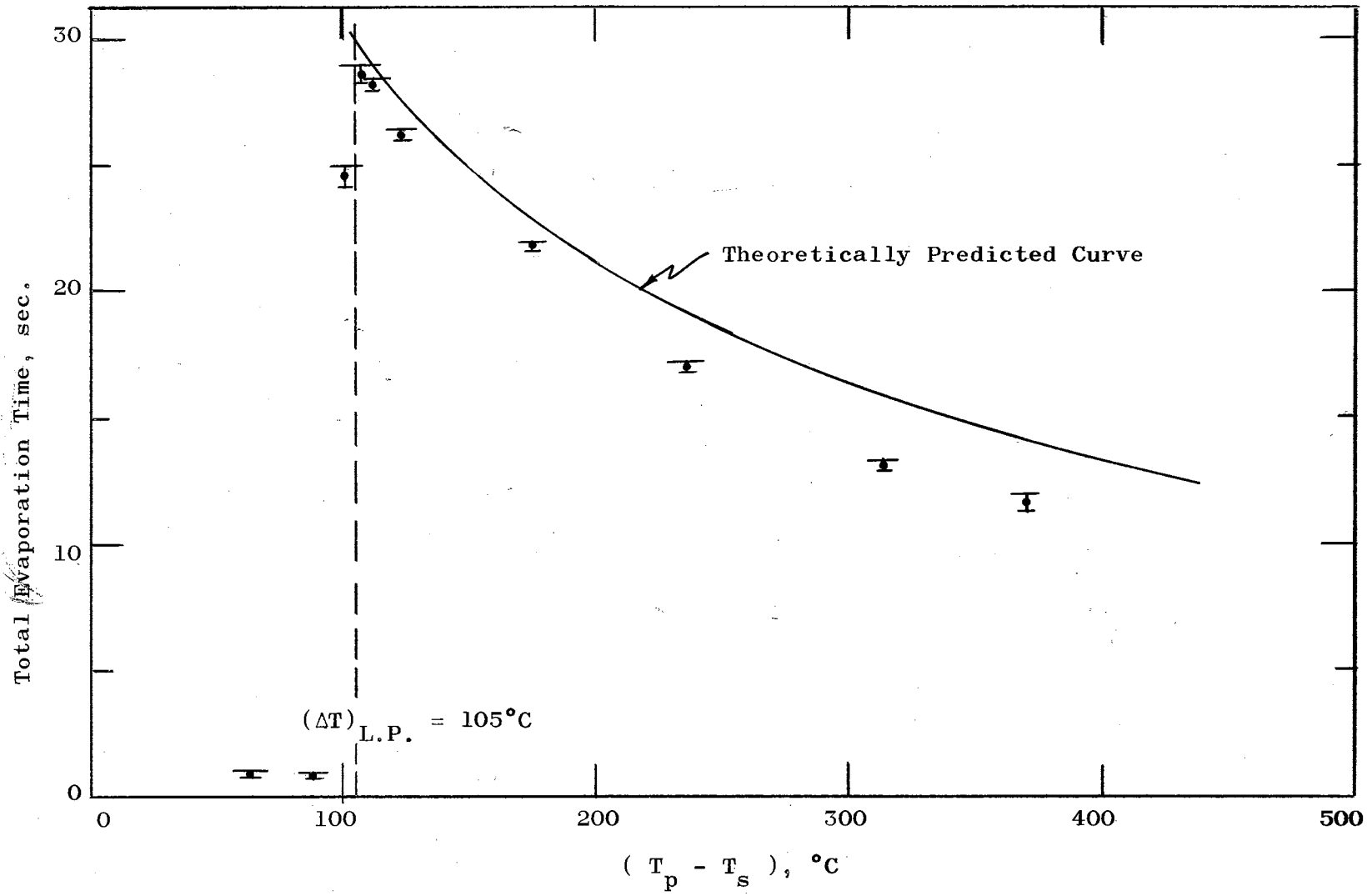

Figure 11 Droplet Evaporation Time vs. ΔT for Benzene Droplets; V_o = 0.01343 ml.

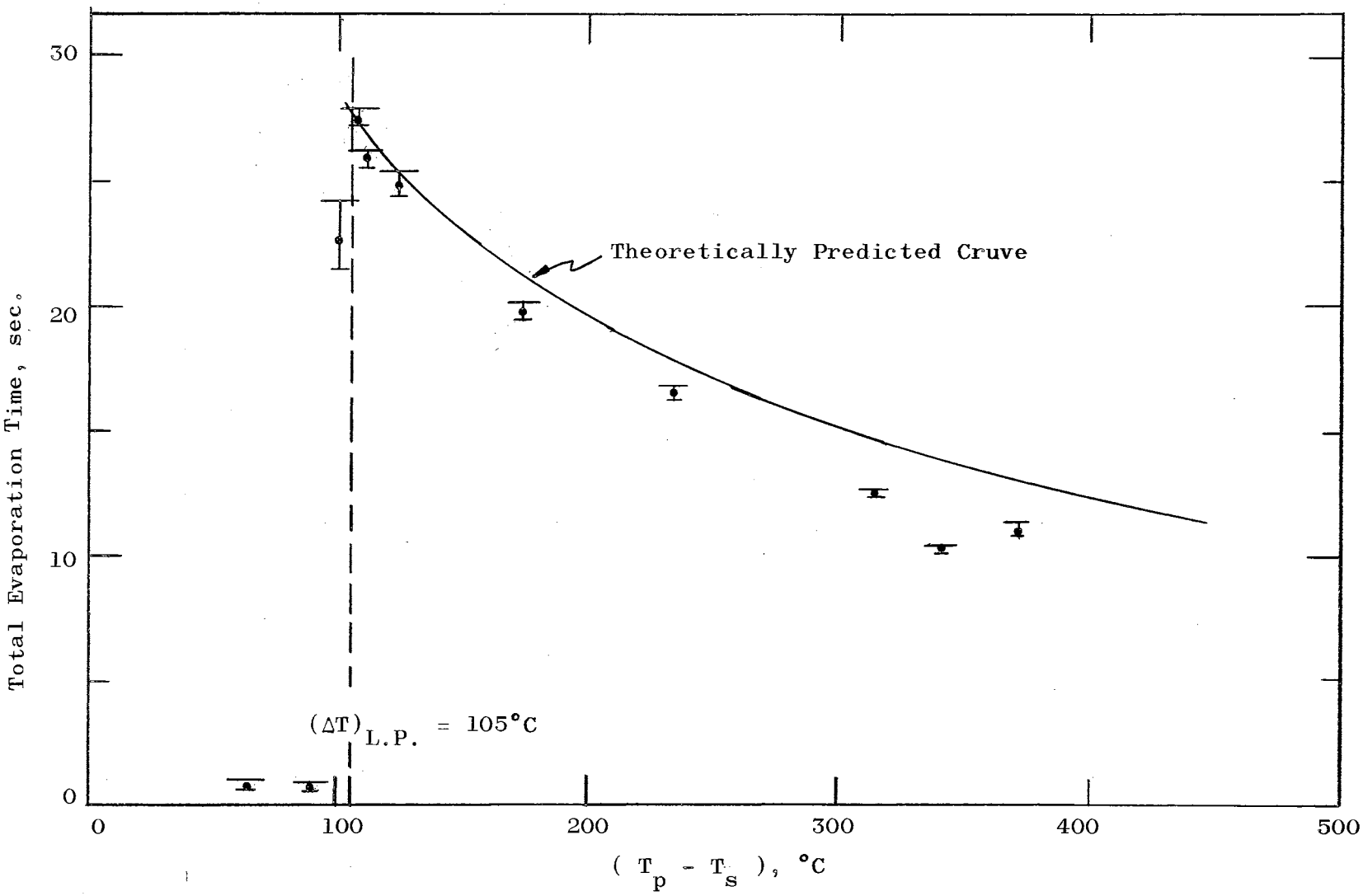

Figure 12 Droplet Evaporation Time vs. ΔT for Benzene Droplets; V_o = 0.01176 ml.

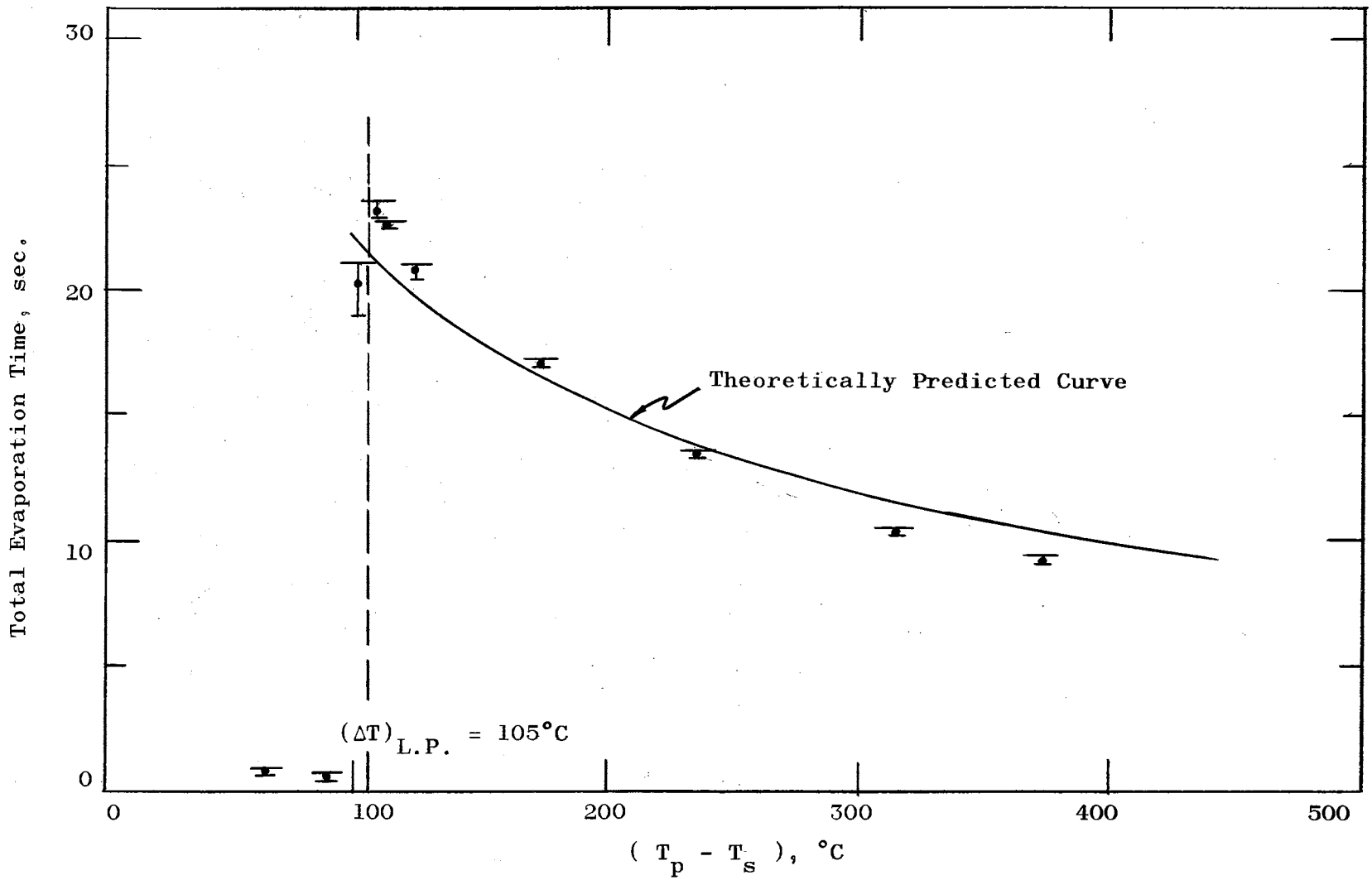

Figure 13 Droplet Evaporation Time vs. ΔT for Benzene Droplets; V_o = 0.00748 ml.

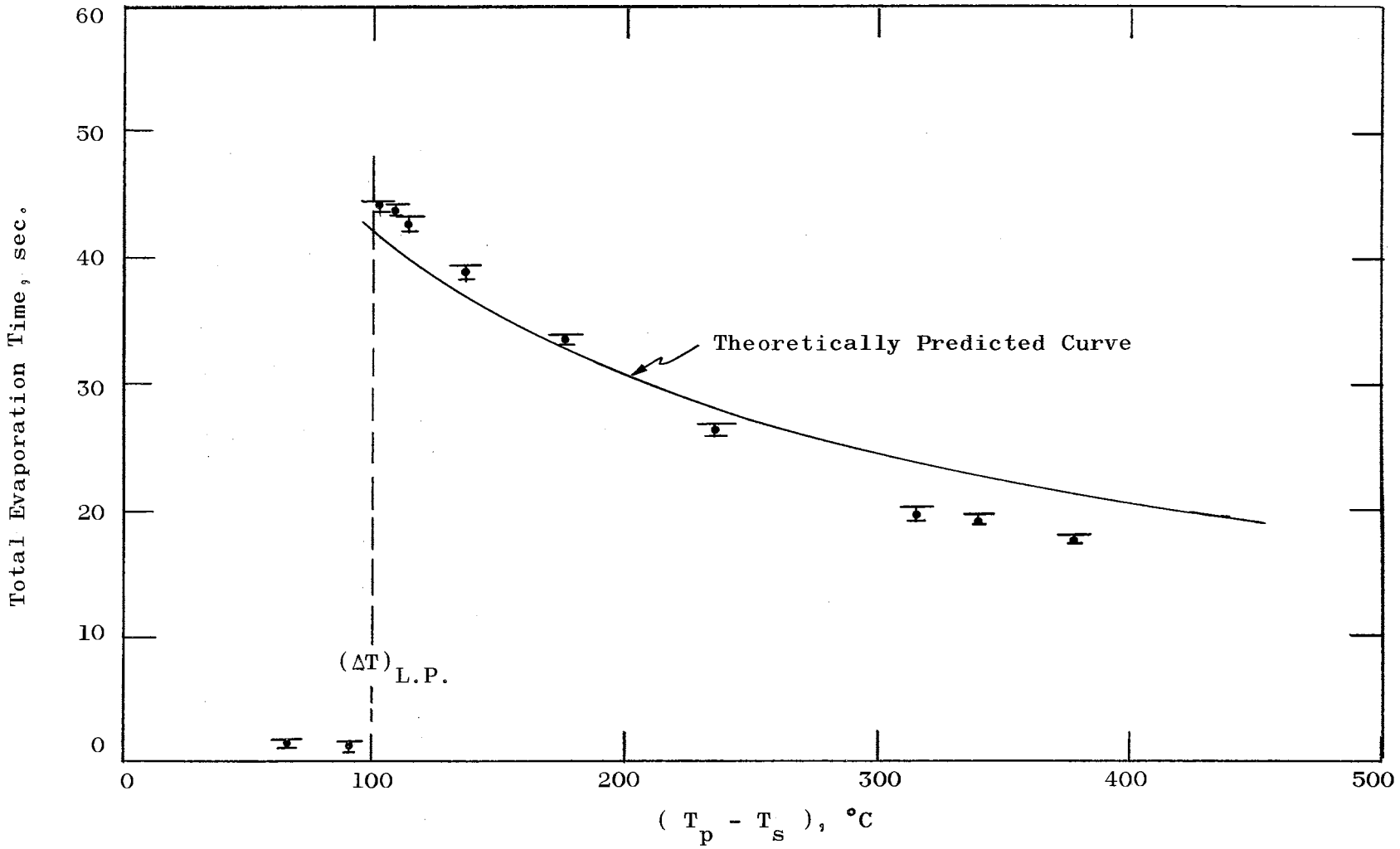
Total Evaporation Time, sec.
60
50
40
30
20
10
0
0
100
200
300
400
500
(T_p - T_s), °C
$(\Delta T)_{L.P.}$
Theoretically Predicted Curve

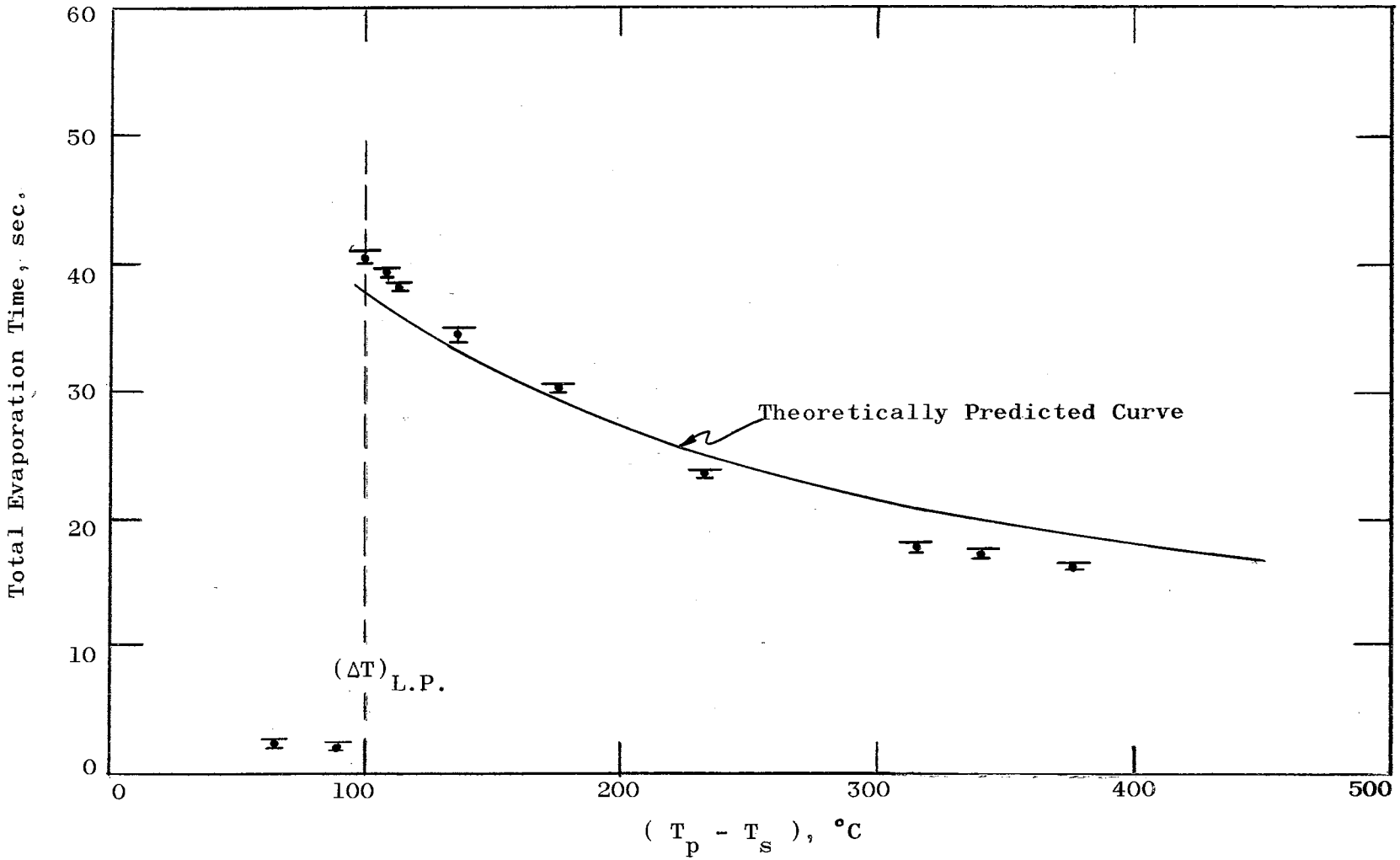

Figure 15 Droplet Evaporation Time vs. ΔT for Ethanol Droplets; V_o = 0.01100 ml.

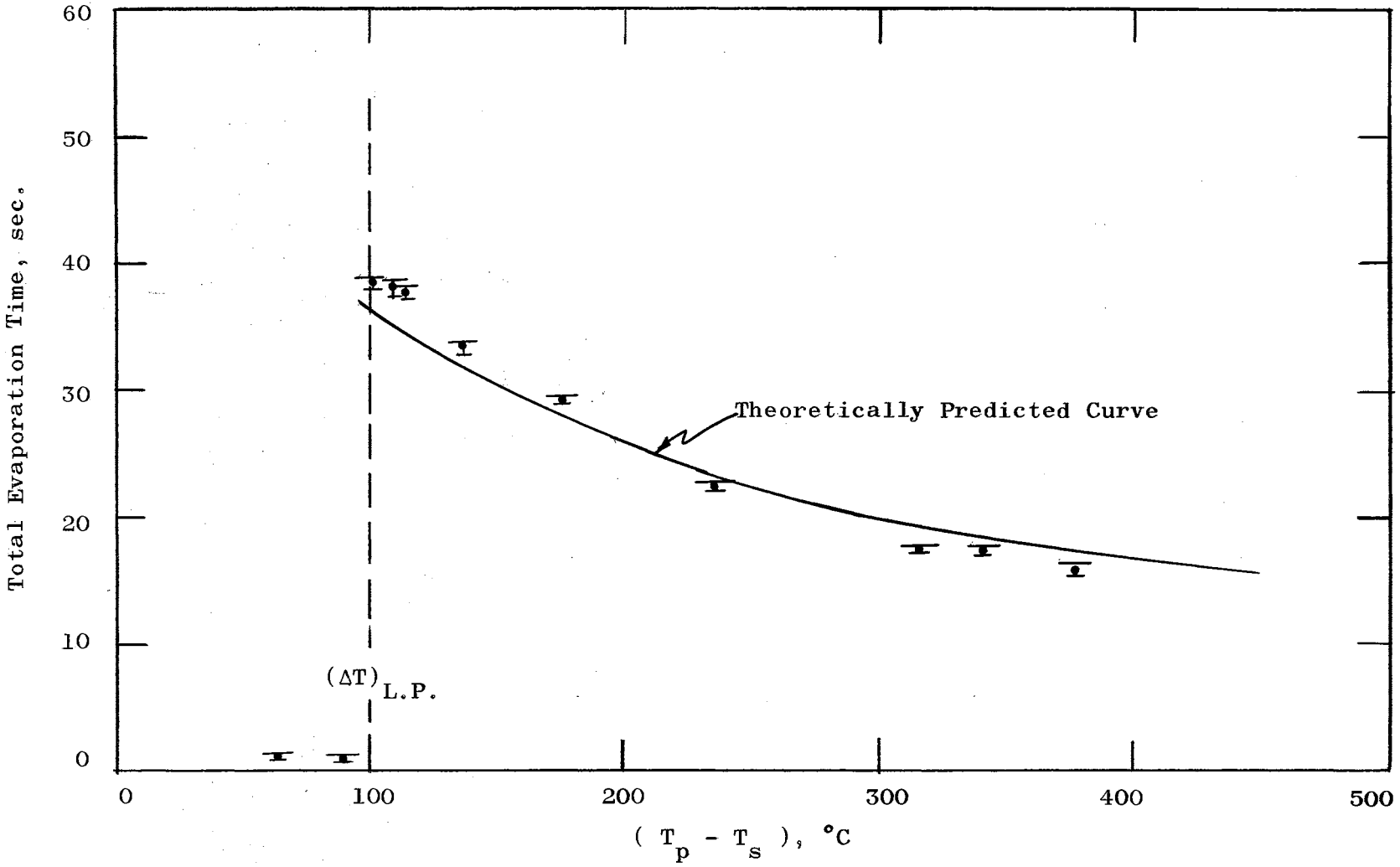

Figure 16 Droplet Evaporation Time vs. ΔT for Ethanol Droplets; V_o = 0.00979 ml.

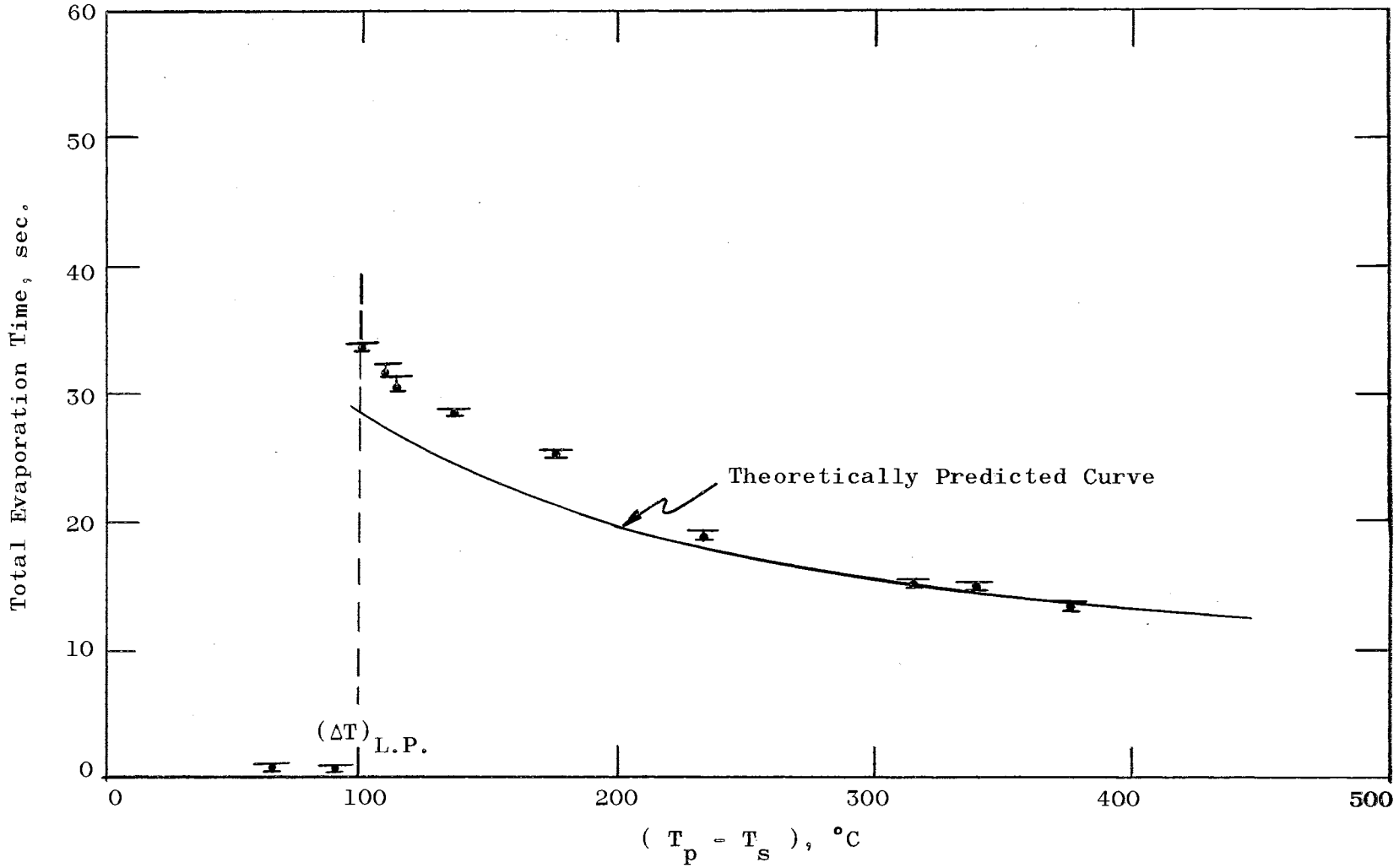

Figure 17 Droplet Evaporation Time vs. ΔT for Ethanol Droplets; V_o = 0.00621 ml.

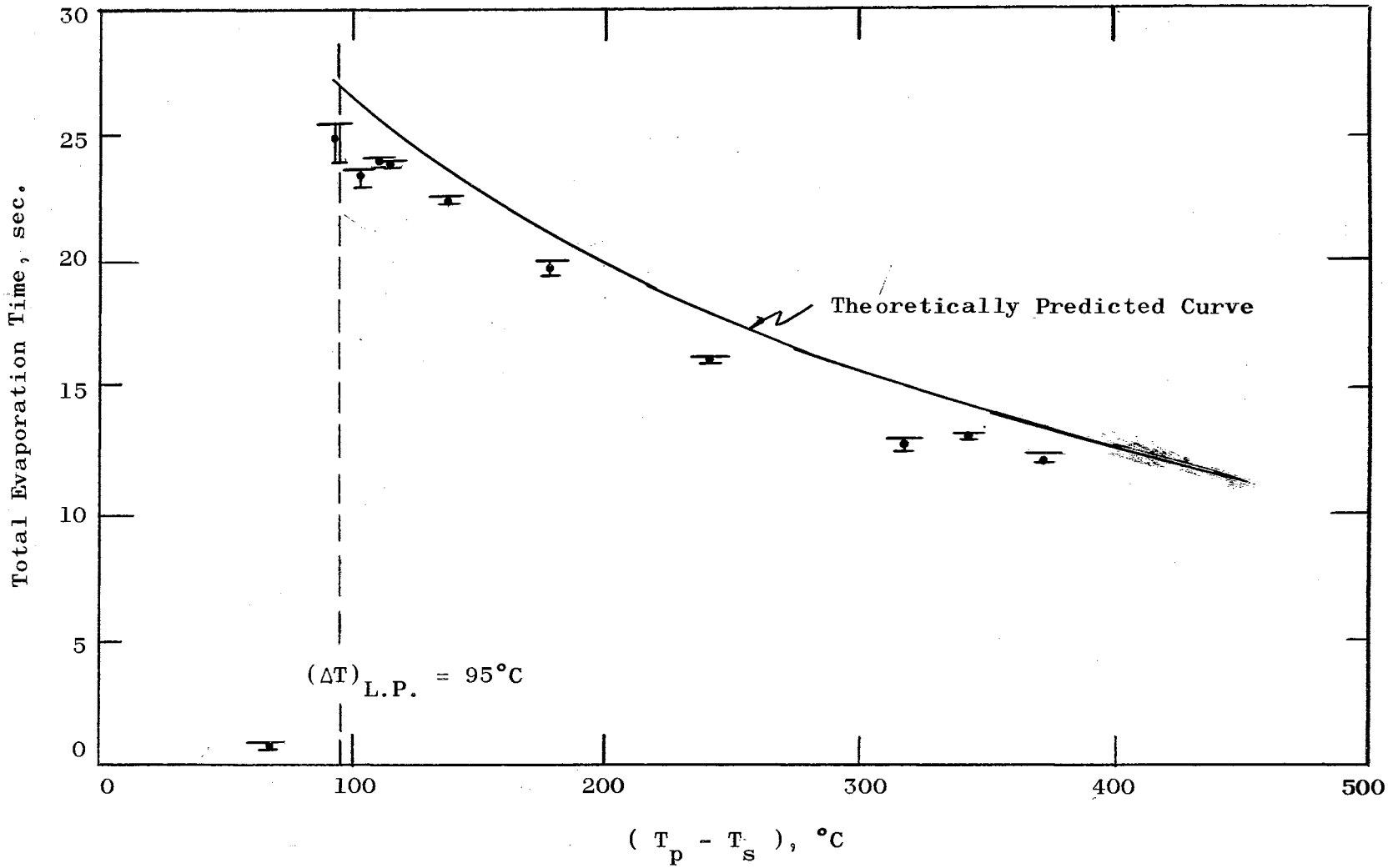

Figure 18 Droplet Evaporation Time vs. ΔT for Carbon-tetrachloride Droplets; V_o = 0.00803 ml.

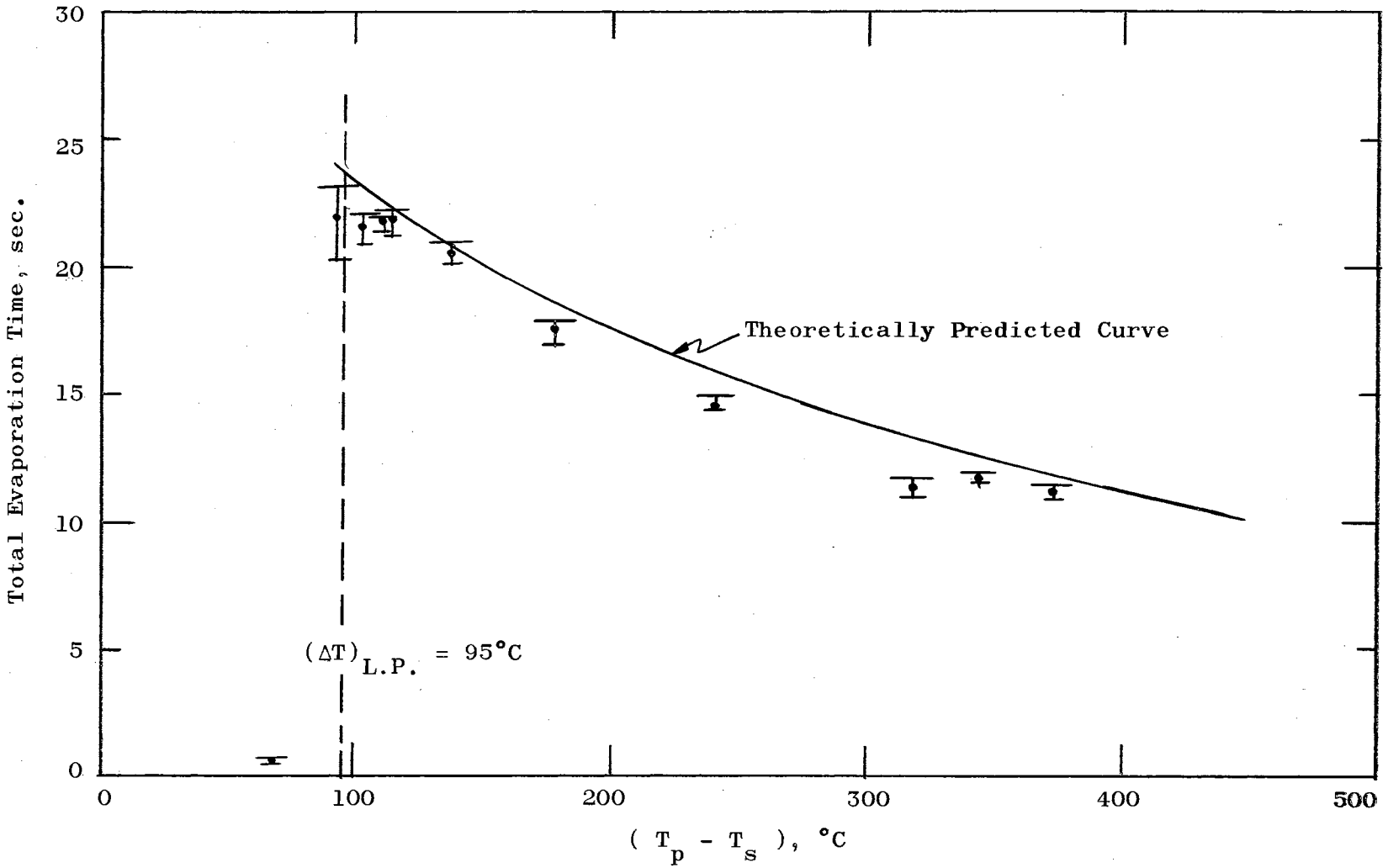

Figure 19 Droplet Evaporation Time vs. ΔT for Carbon-tetrachloride Droplets; V_o = 0.00627 ml.

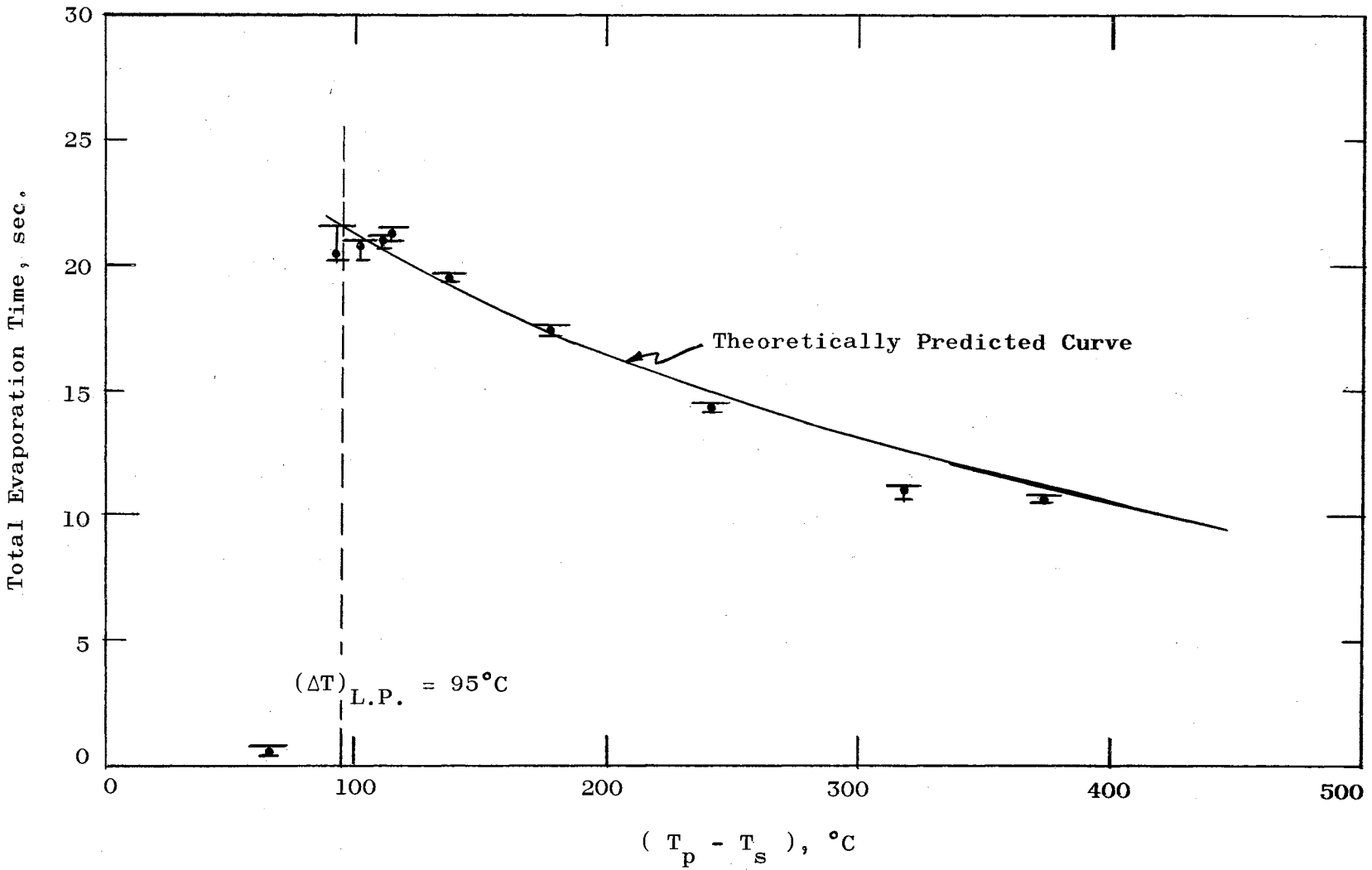

Figure 20 Droplet Evaporation Time vs. ΔT for Carbon-tetrachloride Droplets; V_o = 0.00564 ml.

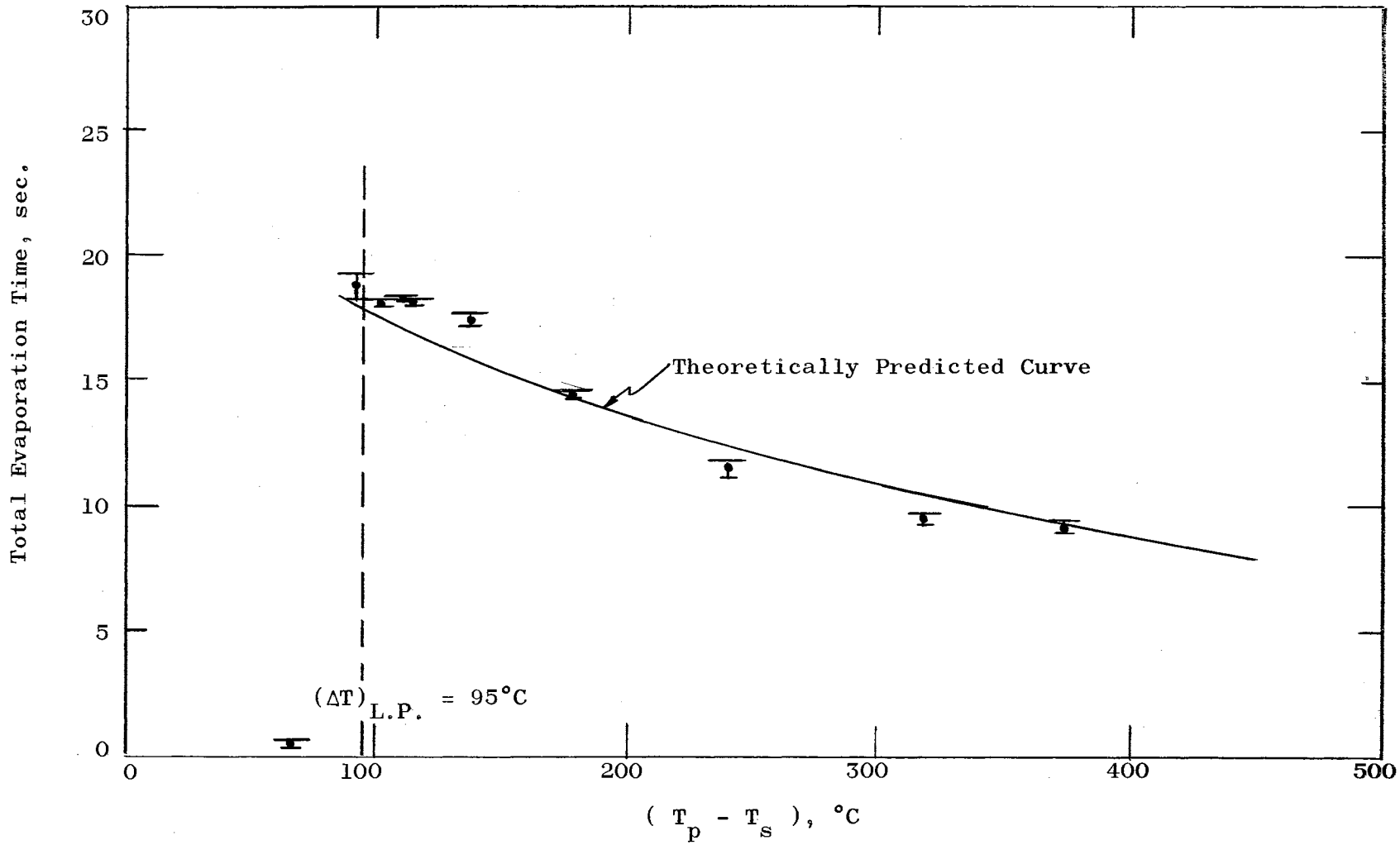

Figure 21 Droplet Evaporation Time vs. ΔT for Carbon-tetrachloride Droplets; V_o = 0.00394 ml.

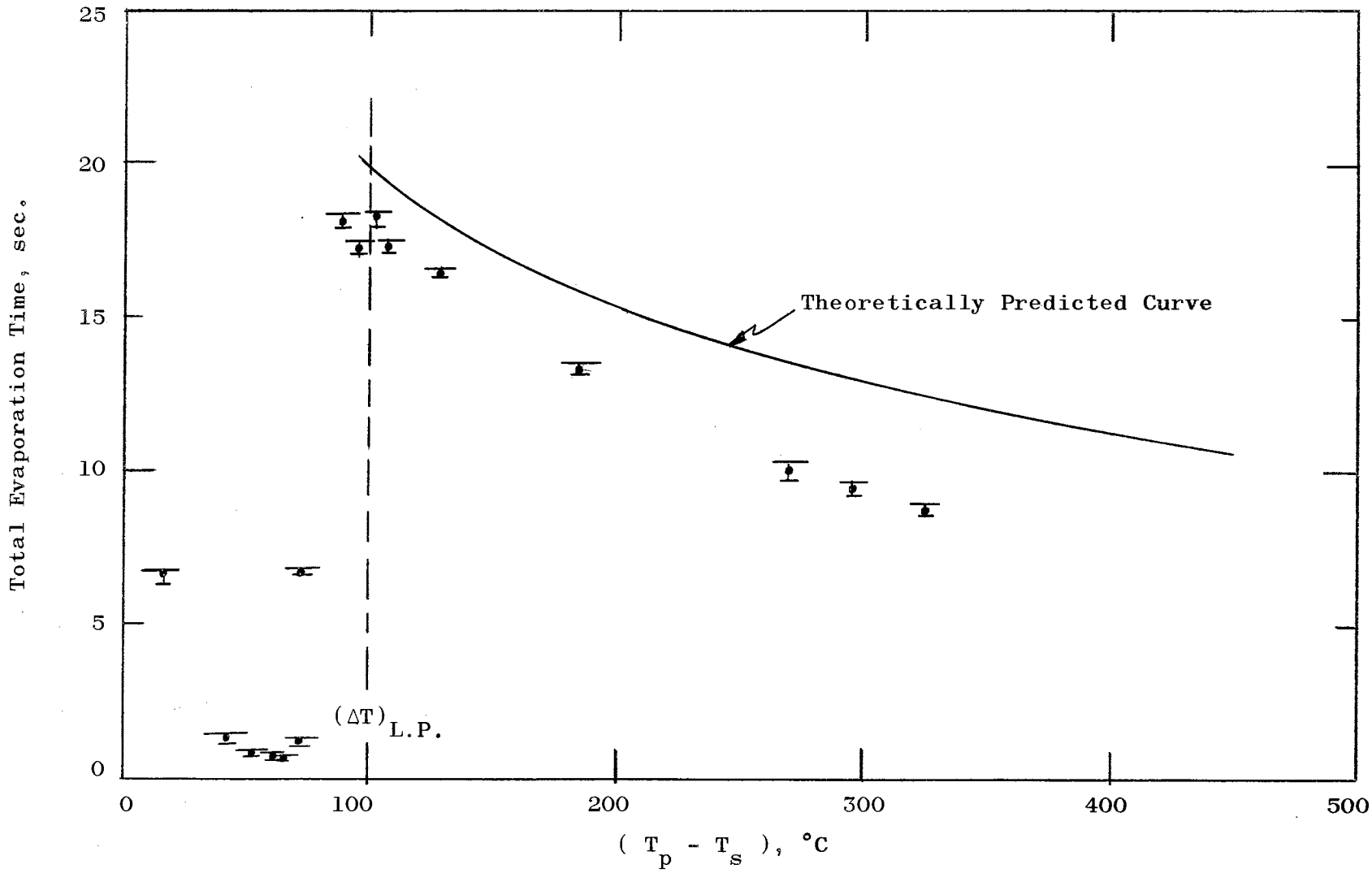

Figure 22 Droplet Evaporation Time vs. ΔT for N-Octane Droplet; V_o = 0.01683 ml.

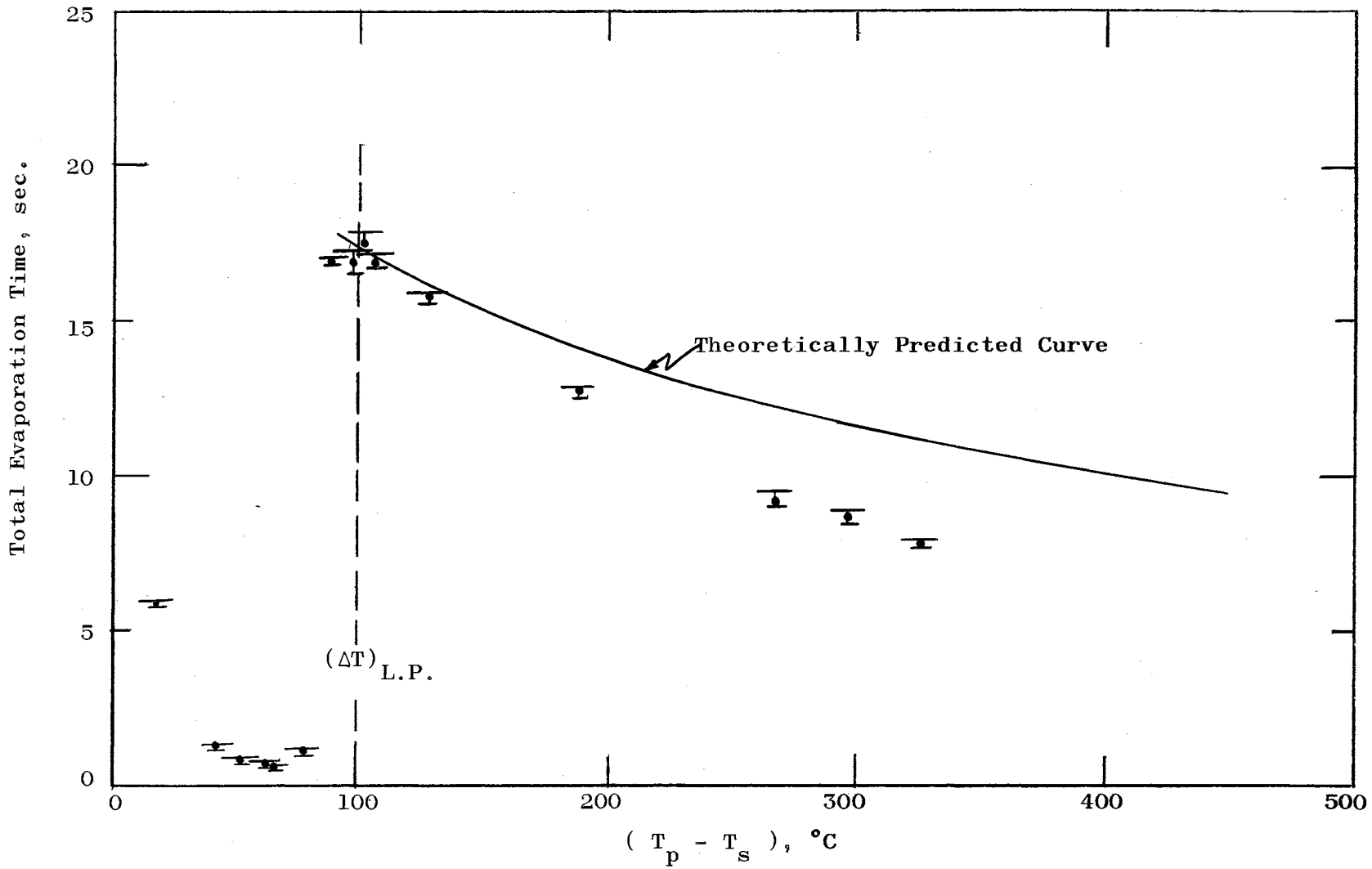

Figure 23 Droplet Evaporation Time vs. ΔT for N-Octane Droplet; V_o = 0.01327 ml.

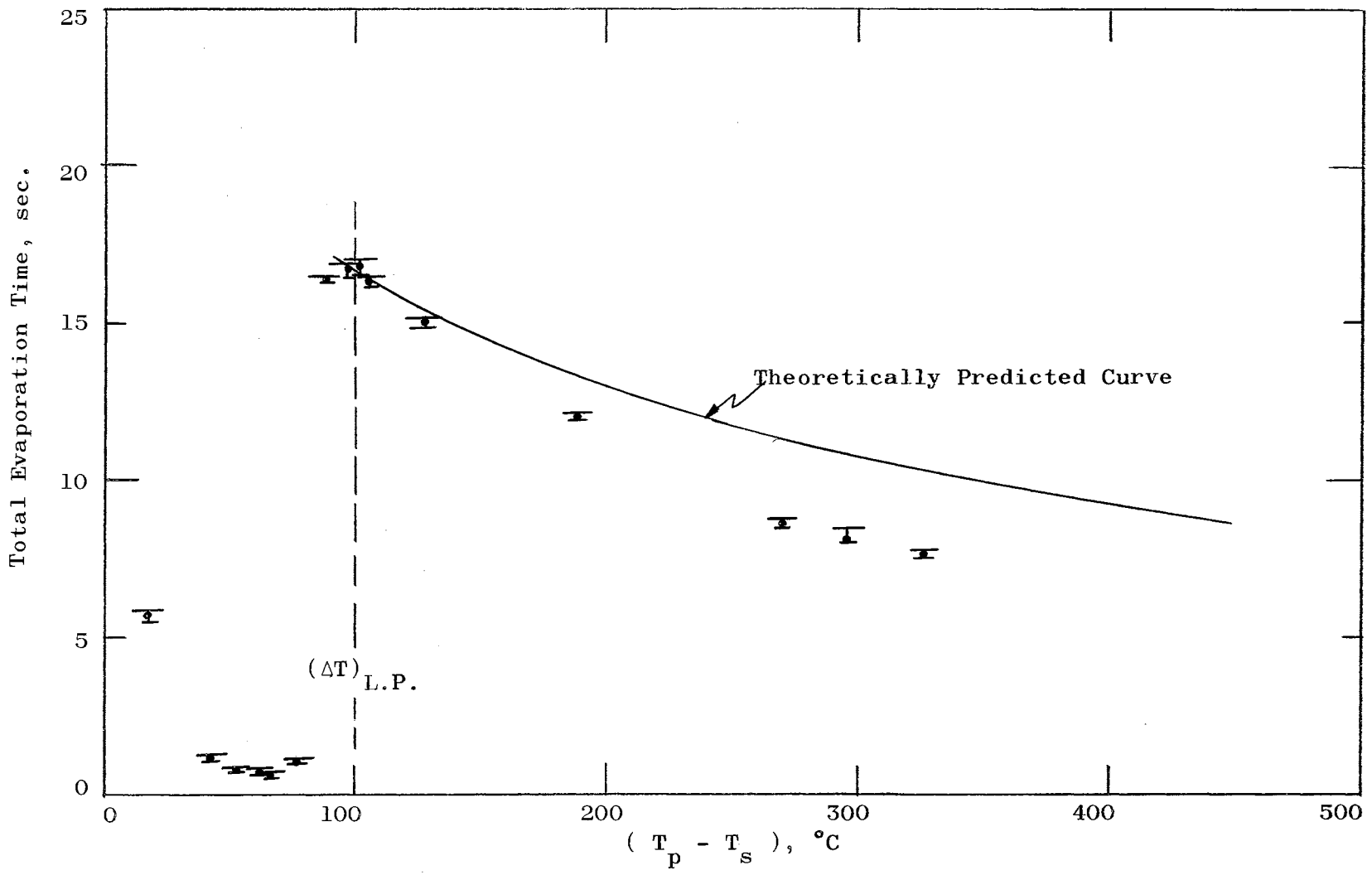

Figure 24 Droplet Evaporation Time vs. ΔT for N-Octane Droplet; V_o = 0.01266 ml.

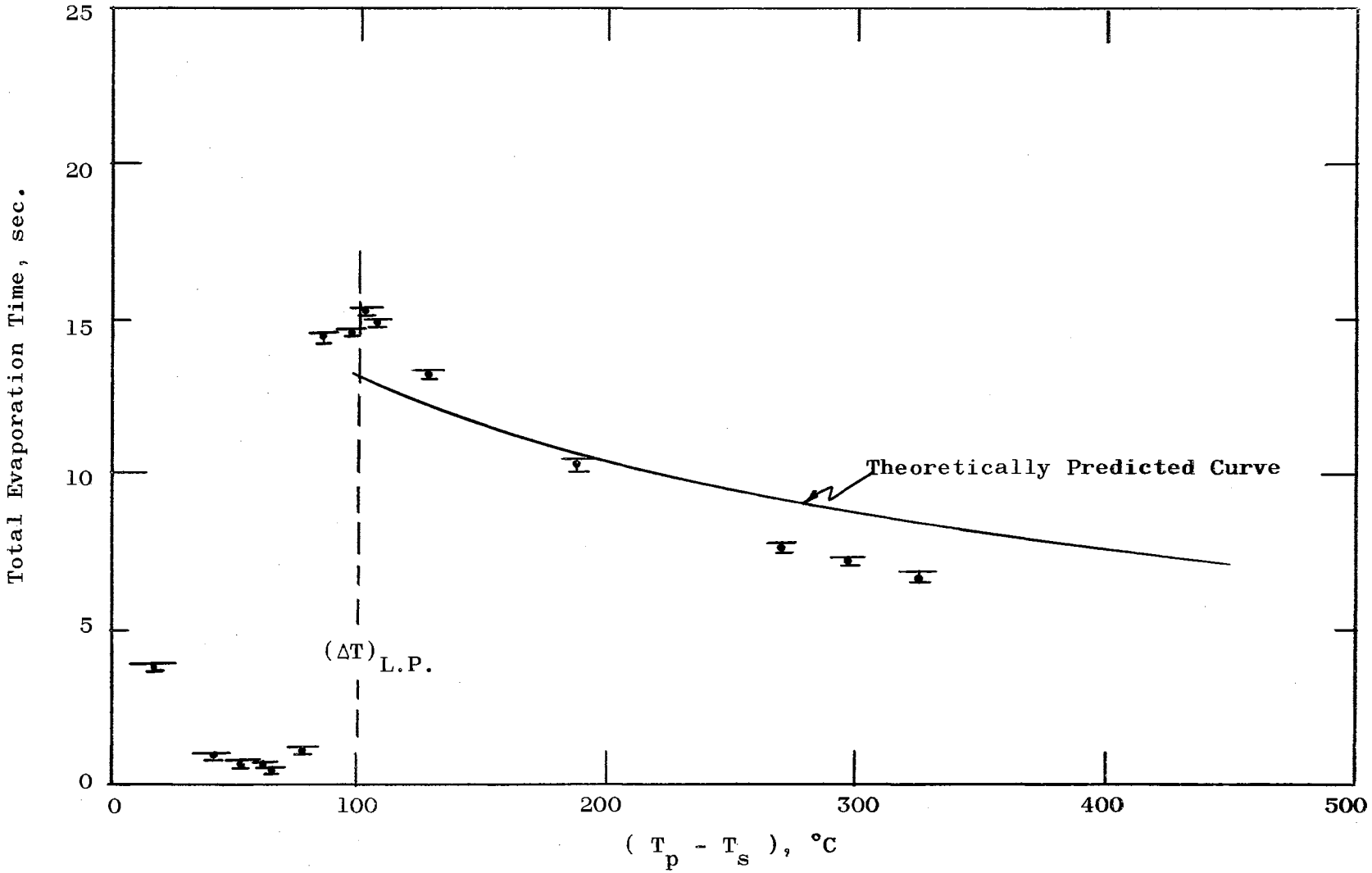

Figure 25 Droplet Evaporation Time vs. ΔT for N-Octane Droplet; V_o = 0.00824 ml.

predicted curves and experimental data points. The weakest agreement appears in the case of normal octane at higher plate temperatures.

The theoretical curve in Figures 10 through 25 for organic liquids seems to overpredict the total droplet evaporation time. Especially, for n-octane, the worst case gives a 30 percent overprediction over the experimental data points. Possible explanations of the discrepancy between experimental and the theoretical model in these cases are many; n-octane and ethyl alcohol have lower surface tension; therefore, the droplets of these liquids may not be spherical in shape. The theoretical model assumes a perfect spherical configuration (more discussion will be found in a later paragraph).

The thermal decomposition or oxidation of organic vapors at higher plate temperatures, although not clearly established, may also be a possible explanation of larger deviations between experiment and theory. For instance, the vapor film which separates the liquid droplet of n-octane from the heating plate during the evaporation process might well be the vapor of some lighter hydrocarbons such as methane or ethane. Marschener (18) in his study on thermal decomposition of n-octane, indicated that at temperatures between 200°C and 600°C, stainless steel apparatus which had been in continuous use for an extended period gave products which contained abnormally large amounts of methane. The thermal conductivity of methane vapor is much higher than the thermal conductivity of n-octane vapor, e.g., at 400°C, the thermal conductivity of methane vapor is about 0.000152 (cal/sec,

cm, °C) as compared to 0.000087 (cal/sec, cm, °C) for the n-octane vapors. If we consider that the vapor generated from the bottom of a 0.02 cc. n-octane droplet, has been decomposed into methane vapor (about 0.003 gm. as calculated from the vapor film thickness), it would require approximately 0.189 cal. of endothermic heat of reaction (about 63 cal/gm) in addition to the total latent heat of 0.772 cal. (71 cal/gm x 0.02 cm^3 x 0.5445 gm/cm^3) in order for the vaporization to take place. That is an increase of about 25 percent in the total heat load; but at the same time, there is an increase of about 75 percent in the heat conductivity for the conducting vapors (methane vs. n-octane). If we consider that the heat transfer due to conduction through the vapor film accounts for about 60 percent of the overall heat transfer, (as it is the case for water at 400°C, see Figure 35) about 20 percent overprediction in the total evaporation time for the n-octane droplet at higher temperatures may be expected. One experimental evidence of the thermal decomposition of n-octane was a change of vapor odor during the process of droplet evaporation at higher temperatures.

Another test for evaluating the theoretical model is found in the comparison of the photographic data on the instantaneous droplet size and the theoretically predicted values. The instantaneous radii from photographic measurements are presented in Table F-2 and plotted in Figures 26 through 33. The solid points represent the average experimental data obtained from direct microscopic measurements on the film slides. The uncertainties of these measurements are indicated by two bars which give the

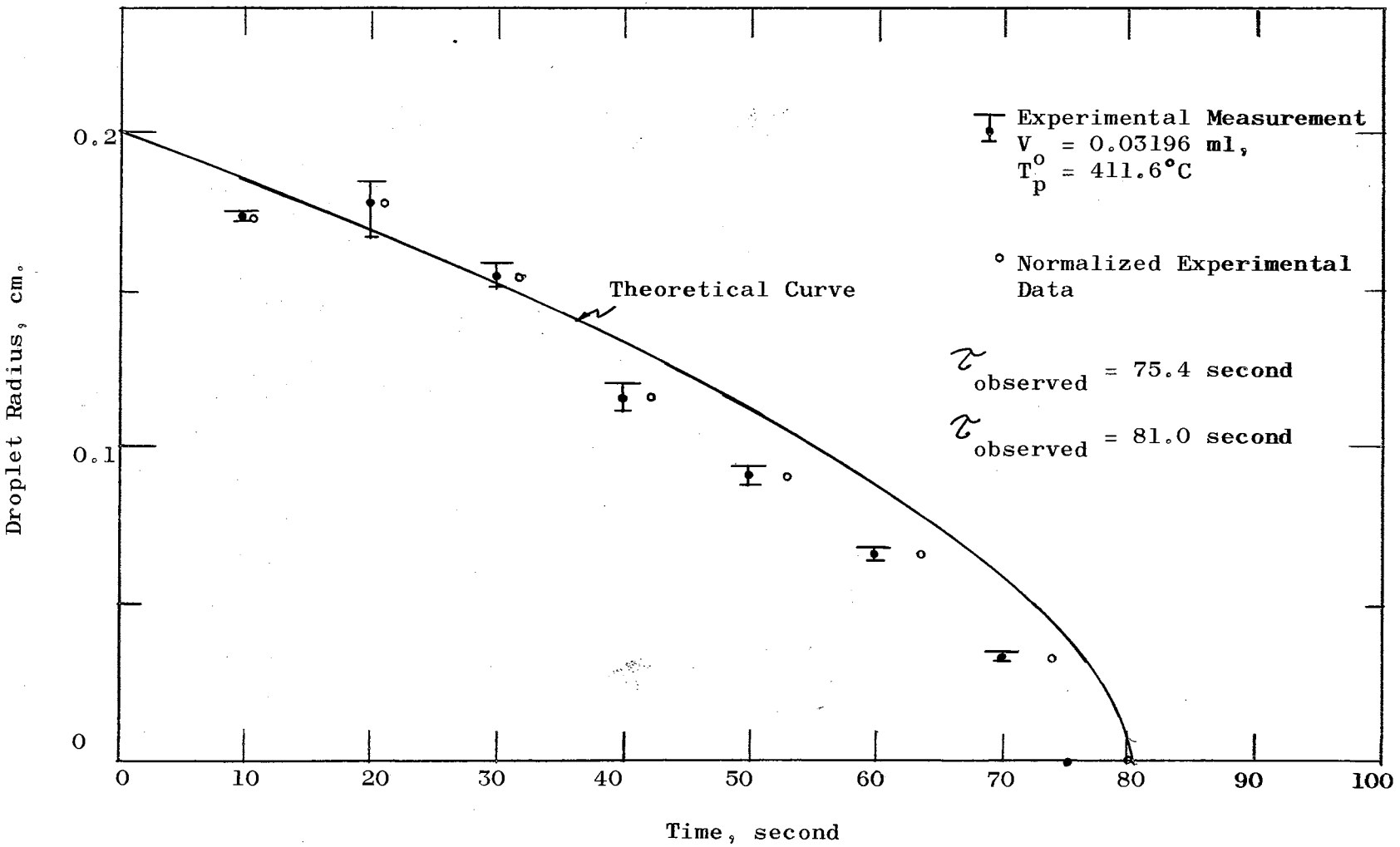

Figure 26 Droplet Radius vs. Time, Water Droplet

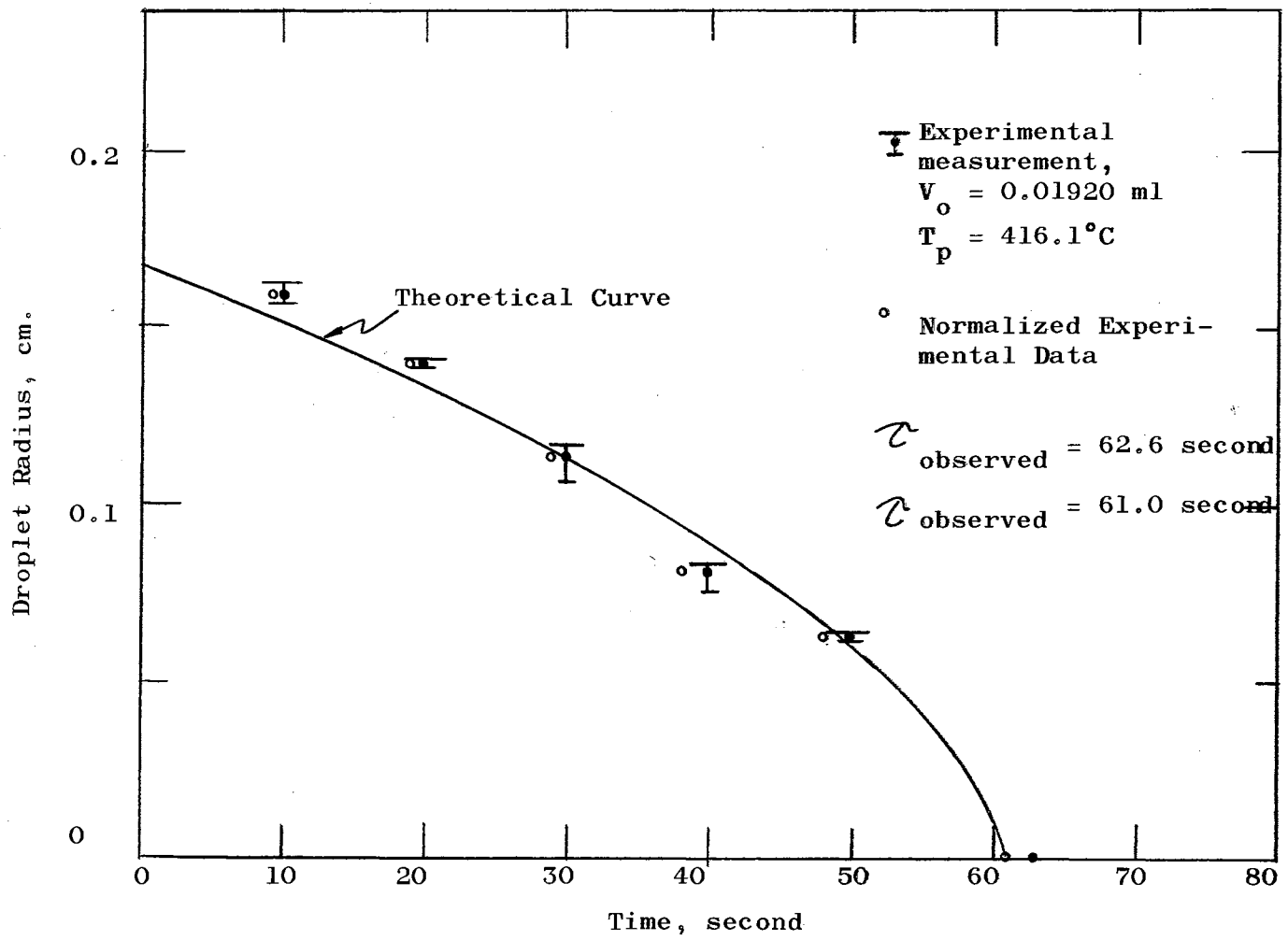

Figure 27 Droplet Radius vs. Time, Water Droplet

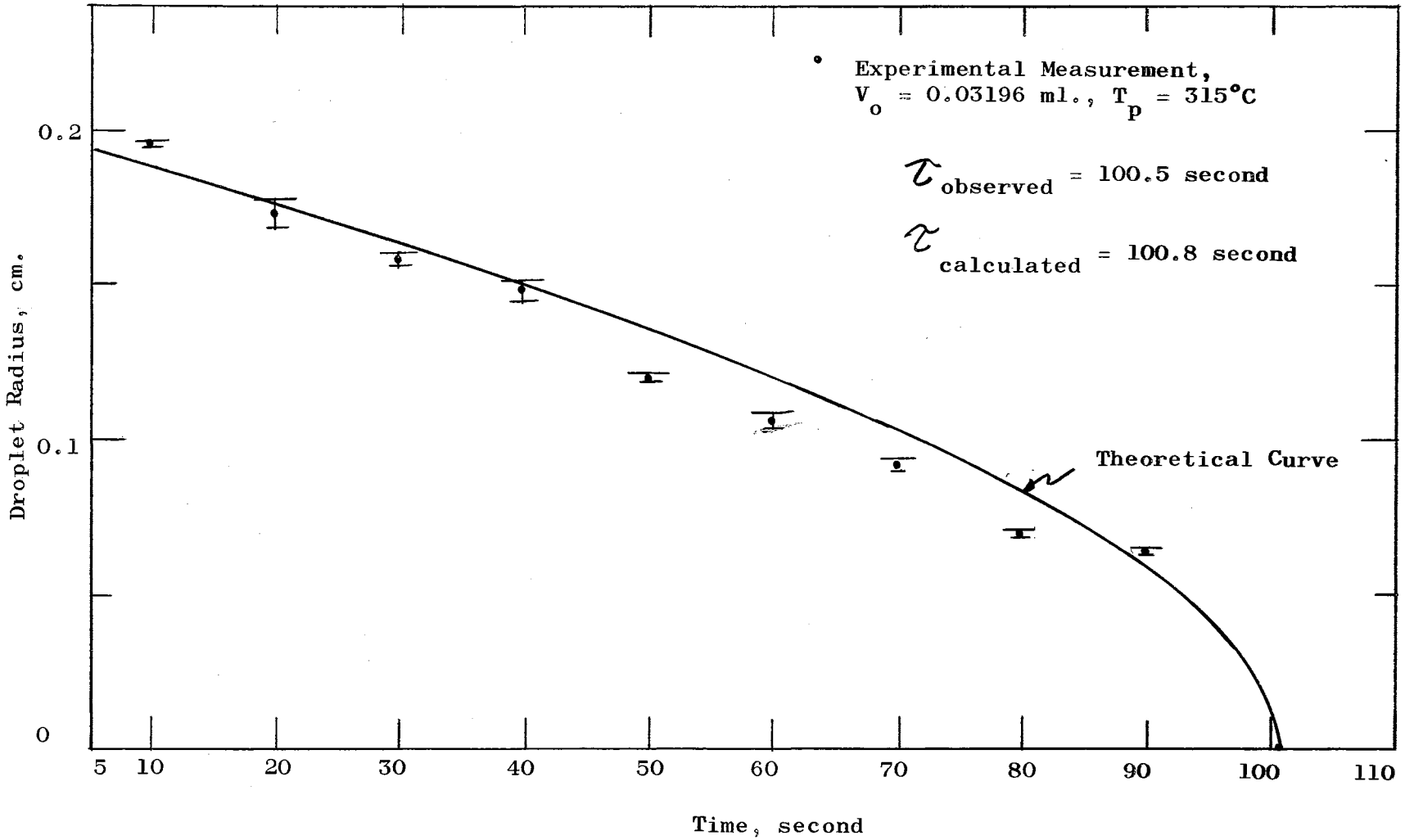

Figure 28 Droplet Radius vs. Time, Water Droplet

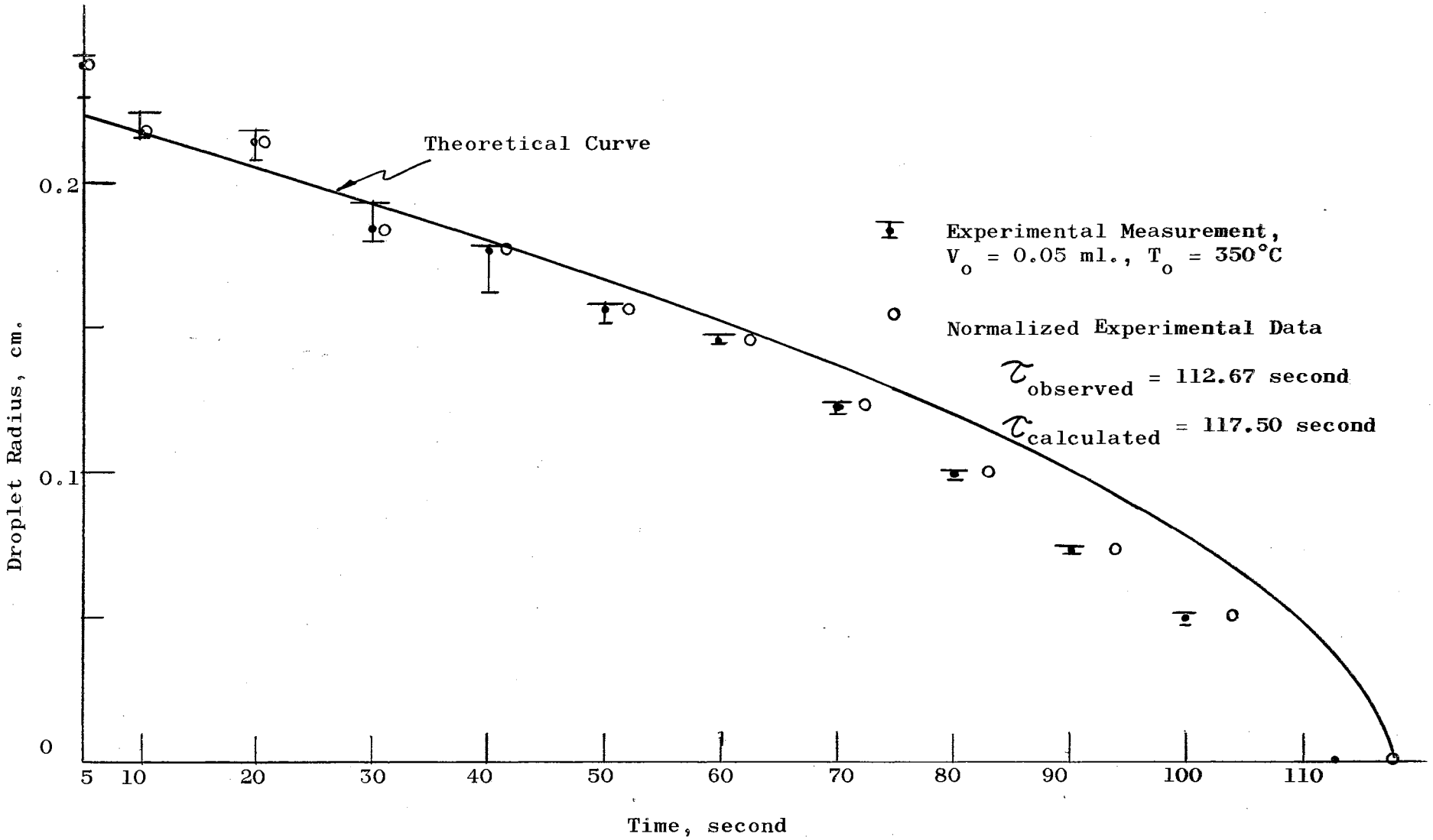

Figure 29 Droplet Radius vs. Time, Water Droplet

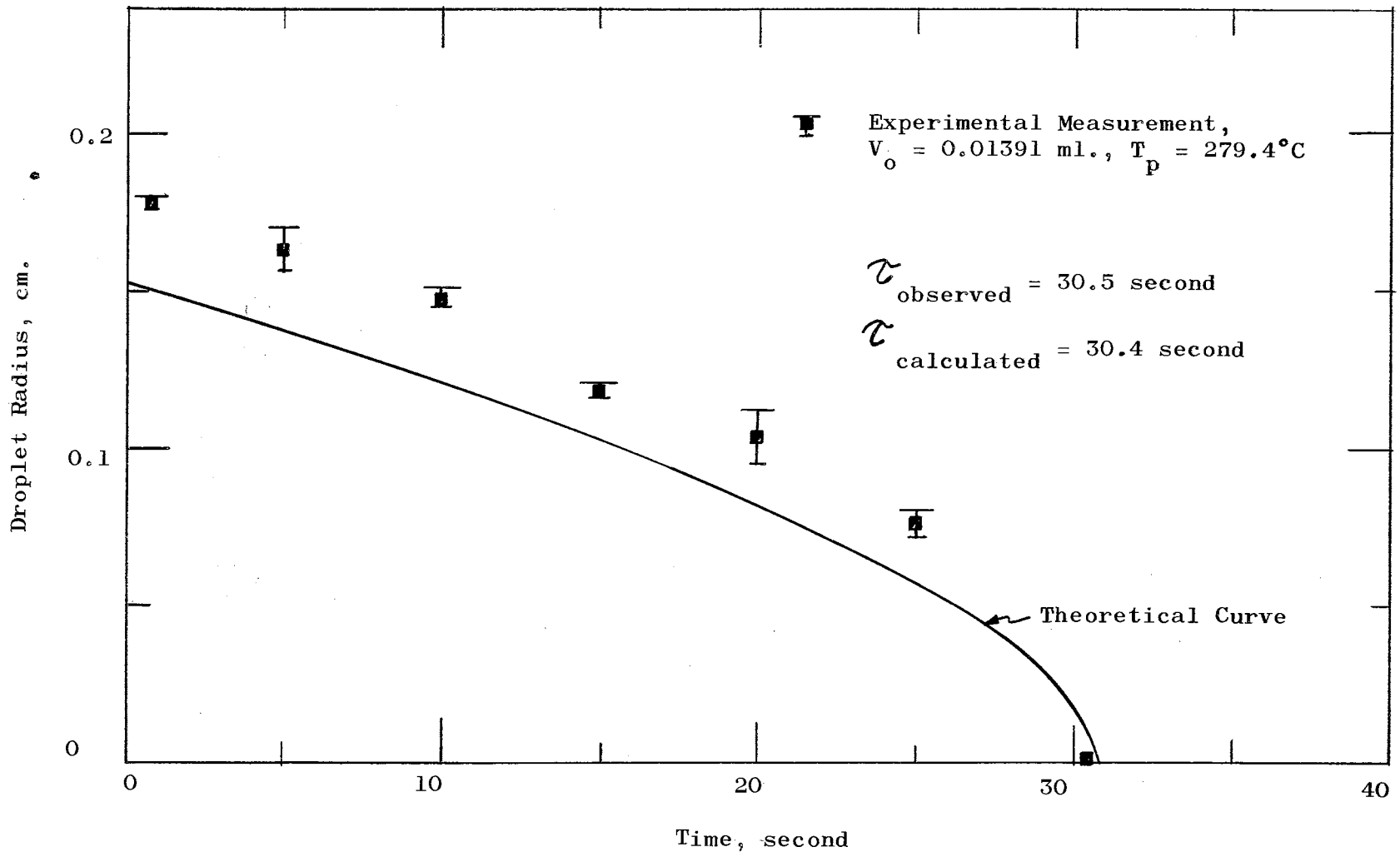

Figure 30 Droplet Radius vs. Time, Ethanol Droplet

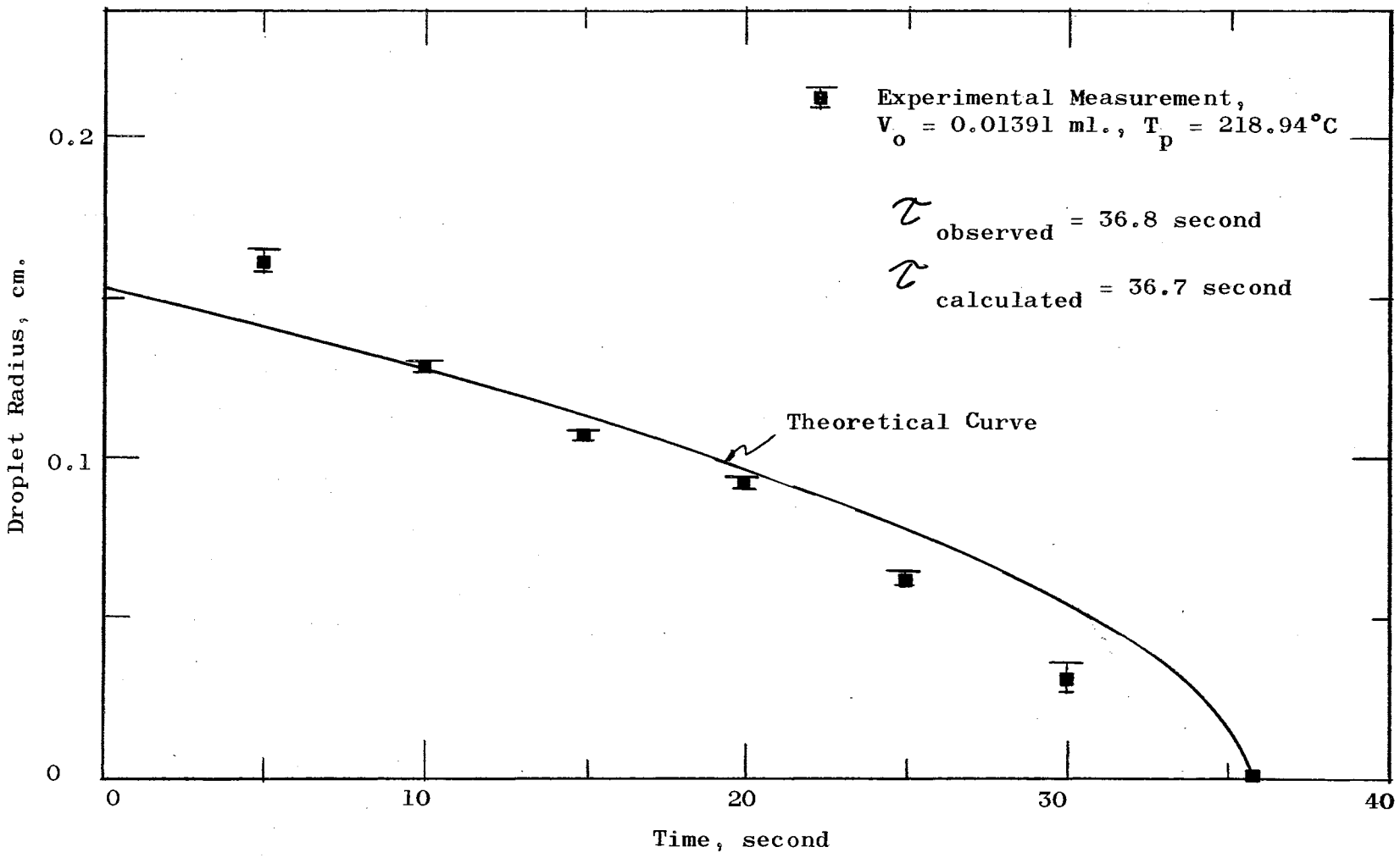

Figure 31 Droplet Radius vs. Time, Ethanol Droplet

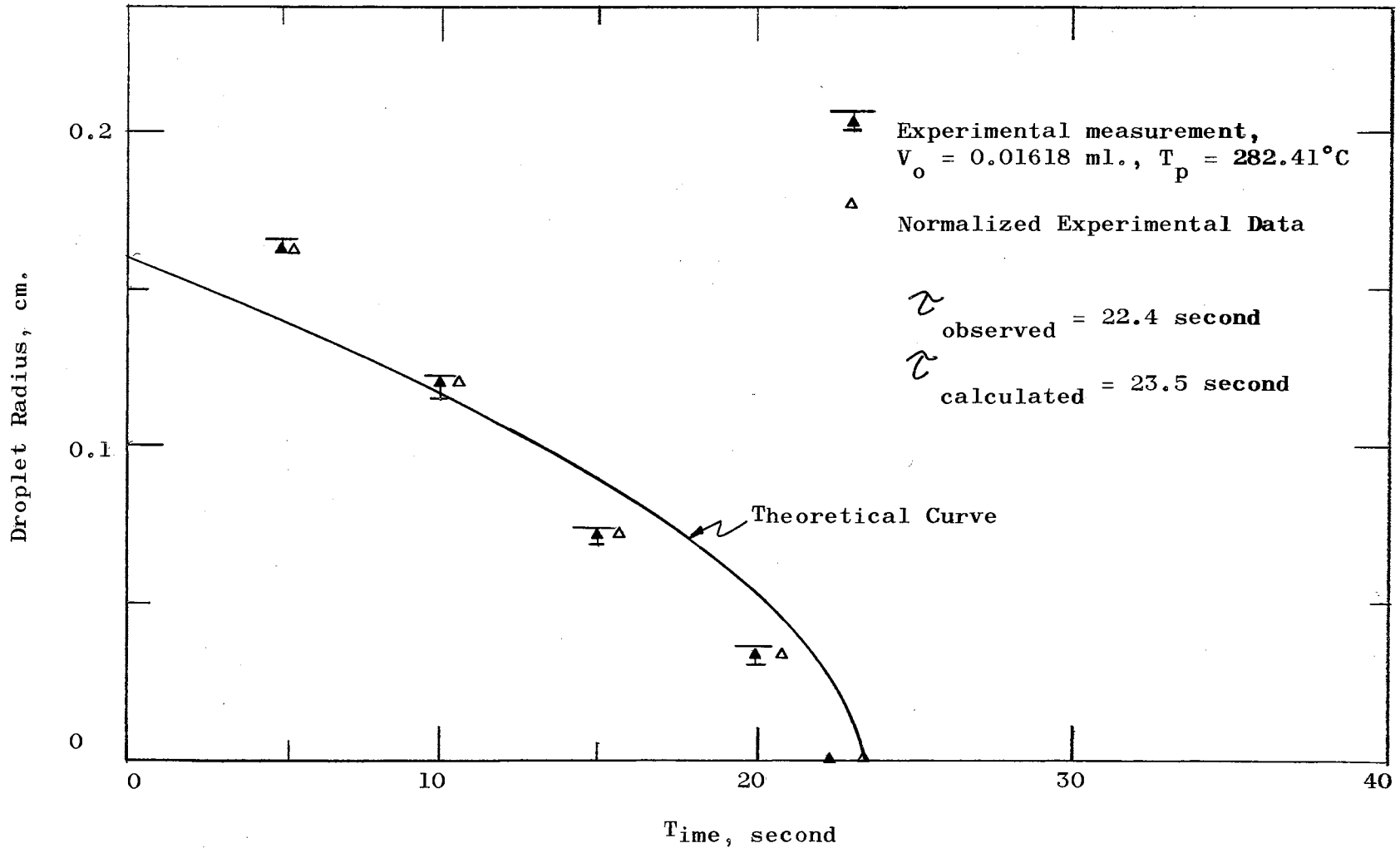

Figure 32 Droplet Radius vs. Time, Benzene Droplet

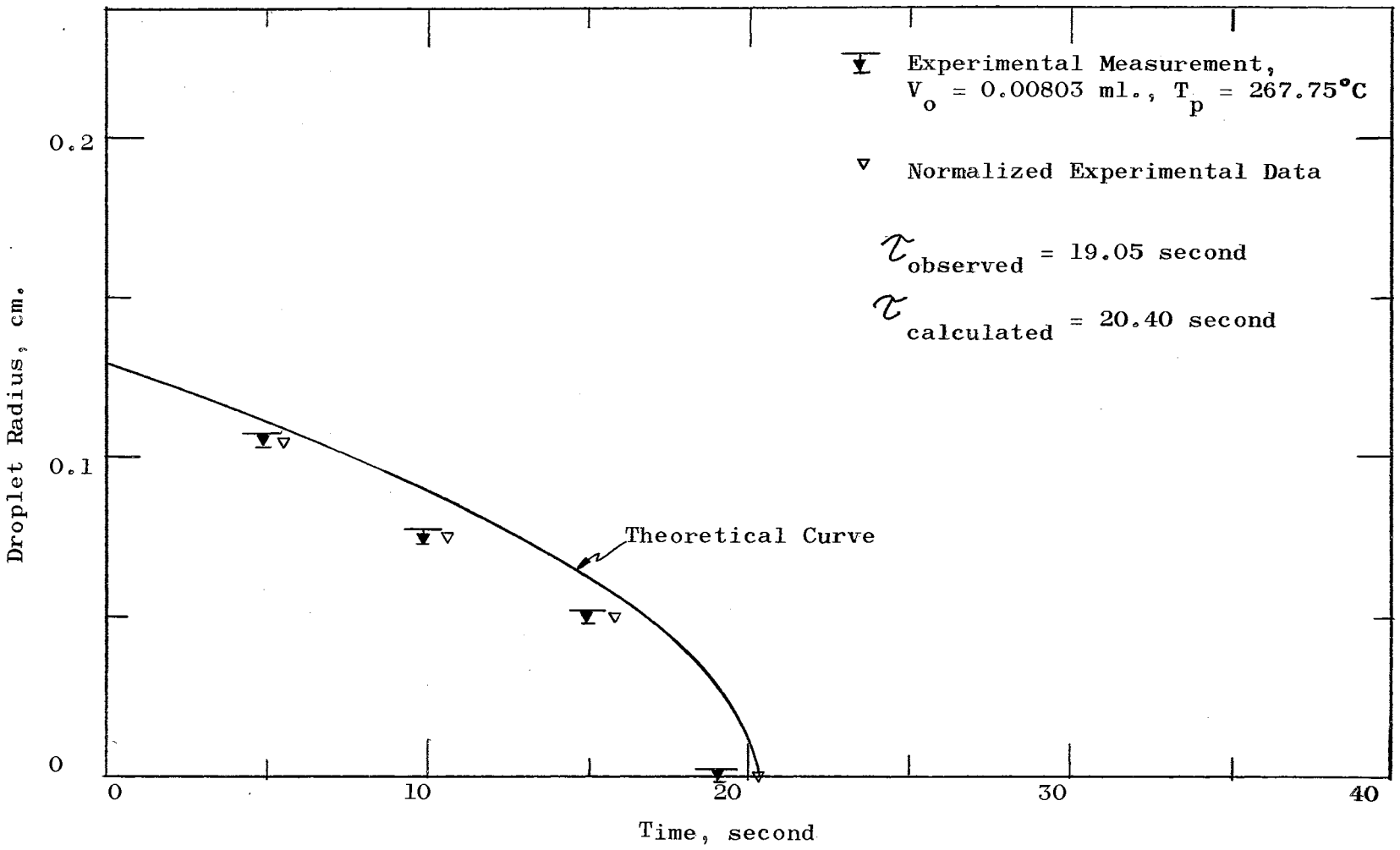

Figure 33 Droplet Radius vs. Time, Carbon-tetrachloride

range of variation. The maximum range of variation is ± 5 percent; and in most cases, it is less than ± 2 percent. The open points in Figures 26 through 33 are the experimental values corrected on the time axis by the ratio of the theoretically predicted evaporation time over the experimental droplet evaporation time. Very good agreement between the theoretical curves and the experimental values for the droplet radius is shown for the case of water in Figures 26 through 28. The maximum deviation of an experimental diameter from the theoretical curve is found to be about 30 percent in the case of water of V_o = 0.05 ml. and at a plate temperature of 350°C. Figures 30 through 33 are similar plots for droplet radius history with organic liquids. With the available still-camera set-up, the shortest interval for studying the history of droplet radius was about 5 seconds. Therefore, only a few experimental points were obtained with organic liquids, which have shorter droplet lifetime.

In general, the theory seems to underpredict the instantaneous droplet radius in the beginning period of evaporation when the droplet size is large, and to overpredict when the droplet has nearly disappeared. The average deviation of the experimental points from the theoretical curves is about ± 5 percent.

The previous evaluation of the theoretical model was made on the basis that all assumptions made in constructing the model were valid. Many of these, however, must be justified. First of all, the assumption that the droplet remains a perfect sphere in the process of evaporation may be questioned. The deviation from sphericity does indeed exist for the larger droplets of liquid

used in this study. Bashforth and Adams (1) described the droplet shape as a function of its volume, density, and surface tension and constructed a table to indicate the degree of deviation from sphericity by using the dimensionless group ($\rho_L g R_o^2/\sigma$) as parameter. The deviation from sphericity is indicated by the ratio of the major and minor radius. (For a perfect sphere, this ratio should be unity.) According to this table in Bashforth and Adams' work, the dimensionless group ($\rho_L g R_o^2/\sigma$) must be equal to or less than 0.57 in order to have an essential sphericity (i.e., the ratio of the major axis to the minor axis is less than 1.10). The following table presents the dimensionless criteria for all the liquids and droplet sizes used in this study.

TABLE I

DIMENSION CRITERION FOR DROPLET SPHERICITY

Liquid	Droplet volume ml.	$\frac{g\rho_L R_o^2}{\sigma}$
CCl_4	0.00803	1.1603
	0.00627	0.9183
	0.00394	0.7213
C_2H_5OH	0.01391	0.9663
	0.01100	0.7610
	0.00621	0.5606
C_6H_6	0.01618	0.9673
	0.01343	0.7840
	0.00748	0.5792
H_2O	0.03196	0.6337
	0.02212	0.4498
	0.01540	0.3129
$n\text{-}C_8H_{18}$	0.01682	1.1956
	0.01266	0.9903
	0.00824	0.7428

From Table I, it is obvious that among the five liquids used in this study, water droplets are most spherical in shape. N-octane droplets, on the other hand, deviate most from the spherical assumption. The maximum deviation from sphericity is about 17 percent (i.e., the ratio between major and minor axis is 1.17) for the largest n-octane droplet.

The two-zone transport mechanism postulated in the theoretical development of Chapter V eliminates the uncertainity of the empirical parameter, X, which was introduced by Gottfried in his work (9). The integral analysis applied in solving the transport problems for the lower half of droplet is an improved procedure over Gottfried's trial-and-error approach. Starting with the geometrical configuration and the fundamental transport equations, the integral analysis gives the explicit functional dependence of W_1 on its controlling variables - Equation (32). The polynomial curve fit for the integral values in Equations (C1, C2, and C3) introduced less than 1 percent error between the curve fit and the values actually obtained by numerical integration, but it simplifies the overall computational scheme to a great extent.

The application of the modified Eulers' method in the numerical analysis is a successful procedure. The instantaneous droplet volume corresponding to a time interval converges to its correct value within two or three iterations in the beginning stage of evaporation, and within fifteen iterations near the end of evaporation. The maximum computing time on IBM 1410 was twenty minutes for the largest droplet lifetime; droplets which have an average droplet lifetime take about three minutes of machine computation

to obtain the droplet total evaporation time.

Figure 34 shows the heat flux history of water droplets at $\Delta T = 180°C$ and $\Delta T = 400°C$ as obtained from the theoretical computation. It is easily seem that at higher plate temperature, the radiative heat flux is about 60 percent of the conductive-convective heat flux, while at the lower plate temperature, the radiative heat flux is only about 30 percent of the conductive-convective heat flux.

A major area of uncertainty lies in the hypothesis for the diffusion mechanism occurring over the upper surface of the droplet. This mechanism is assumed to be a molecular diffusion process, independent of plate temperature. Although the effective diffusion coefficient has been assumed to be equal to the molecular diffusivity of liquid at its boiling point, it is indeed possible that this quantity varies with increasing plate temperature. Gottfried (9) has shown the effect of change in the values for diffusivity on his theoretical prediction of the evaporation time; a change of $\pm$ 20 percent in the diffusion coefficient results in a change in his analytical curves of about $\pm$ 15 percent.

The rates of evaporation per unit area from the lower and upper halves of the droplet, i.e., W_1/A_1 and W_2/A_2 are plotted as a function of time in Figure 35 for the cases of water droplet at 280°C and 500°C plate temperature respectively. It appears that at higher temperatures, the evaporation rate from the lower half of the droplet predominates over the molecular diffusion from the upper half of droplet; at lower plate temperatures, the evaporation due to molecular diffusion, W_2/A_2 becomes relatively

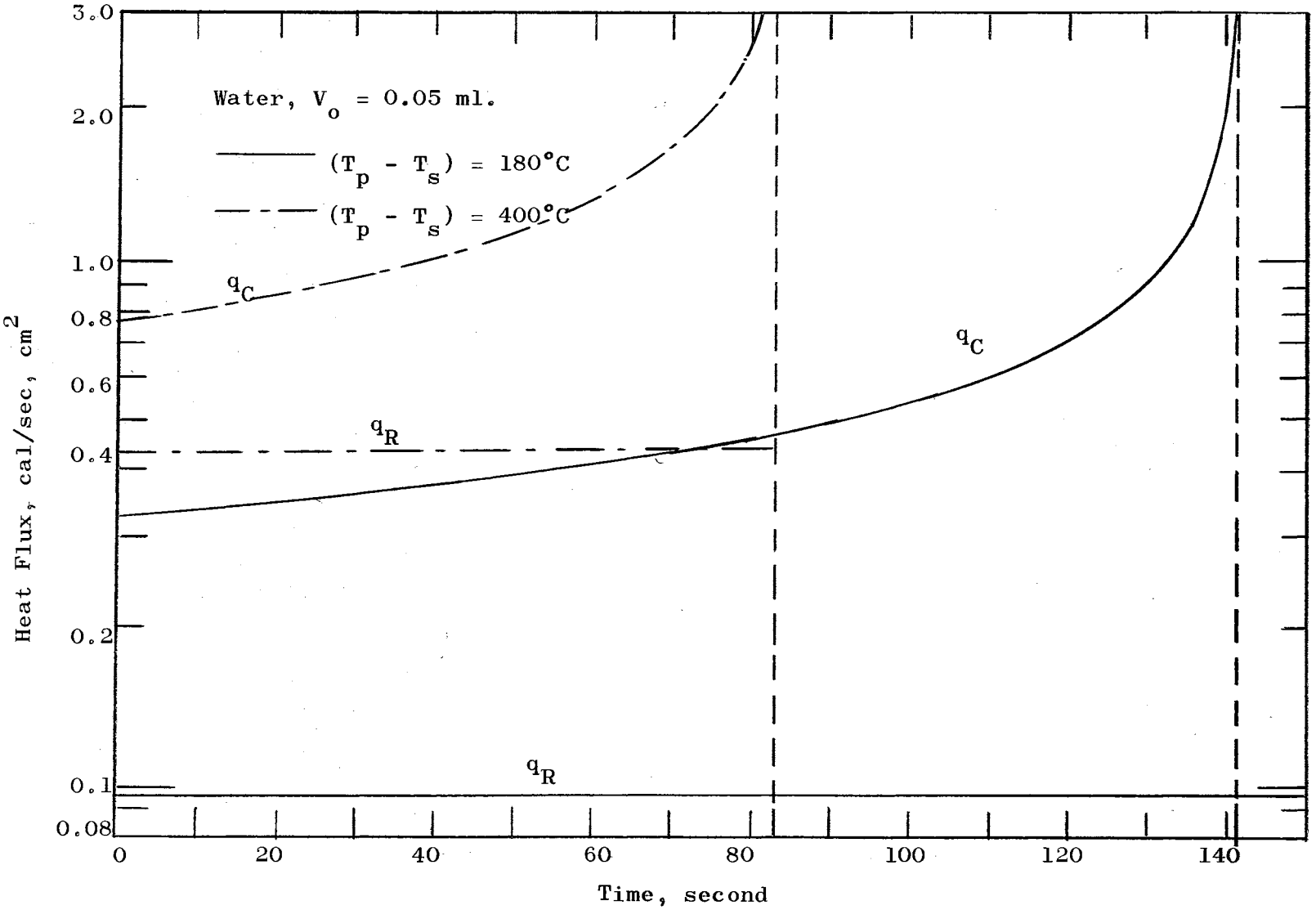

Figure 34 Heat Flux History of Water Droplet

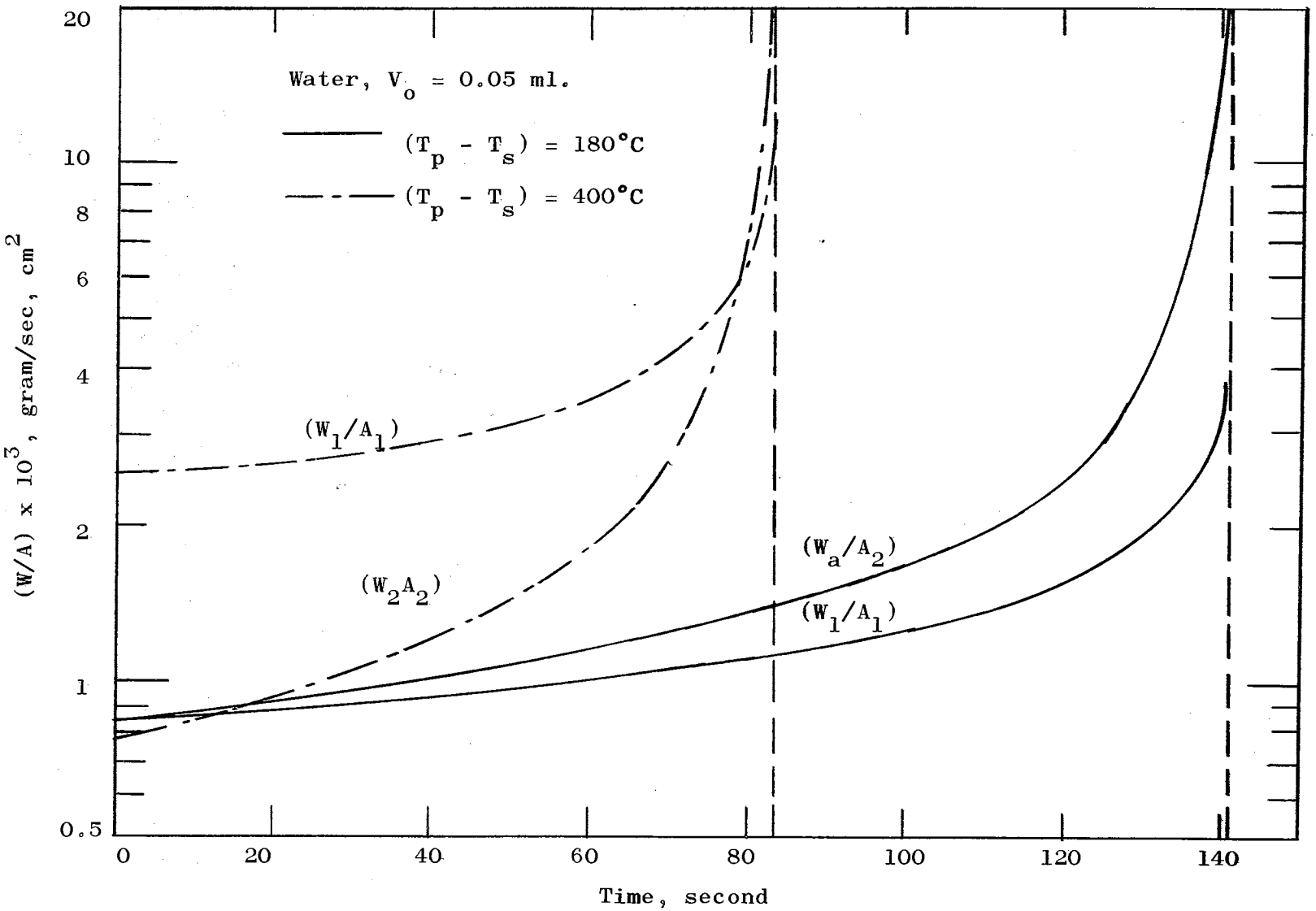

Figure 35 Mass Transfer Rate vs. Time for Water

more important than W_l/A_l, especially towards the end of droplet evaporation.

The droplet volume, V, radius, r, and the vertical distance from bottom of droplet to plate, δ_l, are shown as functions of droplet lifetime in Figure 36. It may be seen that in this case δ_l, is less than about 0.002 centimeters, which is typical of all of the droplets considered in this study. There was no experimental measurement for the magnitude of δ_l in this work. Kistemaker in a recent work measured the vapor film thickness of 0.006 centimeters for water droplet at 500°C plate temperature from his x-ray photographs. The experimental technique of producing the liquid droplet used by Kistemaker, however, is different from that used in this work. Instead of allowing the droplet to have complete freedom of moving around on the hot surface, Kistemaker as well as Gorton (8) confined the liquid droplet at the tip of a delivering pipet. Though they were able to keep the droplet at a constant volume while the droplet was experiencing spheroidal-state boiling, the film thickness measured in their experiment could only be used as rough comparison and is certainly not a good experimental justification for our theoretical model.

The Reynolds number defined as $Re = \rho_v \bar{U} \delta_l / \mu$ for the radial flow of vapor beneath the droplet has been computed for water at $\Delta T = 180°C$, and for carbon tetrachloride, ethyl alcohol, benzene, n-octane, and water at $\Delta T = 400°C$; Figure 37 indicates that at the higher plate temperature, water droplets give higher Reynolds numbers than at lower plate temperatures. In all cases, the Reynolds number decreases as the droplet proceeds to evaporate as

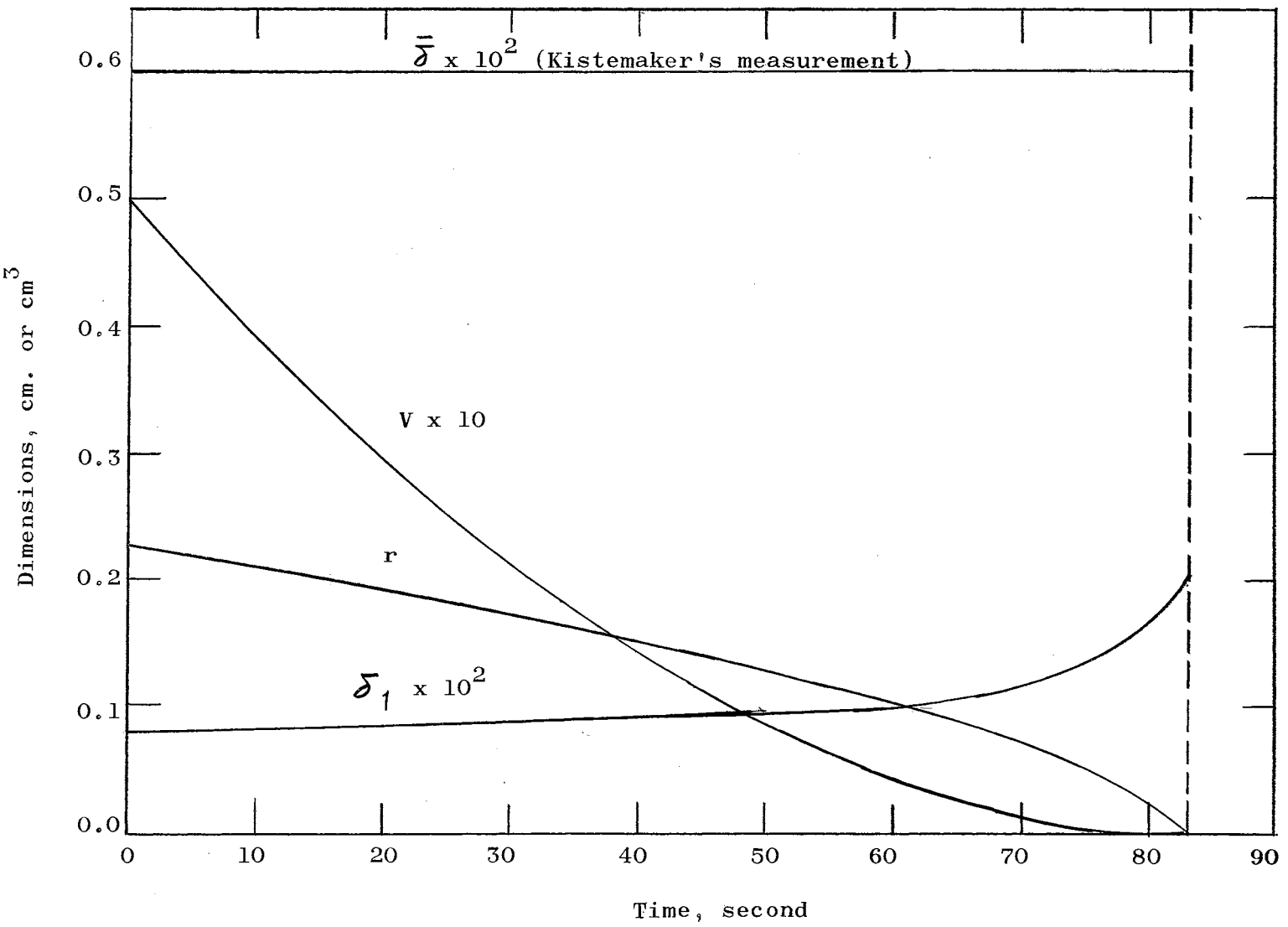

Figure 26 Theoretical History of Droplet Dimensions; Water Droplet at T = 500°C (V_o = 0.05 ml.)

is shown in Figures 37 and 38. It is significant to observe that the Reynolds number never exceeds sixteen for all liquids and conditions studied. These small Reynolds numbers imply laminar flow beneath the droplet and therefore justify one of the assumptions made in the theoretical development.

Seventy-two experimental data on droplet evaporation time were correlated by Equation (60). The constant C_1 and C_2 were obtained by regressional analysis, and the final result is shown in Equation (65) and Figure 39. This equation not only gives a quick estimate for the overall droplet evaporation time, but also furnishes a functional dependence of the overall droplet evaporation rate on the partial contributions due to conductive-convective heat transfer and radiative heat transfer respectively. The heat fluxes calculated from this correlational equation check the values obtained by the theoretical analysis within a maximum error of 35 percent.

The correlational groups are tabulated in Appendix E along with their percent deviation from Equation (65). From this tabulation, it may be seen that the maximum scatter of the experimental points is less than $\pm$ 30 percent, with most of the points exhibiting less than $\pm$ 20 percent deviation. Figure 39 presents the comparison between the experimental data and the values calculated by Equation (65). In view of the assumptions and simplifications made in the derivation of Equation (60), the error of this correlation on the order of $\pm$ 20 percent is to be expected.

From the experimental data shown in Figures 6 through 25, it is also of interest to observe that the Leidenfrost point is

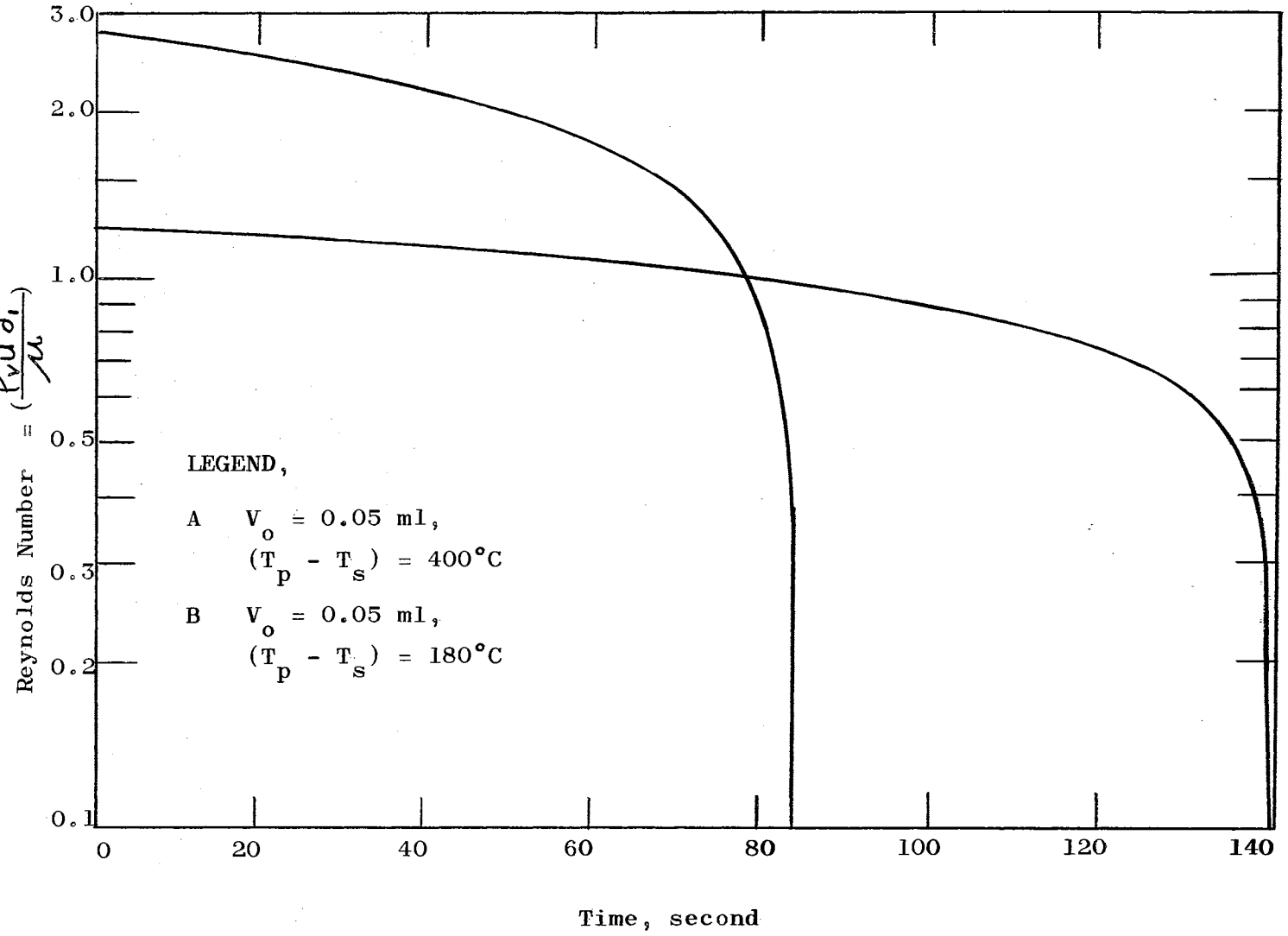

Figure 37 Reynolds Number vs. Time for Water Droplets

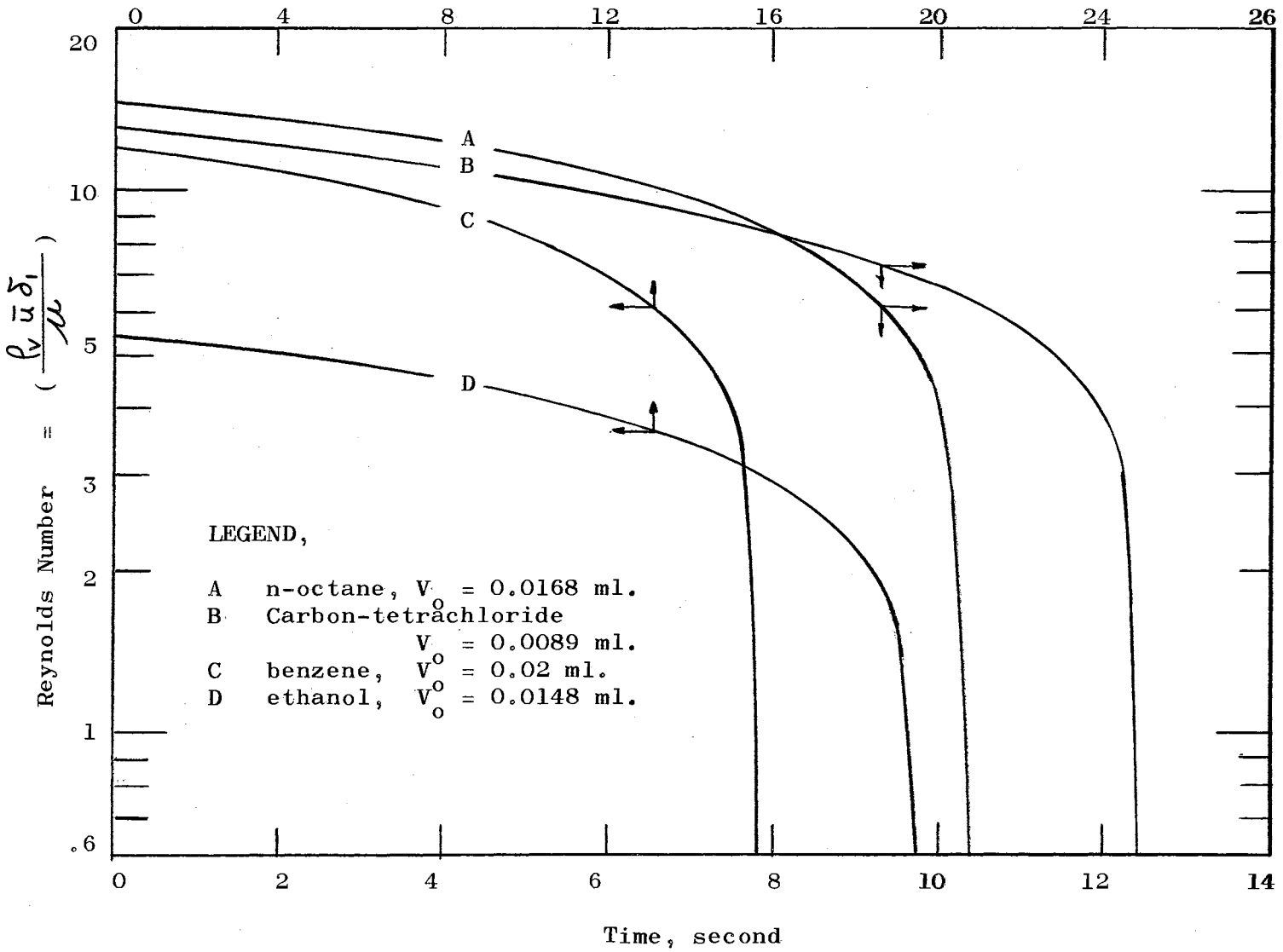

Figure 38 Reynolds Number vs. Time for Organic Liquids at $(T_p - T_s)$ = 400°C

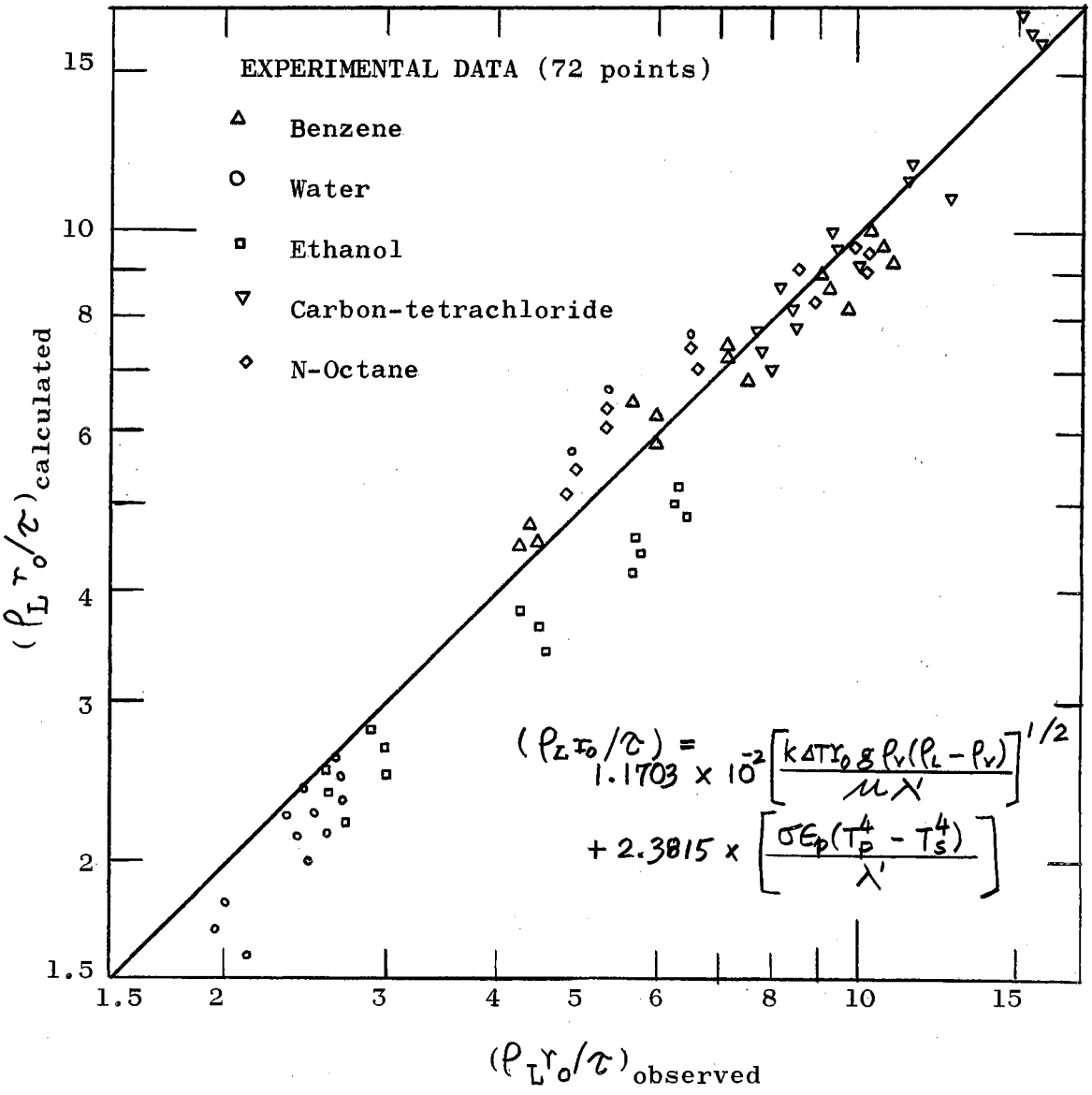

Figure 39 Empirical Correlation

well defined for organic liquids. The water droplets have a wider range of transition from nucleate boiling to stable film boiling. This, therefore, causes some uncertainties in the experimental determination for the Leidenfrost point for water droplets. In the range of droplet volumes studied, the Leidenfrost point is found to be essentially independent of droplet size. Table II summarizes the Leidenfrost point for liquid droplets as experimentally determined in this study, together with the values calculated from the following equation for $(\Delta T)_{min.}$ in pool boiling given by Berenson (2):

$$(\Delta T)_{min.} = 0.127\left(\frac{\rho_v \lambda'}{k}\right)\left[\frac{g(\rho_L-\rho_v)}{(\rho_L+\rho_v)}\right]^{2/3}\left[\frac{g_c\,\bar{\sigma}}{g(\quad_L - \quad_v)}\right]^{1/2}\left[\frac{\mu}{g_c(\quad_L - \quad_v)}\right]^{1/3} \tag{66}$$

It may be noticed that the equation for $(\Delta T)_{min.}$ derived by Berenson does not predict the Leindenfrost point correctly for the liquid droplets, though it gives somewhat better agreement for organic liquids. More study should be done before a general equation which will predict the Leidenfrost point for liquid droplets can be obtained.

TABLE II

SUMMARY FOR $(\Delta T)_{L.p.}$

Liquid	$(\Delta T)_{L.p.}$, °C Experimental Values	$(\Delta T)_{min.}$, °C; from Berenson's Equation
n-octane	100	97.8
Water	180	76.7
Benzene	105	85.7
Alcohol	100	79.8
CCl_4	95	88.7

Another way to evaluate the experimental and theoretical analysis in the present study is to discuss the present results in reference to the existing literature on the Leidenfrost phenomenon. Experimentally, there were two groups of investigators who used two different techniques and measured different experimental variables in studying the spheroidal state boiling. Gorton (8) and Kistemaker (15) used similar techniques to keep a liquid droplet of constant volume at the tip of a pipet positioned above a hot surface. They were more concerned about the vapor film thickness and the mass and heat transfer rates in the gap between the hot surface and the bottom of the liquid droplet. Both Gorton (8) and Kistemaker (15) attempted a theoretical analysis for predicting the thickness of the vapor film from the continuity and momentum equations for vapor flow in the channel underneath the liquid droplet. They assumed that the vapor exhibited perfect fluid behavior and completely ignored the effect of vapor viscosity on the hydrodynamics of this vapor flow. As a consequence, the excess pressure exerted vertically on the liquid droplet was dependent upon the kinetic terms only. This was contradicted by the fact that the radial velocity of the vapor flow in the parallel channel was relatively low. In addition, the vapor viscosity is a very steep function of temperature, and the existence of the drag force both in the vapor-solid and the vapor-liquid interface at any temperature beyond the Leidenfrost point cannot be neglected without any justification. The low Reynolds numbers as presented previously further confirm the importance of the viscous flow existing in the vapor channel.

The expression for the vapor film thickness developed by Kistemaker (15) is as follows:

$$\delta = \frac{1}{2} r_o \left(\frac{m}{\rho_v}\right) \sqrt{\frac{\rho_v}{2\Delta p}}$$

where m is the mass flow rate of vapor in gm/sec, and Δp is the excess pressure (or lifting pressure) existing in the bottom of the droplet. This equation appears unusually simple at the first look. However, there are two quantities, m and Δp, to be determined empirically.

The spheroidal state boiling studied with a liquid droplet restricted both on its motion and volume by the tip of a pipet, is phenomenologically different from what was originally observed by Leidenfrost (17). The droplet performing the Leidenfrost phenomenon is free from any restriction on the motion of droplet. The volume of droplet decreases as the liquid evaporates. The other group of researchers, Rebinder and Pleteneva (23), Borishansky (3), Gottfried (8), and this work were mainly interested in measuring the total evaporation time of a liquid droplet freely moving on a hot plate. Rebinder and Pleteneva (23), and Borishansky (3) gave very good qualitative descriptions of the phenomena. From his experimental data, Borishansky discovered that the ratio τ/r_o (where τ is the total evaporation time, r_o is the initial droplet radius) for a particular liquid at a fixed plate temperature remained constant. He also derived a differential equation from the energy transport mechanism at the vapor-liquid interface but attempted no direct numerical solution to the analytical equations. The dimensional correlation based on the equation and

and applied to the experimental data by Borishansky (3) is

$$\frac{k}{C_{P_L}\rho_L}\,\frac{\tau}{4r_o^2}\left[\frac{4r_o^2}{\sigma}(\rho_L-\rho_V)\right]^{0.5} = \varphi\left(\frac{C_{P_L}\Delta T}{\lambda}, \frac{k_V}{k_L}\right)$$

Neither vapor viscosity nor radiation heat transfer is included in this dimensional correlation. This is inherent in his derivation and therefore introduces a basic conceptual error in the analysis of the Leidenfrost phenomenon.

The present work is an extension of Gottfried's analytical approach to the Leidenfrost phenomenon for small droplets. The physical model remains practically the same as which introduced by Gottfried (9) except that the application of the integral analysis to the lower half of droplet and a different radiative heat transfer analysis eliminates the uncertainty of the magic number X appearing in Gottfried's work.

In the literature, there were no data whatsoever on the history of droplet size for the liquid droplets displaying the Leidenfrost phenomenon.

CHAPTER VIII

CONCLUSIONS AND RECOMMENDATIONS

The following significant conclusions may be drawn from the previous discussions:

Experimental

(1) The liquid droplets produced by the hypodermic syringe technique are reproducible to within $\pm$ 3 percent deviation from the average droplet size.

(2) The droplet evaporation times for all five liquids used in this study are measurable to within a maximum variation of $\pm$ 5 percent in the Leidenfrost regime.

(3) The experimental data on the droplet evaporation time were correlated empirically by Equation (65) with an average error of $\pm$ 20 percent.

(4) The Leidenfrost point is well defined for organic liquids, while for water it is between 250°C and 310°C plate temperature. The Leidenfrost point is found to be essentially independent of droplet size for the range of droplet volumes studied.

(5) The equation derived by Berenson (2) for $(\Delta T)_{min.}$ calculation in pool boiling does not correctly predict the Leidenfrost point for liquid droplets though it gives somewhat better agreement for organic liquids.

Theoretical

(1) The theoretical model is supported reasonably well by the experimental data taken with small droplets of ordinary liquids.

(2) The major contribution to the heat flux is due to the conductive-convective heat transfer mechanism.

(3) The theory predicts the experimental values with an average error of $\pm$ 10 percent in both droplet evaporation time and droplet radius measurements.

(4) Best agreement between experiment and theory on the droplet evaporation time is obtained for the cases of water and carbon tetrachloride.

(5) The radiative heat flux cannot be neglected at plate temperatures beyond the Leidenfrost point of liquids. For the case of water droplets, the radiative heat flux is about 30 percent of the conductive-convective heat flux at the Leidenfrost point (280°C), and about 60 percent at a plate temperature of 500°C.

(6) The radial flow of vapor beneath the droplet is, is in all cases, laminar as indicated by the computed Reynolds numbers.

The following recommendations for further work along this line are made:

(1) A low-speed movie camera should be used in the study of radius history for liquid droplets which have shorter evaporation lifetimes.

(2) The possible thermal decomposition of organic liquids while in spheroidal-state boiling should be further studied.

(3) The theoretical model may be extended to other geometrical shapes, such as ellipsoids for the liquid masses.

(4) Experimental data on droplet evaporation time should be taken with cryogenic liquids or liquid metals in order to check the possibility of generalizing this theoretical model to these classes of liquids.

(5) The Leidenfrost point for liquid droplets should be studied further to obtain a theoretical equation which will predict the Leidenfrost point correctly.

A SELECTED BIBLIOGRAPHY

1. Bashforth, F. and J. C. Adams, An Attempt to Test the Theory of Capillary Action, University Press, Cambridge, 1883.

2. Berenson, P. J., ASME J. Heat Transfer, 83, 3, p. 351, 1961.

3. Borishansky, V. M., AEC Trans. Series, AEC-TR-3405, 1953.

4. Bromley, L. A., "Heat Transfer in Stable Film Boiling," Ph.D. Thesis, University of California, Berkeley, June, 1948.

5. Chang, Y. P., Trans. ASME, 79, pp 1501-1513, 1957.

6. _____ _____, AEC Report, TID-14004, July, 1961.

7. Drew, T. B. and A. C. Mueller, Trans. Am. Inst. Chem. Engrs., 33, pp. 449-71, 1937.

8. Gorton, C. W.,"Heat Transfer to Drops in the Spheroidal State," Ph. D. Thesis, Purdue University, July, 1953.

9. Gottfried, B.S., "The Evaporation of Small Drops on a Flat Plate in the Film Boiling Regime," Ph.D. Thesis, Case Institute of Technology, May, 1962.

10. Gross-Gronomski, L., Combustion and Flame, 7, 3, pp. 217-25, 1963.

11. Hodgman, C. D., Ed., Handbook of Chemistry and Physics, 39th ed., Chemical Rubber Publishing Company, Cleveland, 1958.

12. Hoffman, T. W. and W. H. Gauvin, Can. J. Chem. Engr., 38, p. 129, 1960.

13. Holamn, J. P., Heat Transfer, McGraw-Hill Book Company, Inc., New York, 1963.

14. Hosler, E. R. and J. W. Westwater, Propellants, Combustion and Liquid Rocket Conference, April 26, 1961.

15. Kistemaker, J., Physica, 29, pp. 96-104, 1963.

16. Kunz, K.S., Numerical Analysis, McGraw-Hill Book Company, Inc., New York, 1957.

17. Leidenfrost, J. G., "De Aquae Communis Nonnullis Qualitatibus Tractatus," Duisburgh, 1756, (The original treatise of Leidenfrost has been translated into English by Mrs. Wares of the University of Oklahoma, Norman, Oklahoma, 1963. This is available through Dr. K. J. Bell, School of Chemical Engineering, Oklahoma State University, Stillwater, Oklahoma.)

18. Marschner, R. F., Ind. Eng. Chem., 30, 5, pp. 554-62, 1938.

19. McAdams, W. H., Heat Transmission, McGraw-Hill Book Company, Inc., 3rd ed., New York, 1954.

20. Nukiyama, S., J. Soc. Mech. Engrs., Japan, 37, pp. 367-74, 1934. (The original Japanese article has been translated by C. J. Lee, School of Chemical Engineering, Oklahoma State University, 1962.)

21. Patel, B. M., Unpublished Ph.D. Thesis, School of Chemical Engineering, Oklahoma State University, 1965.

22. Perry, J. H., Chemical Engineering Handbook, 3rd ed., McGraw-Hill Book Company, Inc. New York, 1950.

23. Pleteneva, N. A. and P. A. Rebinder, Russian J. Phy. Chem., 20, 9, p. 961, 1946. (English translations are available through Dr. K. J. Bell, School of Chemical Engineering, Oklahoma State University, Stillwater, Oklahoma.)

24. Rebinder, P.A. and N. A. Pleteneva, Russian J. Phy. Chem., 20, 9, p. 973, 1946.

25. Reid, R. C. and T. K. Sherwood, The Properties of Gases and Liquids, McGraw-Hill Book Company, Inc., New York, 1958.

26. Rossini, F. D., et al., Selected Values of Physical and Thermodynamic Properties of Hydrocarbons and Related Compounds, Carnegie Press, Pittsburgh, 1953.

27. Salvadori, M. G. and M. L. Baron, Numerical Methods in Engineering, Prentice-Hall, Inc., New Jersey, 1961.

28. Savic, P., National Research Council of Canada Report MT-26, May, 1955.

29. Savic, P., National Research Council of Canada Report MT-37, April, 1958.

30. Schlichting, H., Boundary Layer Theory, 4th ed., McGraw-Hill, New York, 1960.

31. Sparrow, E. M., Int. J. Heat and Mass Transfer, 7, pp. 229-38, 1964.

32. Washburn, E. W., Ed., International Critical Table, McGraw-Hill Book Company, Inc., New York, 1926.

33. Westwater, J. W., Chapter on boiling, Advances in Chemical Engineering, Vol. I, Academic Press, 1959.

34. Zuber, N., "Hydrodynamic Aspects of Boiling Heat Transfer," Ph.D. Thesis, University of California, Los Angeles, 1959.

35. Zuber, N. and M. Tribus, AEC Report, AECU-3631, January, 1958.

NOMENCLATURE

A	total surface area of droplet, cm^2
A_1	surface area of lower-half droplet, cm^2
A_2	surface area of upper-half droplet, cm^2
A_p	projected area of liquid droplet, cm^2
A_s	area of stainless steel plate, cm^2
C_1, C_2	correlational constants from experimental data, dimensionless
C_p	mean specific heat of vapor cal/gm, °C
C_{P_L}	mean specific heat of liquid, cal/gm, °C
C_s	concentration of vapor in air at upper half droplet surface, g-mole/cm^3
C_∞	concentration of vapor in air at infinite distance from droplet, g-mole/cm^3
D	vapor to air molecular diffusion coefficient, cm^2/sec
F	total upward force exerted on droplet, dynes
F_{dA-Ap}	configuration factor for radiation from surface element dA to surface Ap, dimensionless
$\bar{F}_1$, $\bar{F}_2$	configuration factor for radiation from hot plate to liquid droplet, dimensionless
$\mathcal{F}_1$, $\mathcal{F}_2$	overall configuration factor for radiation from hot plate to droplet, dimensionless
f	function of one or more variables, dimensionless
g	gravitational acceleration, cm/sec^2
g_c	conversion factor, 980 dyne-cm/gm-sec^2
$I_1(\delta_1/r, \Theta')$	first integral defined in Equation(28)

$I_2(\delta_1/r,\Theta'')$	double integral defined in Equation (27)
$I_3(\delta_1/r)$	triple integral defined in Equation (26)
k	mean thermal conductivity of vapor, cal/sec, cm, °C
k_e	effective thermal conductivity as defined in equation (23), cal/sec, cm°C
k_L	mean thermal conductivity of liquid, cal/sec, cm, °C
K	correction factor defined as $k(1+K) = k_e$, dimensionless
k_c	mass transfer coefficient based on concentration, cm/sec
M	molecular weight of vapor, gm/g-mole
m	vapor mass flow rate, gm/sec
P	excess pressure beneath droplet, dyne/cm^2
$P(\Theta'')$	excess pressure at angular position Θ'', dyne/cm^2
P_s	partial pressure of the diffusing vapor, dyne/cm^2
Q_c	total heat conducted through the vapor film generated in bottom of droplet, cal/sec
Q_{R1}, Q_{R2}	heat flow due to radiation from plate to liquid droplet, cal/sec
q_c	conductive-convective heat flux through the vapor film, cal/sec, cm^2
q_{R1}, q_{R2}	radiative heat fluxes, cal/sec, cm^2
Re	Reynolds number for vapor flow between the heating surface and the bottom of droplet, dimensionless
r	radius of droplet at any time, cm
r_o	radius of initial droplet, cm
Sc	Schmidt number for mean flow around droplet, dimensionless
T_p	plate temperature, °C
T_s	boiling temperature of liquid droplet, °C
T_v	mean vapor temperature beneath droplet, °C

ΔT	$T_p - T_s$, °C
t	time variable, sec
U	radial vapor velocity beneath droplet, cm/sec
$\bar{u}$	mean radial vapor velocity beneath droplet, cm/sec
V	droplet volumne, cm^3
V_i, V_{i+1}	volume variables in the numerical iteration process, cm^3
W_1	rate of evaporation over lower droplet, gm/sec
W_2	rate of evaporation over upper droplet, gm/sec
X_1	correlational group defined in Equation (62)
X_2	correlational group defined in Equation (63)
x	radial space variable beneath droplet, cm
Y	correlational group defined in Equation (61)
y	axial space variable beneath droplet, cm

Greek Letters

δ	vertical distance from some point on lower droplet surface to plate, cm
δ_o	vertical distance from bottom of droplet to plate at initial droplet volume, cm
δ_1	vertical distance from bottom of droplet to plate at any time
ϵ_L	thermal emissivity of liquid, dimensionless
ϵ_S	thermal emissivity of stainless steel, dimensionless
φ	function of some variables
λ	heat of vaporizarion of saturated liquid, cal/gm
λ'	$= \lambda + \frac{\Delta T}{2} C_p$, cal/gm
μ	mean viscosity of vapor gm/cm-sec
ρ_L	density of saturated liquid, gm/cm^3

ρ_V	density of vapor, gm/cm^3
σ	Stefen-Boltzman constant, 1.355×10^{-2} $cal/(°C)^4\text{-}cm^2$
σ_l	surface tension of liquid, dyne/cm
τ	total droplet evaporation time, sec
θ	angular variable in droplet, radian
θ', θ''	dummy angular variables in droplet
Ω	general symbol for field force, dyne

APPENDIX A

PHYSICAL PROPERTIES

TABLE A1

PHYSICAL PROPERTIES

Physical Property	Water H_2O	Ethanol C_2H_5OH	Benzene C_6H_6	Carbon Tet. $C\ Cl_4$	n-Octane C_8H_{18}	Reference
Boiling point, °C	100.0	78.5	80.1	76.8	125.7	11
Molecular wt., gm	18.0	46.1	78.0	153.8	114.0	11
Density (l) gm/cm^3	0.958	0.737	0.817	1.433	0.545	3
Latent heat, cal/gm	539.0	204.3	94.1	46.4	71.0	22
Emissivity ---	0.96	0.96*	0.96*	0.96*	0.96*	19
Diffusivity cm^2/sec	0.353	0.180	0.133	0.113	0.108	25

* estimated values

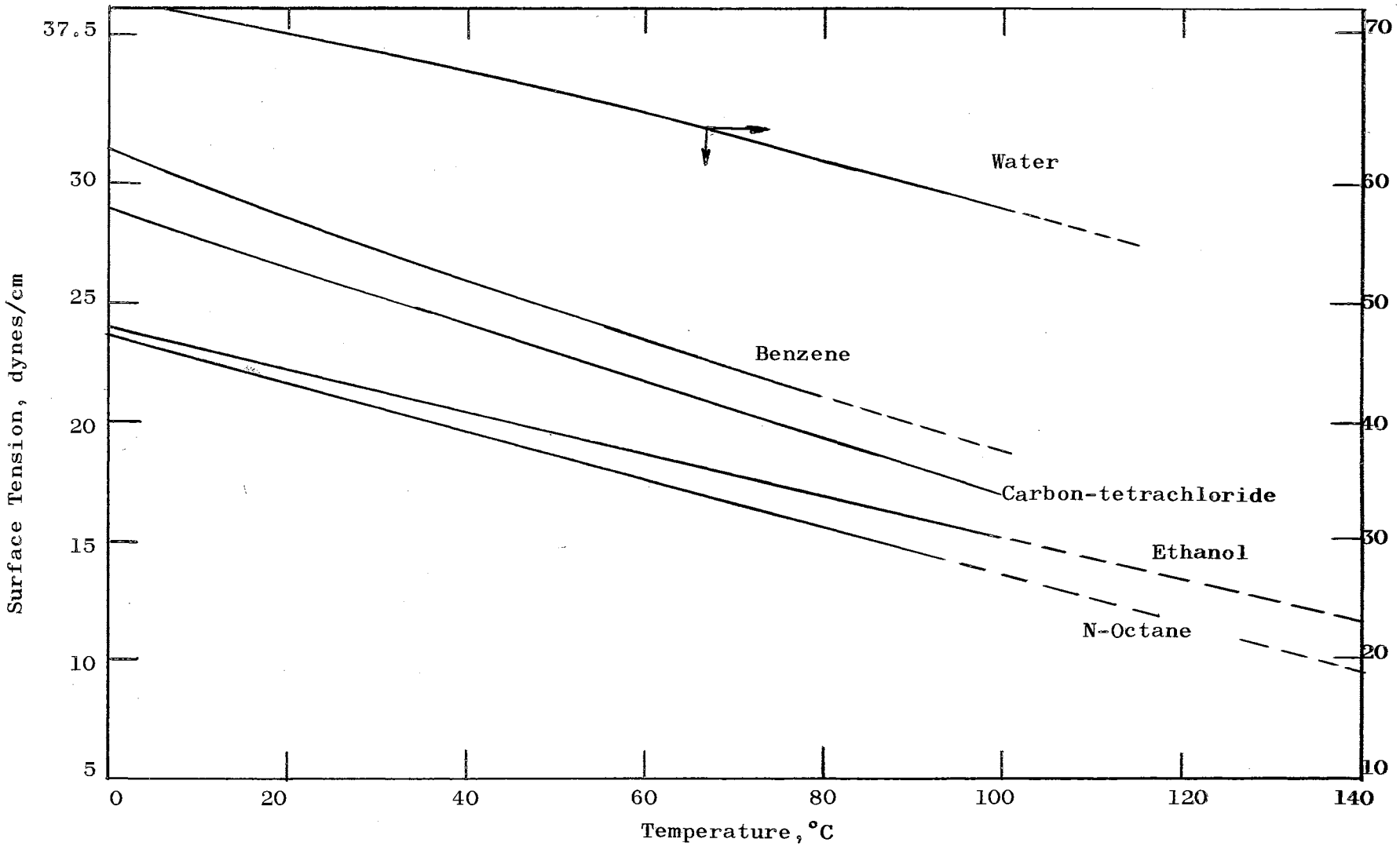

Figure A1 Surface Tension of Liquids (32)

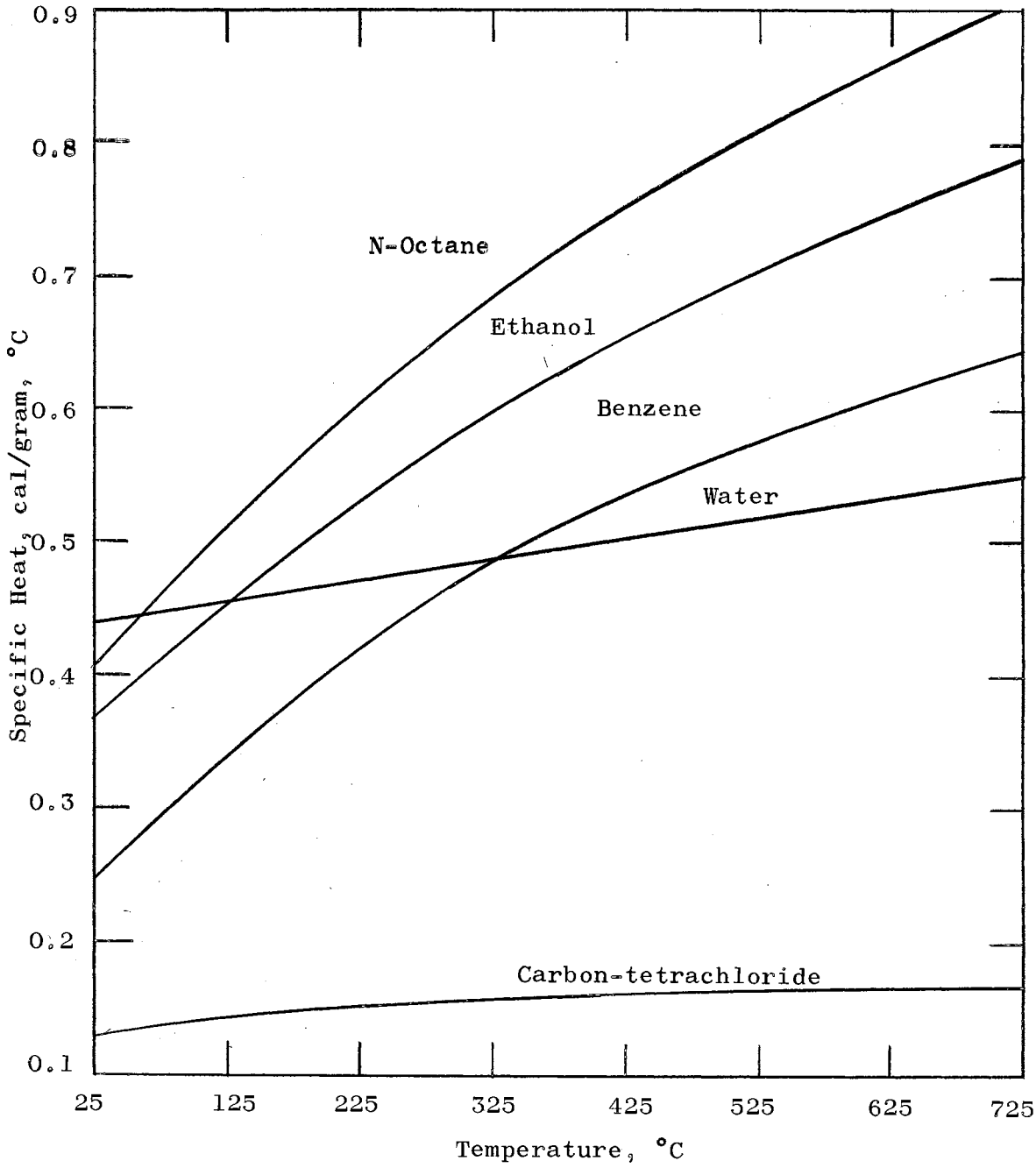

Figure A2 Specific Heat of Gases (11)

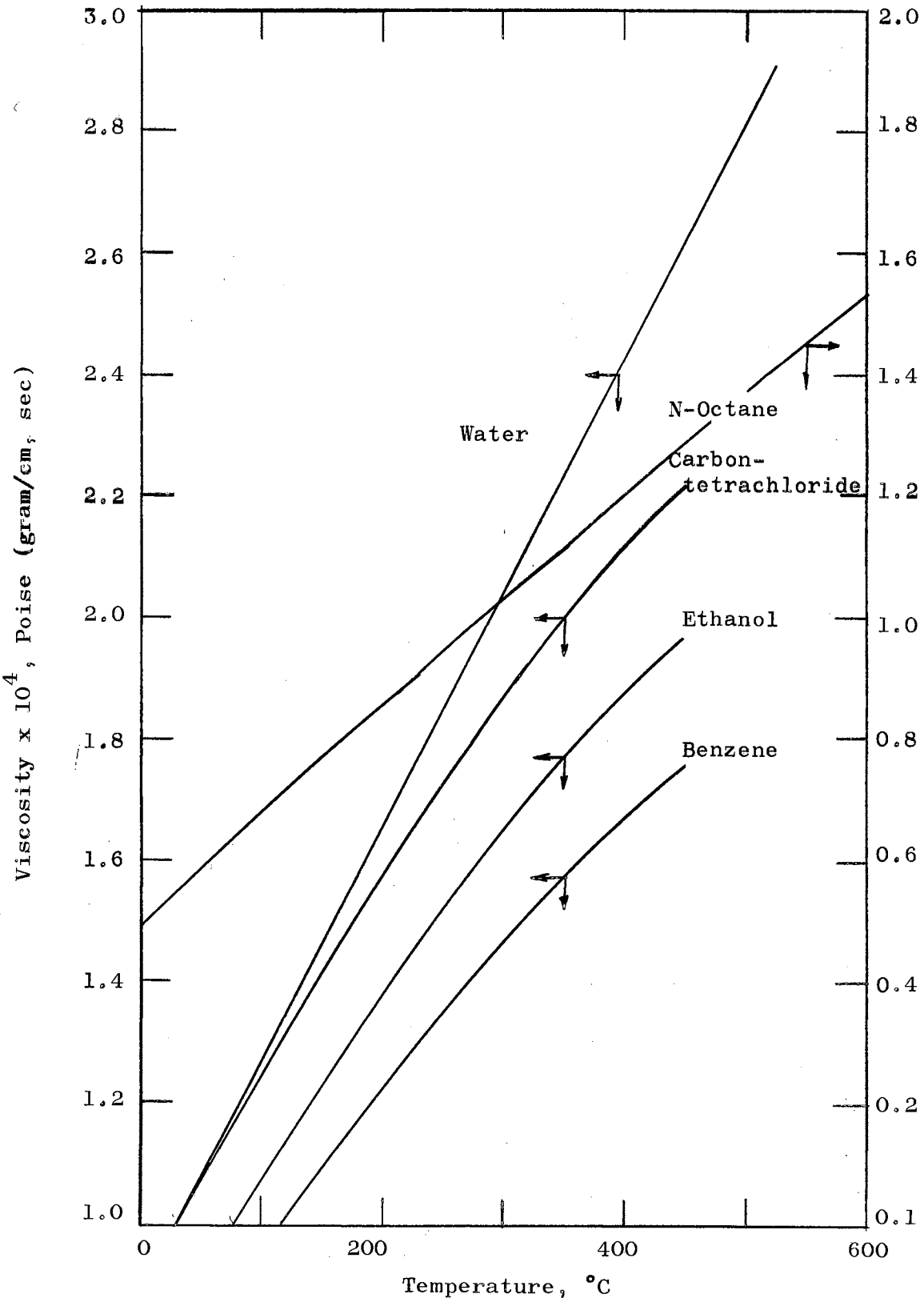

Figure A3 Viscosity of Gases (25)

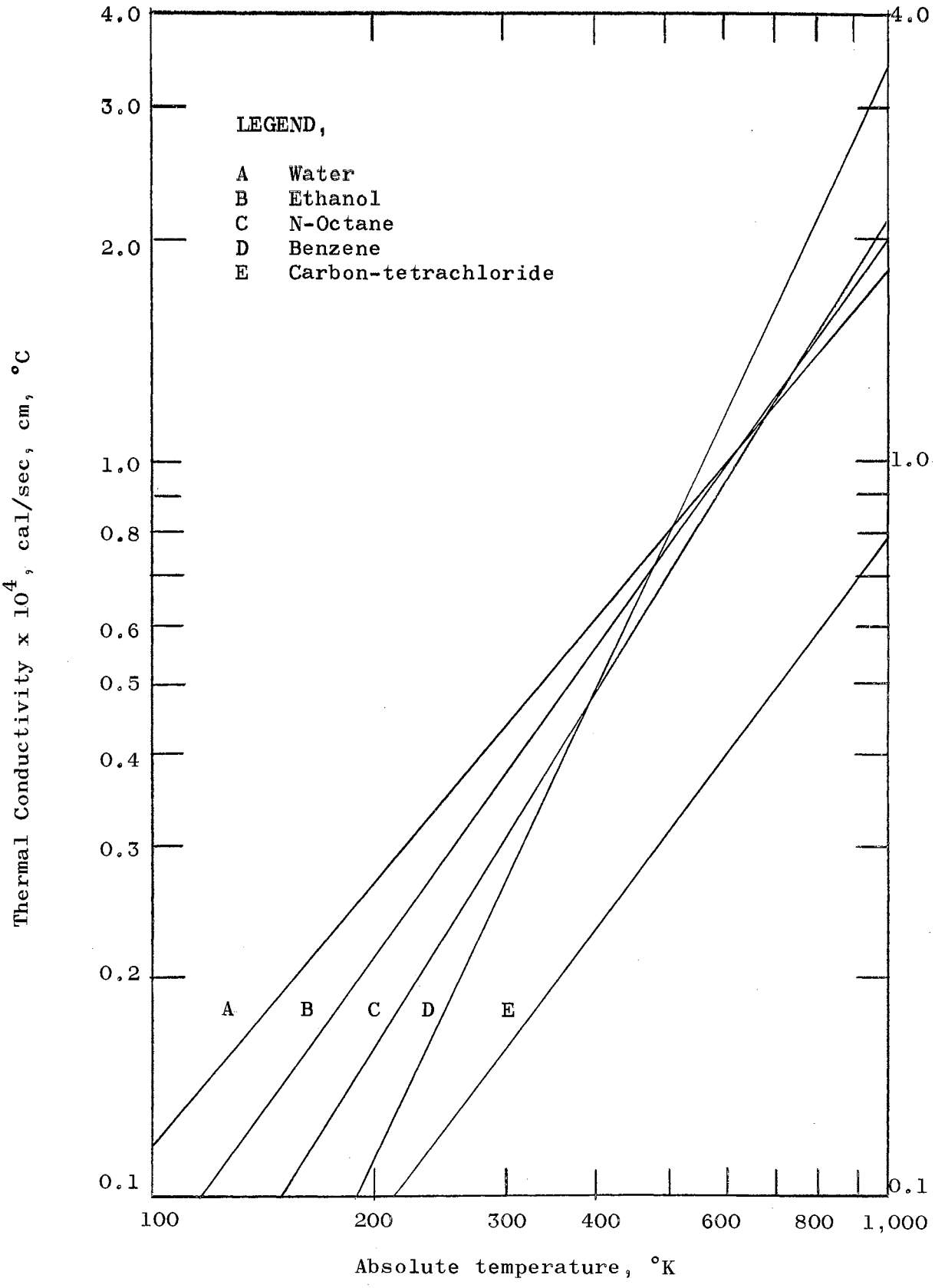

Figure A4 Thermal Conductivity of Gases (19)

APPENDIX B

HYPODERMIC NEEDLE CALIBRATIONS

TABLE B1

MEAN DROP VOLUMES AT ROOM TEMPERATURE (IN CC)

Liquid	Gage 13 needle	Gage 16 needle	Gage 17 needle	Gage 21 needle
CCl_4	0.00803 ± 2.82%	0.00627 ± 2.69%	0.00564 ± 2.89%	0.00394 ± 2.90%
EtOH	0.01391 ± 1.56%	0.01100 ± 1.74%	0.00979 ± 2.55%	0.00621 ± 1.89%
C_6H_6	0.01618 ± 2.39%	0.01343 ± 1.89%	0.01176 ± 1.63%	0.00748 ± 1.84%
H_2O	0.03196 ± 0.95%	0.02212 ± 1.49%	0.01920 ± 1.48%	0.01540 ± 0.72%
n-Octane	0.01682 ± 1.03%	0.01327 ± 1.72%	0.01266 ± 2.07%	0.00824 ± 2.25%

TABLE B2

HYPODERMIC NEEDLE CALIBRATIONS
(CARBON TETRACHLORIDE)

Fluid and needle size	Wt. per drop, g.	Deviation from mean, %	Fluid and needle size	Wt. per drop, g.	Deviation from mean, %
CCl_4 at 26°4C, gage 13 needle	0.01348	5.15	CCl_4 at 26.3°C. gage 16 needle	0.01028	2.69
	0.01247	- 2.72		0.01007	0.59
	0.01240	- 3.26		0.01014	1.29
	0.01328	3.59		0.01042	4.09
	0.01267	- 1.17		0.01017	1.59
	0.01249	- 2.57		0.00977	- 2.40
	0.01275	- 0.54		0.00970	- 3.10
	0.01245	- 2.88		0.00963	- 3.80
	0.01349	5.23		0.00960	- 4.10
	0.01268	- 1.09		0.01034	3.29
Ave.	0.01282	± 2.82	Ave.	0.01001	± 2.69
CCl_4 at 26.4°C, gage 17 needle	0.00948	5.22	CCl_4 at 26.6°C, gage 21 needle	0.00629	0.00
	0.00918	1.89		0.00611	- 2.86
	0.00903	0.22		0.00629	0.00
	0.00916	1.66		0.00659	4.77
	0.00938	4.11		0.00620	- 1.43
	0.00911	1.11		0.00605	- 3.81
	0.00885	- 1.77		0.00611	- 2.86
	0.00870	- 3.44		0.00611	- 2.86
	0.00870	- 3.44		0.00624	- 0.79
	0.00847	- 5.99		0.00690	9.70
Ave.	0.00901	± 2.89	Ave.	0.00629	± 2.90

TABLE B3

HYPODERMIC NEEDLE CALIBRATIONS
(ETHANOL)

Fluid and needle size	Wt. per drop, g.	Deviation from mean, %	Fluid and needle size	Wt. per drop, g.	Deviation from mean, %
Ethanol at 25.6°C, gage 13 needle	0.01085	- 0.55	Ethanol at 25.5°C, gage 16 needle	0.00863	0.00
	0.01091	0.00		0.00838	- 2.89
	0.01053	- 3.51		0.00882	2.21
	0.01113	2.02		0.00847	- 1.85
	0.01117	2.39		0.00906	4.98
	0.01128	3.40		0.00863	0.00
	0.01072	- 1.75		0.00860	- 0.34
	0.01085	- 0.56		0.00840	- 2.66
	0.01090	- 0.09		0.00875	1.39
	0.01077	- 1.29		0.00854	- 1.04
Ave.	0.01091	± 1.56	Ave.	0.00863	± 1.74
Ethanol at 25.6°C, gage 17 needle	0.00757	- 1.42	Ethanol at 25.6°C, gage 21 needle	0.00458	- 5.96
	0.00763	- 0.65		0.00484	- 0.62
	0.00792	3.13		0.00498	2.26
	0.00752	- 2.08		0.00492	1.02
	0.00770	0.26		0.00485	- 0.41
	0.00807	5.08		0.00493	1.23
	0.00736	- 4.16		0.00488	0.20
	0.00793	3.26		0.00492	1.02
	0.00775	0.91		0.00505	3.69
	0.00731	- 4.51		0.00475	- 2.47
Ave.	0.00768	± 2.55	Ave.	0.00487	± 1.89

TABLE B4

HYPODERMIC NEEDLE CALIBRATIONS (BENZENE)

Fluid and needle size	Wt. per drop, g.	Deviation from mean, %	Fluid and needle size	Wt. per drop, g.	Deviation from mean, %
Benzene at 25.6°C, gage 13 needle	0.01378	- 3.16	Benzene at 25.7°C, gage 16 needle	0.01182	0.09
	0.01400	- 1.61		0.01225	3.73
	0.01426	0.21		0.01220	3.30
	0.01432	0.63		0.01163	- 1.52
	0.01485	4.36		0.01179	- 0.16
	0.01386	- 2.60		0.01164	- 1.44
	0.01370	- 3.72		0.01209	2.37
	0.01479	3.96		0.01145	- 3.04
	0.01409	- 0.98		0.01171	- 0.84
	0.01460	2.60		0.01150	- 2.62
Ave.	0.01423	± 2.39	Ave.	0.01181	± 1.89
Benzene at 25.7°C, gage 17 needle	0.01025	- 0.87	Benzene at 25.7°C, gage 21 needle	0.00648	- 1.52
	0.01056	2.12		0.00651	- 1.06
	0.01042	0.77		0.00637	- 3.19
	0.01030	- 0.39		0.00652	- 0.91
	0.01024	- 0.97		0.00675	2.74
	0.01027	- 0.68		0.00642	- 2.43
	0.01006	- 2.71		0.00657	- 0.15
	0.01075	3.96		0.00663	0.91
	0.01049	1.45		0.00666	1.21
	0101010	- 2.33		0.00685	4.26
Ave.	0.01034	± 1.63	Ave.	0.00658	± 1.84

TABLE B5

HYPODERMIC NEEDLE CALIBRATIONS
(WATER)

Fluid and needle size	Wt. per drop, g.	Deviation from mean, %	Fluid and needle size	Wt. per drop, g.	Deviation from mean, %
Water at 25.4°C, gage 13 needle	0.03225	1.19	Water at 25.5°C, gage 16 needle	0.02229	1.04
	0.03250	1.97		0.02152	- 2.45
	0.03173	- 0.44		0.02129	- 3.49
	0.03182	- 0.16		0.02268	2.81
	0.03135	- 1.64		0.02236	1.36
	0.03165	- 0.70		0.02203	- 0.14
	0.03173	- 0.45		0.02222	0.72
	0.03238	1.60		0.02207	0.04
	0.03167	- 0.63		0.02239	1.49
	0.03164	- 0.72		0.02176	- 1.36
Ave.	0.03187	± 0.95	Ave.	0.02206	± 1.49
Water at 25.7°C, gage 17 needle	0.01919	0.21	Water at 25.2°C, gage 21 needle	0.01510	- 1.66
	0.01901	- 0.73		0.01538	0.15
	0.01895	- 1.05		0.01530	- 0.36
	0.01852	- 3.30		0.01555	1.26
	0.01893	- 1.15		0.01518	- 1.14
	0.01893	- 1.15		0.01536	0.02
	0.01952	1.92		0.01529	- 0.42
	0.01985	3.65		0.01547	0.74
	0.01928	0.68		0.01550	0.93
	0.01933	0.94		0.01543	0.48
Ave.	0.01915	± 1.48	Ave.	0.01536	± 0.72

TABLE B6

HYPODERMIC NEEDLE CALIBRATIONS
(NORMAL OCTANE)

Fluid and needle size	Wt. per drop, g.	Deviation from mean, %	Fluid and needle size	Wt. per drop, g.	Deviation from mean, %
n-Octane	0.01199	1.26	n-Octane	0.00957	2.44
at 21.1°C,	0.01213	2.44	at 21.1°C,	0.00913	- 2.26
gage 13	0.01191	0.59	gage 16	0.00908	- 2.80
needle	0.01185	0.08	needle	0.00958	1.47
	0.01163	- 1.77		0.00921	- 1.42
	0.01184	0.00		0.00911	- 2.49
	0.01165	- 1.61		0.00943	0.93
	0.01167	- 1.44		0.00933	- 0.13
	0.01194	- 0.84		0.00953	2.00
	0.01181	- 0.25		0.00946	1.25
Ave.	0.011842	± 1.03	Ave.	0.00934	± 1.72
n-Octane	0.00908	1.90	n-Octane	0.00600	3.44
at 21.1°C,	0.00891	0.00	at 21.1°C,	0.00594	2.41
gage 17	0.00892	0.11	gage 21	0.00588	1.37
needle	0.00875	- 1.79	needle	0.00578	- 0.34
	0.00918	3.03		0.00562	- 3.10
	0.00915	2.69		0.00568	- 2.06
	0.00868	- 2.58		0.00567	- 2.24
	0.00869	- 2.46		0.00572	- 1.37
	0.00914	2.58		0.00567	- 2.24
	0.00859	- 3.59		0.00603	3.96
Ave.	0.00891	± 2.07		0.00580	± 2.25

APPENDIX C

NUMERICAL EVALUATION FOR INTEGRALS

The numerical values of the integrals $I_1(\delta_1/r, \pi/2)$, $I_2(\Theta'', \delta_1/r)$, and $I_3(\delta_1/r)$ of Equations (26), (27), and (28) were obtained by applying the Trapezoidal Rule for the numerical double integration (23). These integrations were carried out in a separate computer program for a wide range of the parameter δ_1/r. The prupose was to simplify the overall computational scheme in solving the non-linear implicit differential equation; $-\rho_L \frac{dV}{dt} = (W_1 + W_2)$, by an effort to express both $I_1(\delta_1/r, \pi/2)$ and δ_1/r as explicity functions of $I_3(\delta_1/r)$. Therefore, W_1 can be computed from the value of the instantaneous droplet dimension from Equation (29).

The computer program (in Fortran language) for the integrations is listed on the next page and the results are tabulated as the following:

TABLE C-1

RESULTS FOR NUMERICAL INTEGRATION

δ_1/r	$I_1(\delta_1/r, \pi/2)$	$I_3(\delta_1/r)$
1.0	0.3862	0.0198
0.5	0.6478	0.1572
0.2	1.1500	1.7602
0.1	1.6375	9.0692
0.05	2.1965	42.0310

```
C      LEIDENFROST INTEGRALS,   K. J. BELL
       PUNCH 100
  100 FORMAT(22H LEIDENFROST INTEGRALS//)
    1 READ 101, DELTA
  101 FORMAT(F8.4)
       PUNCH 104, DELTA
       DIMENSION A(160),D(160),E(160),F(160)
  104 FORMAT(7H DELTA ,F8.4)
       U = 0.00
       I = 1
    5 A(I) = ((SIN (U))*(COS (U)))/(DELTA + 1.0 - (COS (U)))
       U = U + 0.01
       I = I + 1
       IF (158 - I) 10, 5, 5
   10 I = 2
       D(1) = 0.0
   15 D(I) = D(I - 1) + (0.005*(A(I) + A(I -1)))
       I = I + 1
       IF (158 - I) 20, 15, 15
   20 A(1) = 0.0
       U = 0.01
       I = 2
   25 A(I) = ((COS(U))*(D(I)))/((SIN(U))*((DELTA+1.0-(COS(U)))**3))
       U = U + 0.01
       I = I + 1
       IF (158 - I) 30, 25, 25
   30 I = 2
       E(1) = 0.0
   35 E(I) = E(I - 1) + (0.005*(A(I) + A(I - 1)))
       I = I + 1
       IF (158 - I) 40, 35, 35
   40 I = 1
   45 E(I) = E(158) - E(I)
       I = I + 1
       IF (158 - I) 50, 45, 45
   50 I = 1
       U = 0.00
   55 A(I) = ((SIN (U))*(COS (U))*(E(I)))
       U = U + 0.01
       I = I + 1
       IF (158 - I) 60, 55, 55
   60 I = 2
       F(1) = 0.0
   65 F(I) = F(I-1) +((0.005)*((A(I-1)) + (A(I))))
       I = I + 1
       IF (158 - I) 70, 65, 65
   70 I = 158
   71 PUNCH 103,I, D(I), F(I)
  103 FORMAT (I6, F12.4,F12.1)
  105 GO TO 1
       END
```

TABLE C-1 (continued)

δ_1/r	$I_1(\delta_1/r, \pi/2)$	$I_3(\delta_1/r)$
0.02	3.0100	290.0000
0.01	3.6604	1201.5975
0.007	4.0023	2478.7
0.005	4.3281	4890.8
0.004	4.5454	7667.8
0.003	4.8267	13672.6
0.002	5.2248	30820.7
0.0015	5.5079	54804.7
0.0010	5.9072	123075.3
0.0007	6.2581	250326.5
0.0005	6.5882	487879.4
0.0003	7.0860	1337422.9
0.0002	7.4761	2959405.8
0.0001	8.1222	11213855.0

The numerical values of Table C-1 were then simply fitted in algebraic equations. The results are as follows:

for $0.0198 \leqslant I_3(\delta_1/r) \leqslant 11213855.0$

$$\ln(\delta_1/r) = -1.3832 - 0.3980 \ln\left[I_3(\delta_1/r)\right] - 0.0104 \left\{\ln\left[I_3(\delta/r)\right]\right\}^2 + 0.0003547 \left\{\ln\left[I_3(\delta_1/r)\right]\right\}^3 \qquad \text{(C-1)}$$

for $0 < \delta_1/r \leqslant 0.01$,

$$I_1(\delta_1/r, \pi/2) = -0.8321 - 0.97464 \ln(\delta_1/r) \qquad \text{(C-2)}$$

for $0.01 < \delta_1/r$,

$$I_1(\delta_1/r, \pi/2) = 0.3874 - 0.2835 \ln(\delta_1/r) + 0.1328 \left[\ln(\delta_1/r)\right]^2 + 0.0087 \left[\ln(\delta_1/r)\right]^3 \qquad \text{(C-3)}$$

APPENDIX D

FLOW DIAGRAM AND FORTRAN PROGRAM

FOR DIGITAL COMPUTATION

FLOW DIAGRAM FOR THE FORTRAN PROGRAM

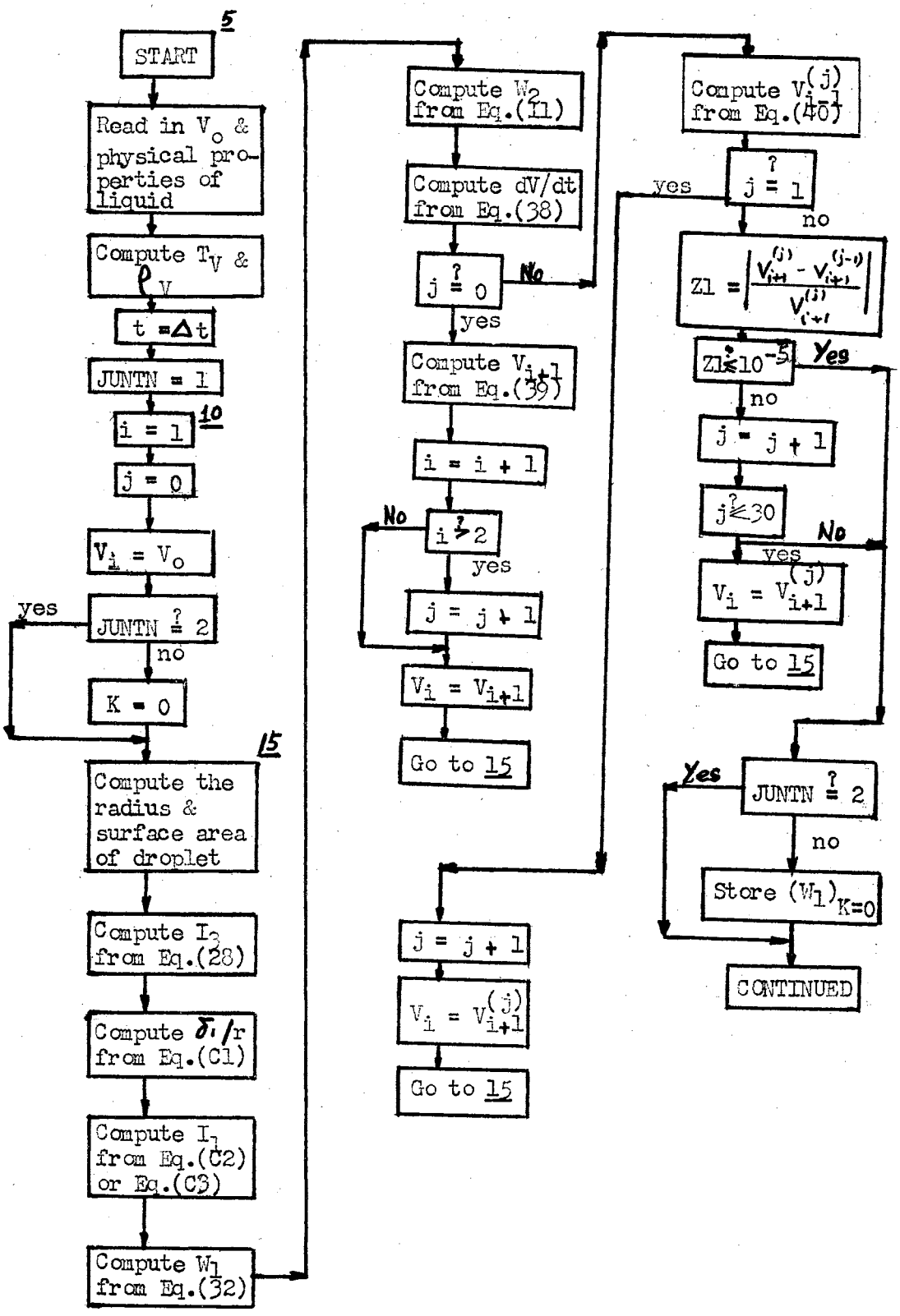

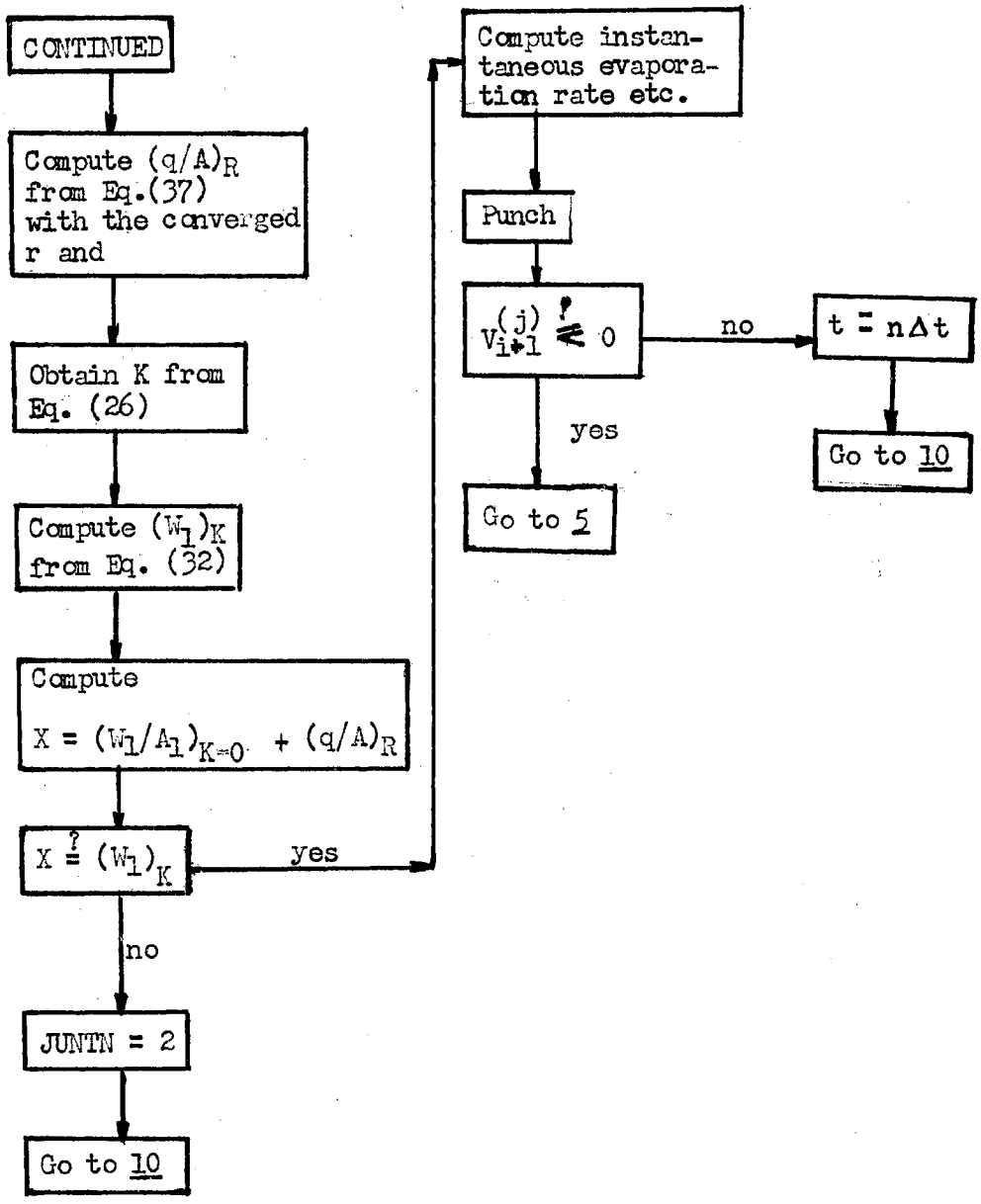
CONTINUED
Compute $(q/A)_R$ from Eq.(37) with the converged r and
Obtain K from Eq. (26)
Compute $(W_1)_K$ from Eq. (32)
Compute
$X = (W_1/A_1)_{K=0} + (q/A)_R$
$X \stackrel{?}{=} (W_1)_K$
yes
no
JUNTN = 2
Go to 10
Compute instantaneous evaporation rate etc.
Punch
$V_{i+1}^{(j)} \stackrel{?}{\leq} 0$
no
yes
$t = n\Delta t$
Go to 10
Go to 5

```
C     BOILING STUDIES PROGRAM NO. 0
    1 FORMAT(F10.3,F10.2,F10.3,F10.4,F10.4,F10.7,F10.5)
    2 FORMAT(F10.3,3F10.7)
    3 FORMAT(F10.7,F10.6,2F10.7)
   60 FORMAT(1H2,3HTS=F10.3,9H  MOL WT=F8.2,5H  TP=8.2,5H  VO=F8.5//)
 2050FORMAT(1H-,78H   TIME    RADIUS      INS VOL     INS RATE      J     DE
    1LTA      SQRAD       AV DETA)
 2060FORMAT(1H ,82H       COND Q     RADQ             WAQ1       WAQ2
    1RADK         Q1             QRAD2)
 2000FORMAT(1H0F8.2,1XF8.4,2XF10.5,2XE11.5,2XI3,2XF10.7,5XE10.4,2XE10.4
    1)
 2010FORMAT (1H ,2H  F10.4,2XE11.5,2XF10.4,2XF10.5,2XF8.4,5XE10.4,2XE10
    1.4)
  105 FORMAT(1H ,5HEROR=E14.8,9H      VOL=E14.8,7H  NO J=I3/)
  106 FORMAT(1H ,3HZ2=E14.8,6H RADK=F10.5,7H  NO I=I3/)
  300 FORMAT(1H0,15HTOTL VAP TIME= F8.3,15H   TOTL HEAT = E14.8)
  301 FORMAT(1H ,12H FINL RADUS=E14.8,12H   FINL VOL=E14.8)
  400 READ INPUT TAPE5,1,TS,VAPH,WT,D,RHOL,VO,EPSL
      READ INPUT TAPE5,2,TP,COND,VISC,CP
      READ INPUT TAPE5,3,EROR,DELAT,DELTT,VLIMT
      WRITE OUTPUT TAPE6,60,TS,WT,TP,VO
      WRITE OUTPUT TAPE6,205
      WRITE OUTPUT TAPE6,206
      TV=(TS+TP)/2.
      RHOV=WT/(82.06*(TV+273.))
      CPP=VAPH+(((TP-TS)/2.)*CP)
      X1=((18.*VISC)*COND)/((980.*RHOV)*((RHOL-RHOV)*CPP))
      WA2R=(WT*D)/(82.06*(TS+273.))
      BOLZ=1.355*((((TP+273.)/1000.)**4)-(((TS+273.)/1000.)**4))
      QRAD=BOLZ/(1.0/0.682+1.0/EPSL-1.0)
      QRAD2=BOLZ/(1.0/0.318+1.0/EPSL-1.0)
      TIME=DELAT
      V=VO
      V1=VO
      QALL=0.0
   47 RADK=0.0
      JUNTN=1
      I=0
   90 VN=V1
      GO TO (48,49),JUNTN
   48 X2=X1*(TP-TS)
      WA0R=(6.283185*COND*(TP-TS))/CPP
      WA1R=WA0R
      GO TO 95
   49 X2=X1*((TP-TS)*(1.+RADK))
      WA1R=((6.283185*COND)*((TP-TS)*(1.+RADK)))/CPP
   95 J=0
```

```
      KEY=1
  100 IF(V1)76,76,5
    5 R=(0.23873241*V1)**0.33333333
      A=12.566371*(R**2)
      S3=(R**3)/X2
      S3=LOGF(S3)
      THIK=-1.383204+S3*(S3*(0.0003547*S3-0.010403)-0.398007)
      IF (THIK+4.9627)14,14,15
   14 S1=(-0.8321)+(0.97464*(-THIK))
      GO TO 16
   15 S1=0.3874+THIK*(THIK*(0.0087*THIK+0.1328)-0.2835)
   16 GO TO (36,37),JUNTN
   36 WA0=WA0R*(R*S1)
      WA1=WA0
      GO TO 34
   37 WA1=WA1R*(R*S1)
      WA0=WA0R*(R*S1)
   34 WA2=(WA2R*(0.5*A))/R
      GO TO (72,85),KEY
   72 FUN1=(WA1+WA2)/RHOL
      IF (J-1)20,25,30
   20 V2=V1-(DELAT*FUN1)
      J=J+1
      V1=V2
      GO TO 100
   25 FUN2=(WA1+WA2)/RHOL
      V2=V-((0.5*DELAT)*(FUN1+FUN2))
      J=J+1
      V1=V2
      FUN=FUN1
      GO TO 100
   30 FUN3=(WA1+WA2)/RHOL
      V3=V-((0.5*DELAT)*(FUN+FUN3))
      Z1=ABSF(((ABSF(V3))-(ABSF(V2)))/(ABSF(V3)))
      IF (Z1-EROR)31,31,32
   32 J=J+1
      IF (30-J)41,41,43
   41 WRITE OUTPUT TAPE6,105,Z1,V3,J
      GO TO 31
   43 V2=V3
      V1=V3
      GO TO 100
```

```
   31 IF (V3)76,76,73
   73 V1=V3
      KEY=2
      GO TO 100
   85 WAQ0=WA0*CPP
      WAQ1=WA1*CPP
      WAQ2=WA2*VAPH
      DELTA=(EXPF(THIK))*R
      QRAD1=QRAD*0.5*A
      QRAD3=QRAD2*0.5*A
      ADELTA=1.0/((2.0*(DELTA+R))/(R**2)*LOGF((DELTA+R)/DELTA)-2.0/R)
      QC=(COND*(TP-TS)*A)/(4.0*ADELTA)
      RADK=QRAD1/QC
      I=I+1
      IF(I-1)98,98,97
   97 Q1=QRAD1+QRAD3+QC
      Q2=WAQ1+WAQ2
      Z2=ABSF((Q2-Q1)/Q2)
      IF(Z2-0.01)21,21,22
   22 I=I+1
      IF(20-I)51,51,52
   51 WRITE OUTPUT TAPE6,106,Z2,RADK,I
      GO TO 21
   52 RADK=((Q1+Q2)/2.0-WAQ2)/QC-1.0
      QRAD2=WAQ2/(0.5*A)
   98 JUNTN=2
      V1=VN
      GO TO 90
   21 RATE=(V-V3)/DELTA
      QALL=QALL+Q2
      WRITE OUTPUT TAPE6,200,TIME,R,V3,RATE,J,DELTA,Q2,ADELTA
      WRITE OUTPUT TAPE6,201,WAQ0,QRAD1,WAQ1,WAQ2,RADK,Q1,QRAD3
      IF(V3-VLIMT)91,91,77
   91 IF(DELAT-DELTT)77,77,82
   82 DELAT=DELAT/2.0
   77 V=V3
      V1=V3
      TIME=TIME+DELAT
      GO TO 47
   76 WRITE OUTPUT TAPE6,300,TIME,QALL
      WRITE OUTPUT TAPE6,301,R,V3
      GO TO 400
      END
*     DATA
```

TABLE D-1

TYPICAL COMPUTER OUTPUT*

TS# 100.000 MOL WT# 18.00 TP# 500.00 VO# 0.05000

TIME	RADIUS	INS VOL	INS RATE	J	DELTA	SQRAD	AV DETA
COND	Q	RADQ	WAQ1	WAQ2	RADK	Q1	QRAD2
2.00	0.2258	0.04823	0.26576E 01	2	0.0006668	0.5110E 00	0.2330E-01
0.2590	0.97212E-01		0.3523	0.15875	0.3753	0.5150E 00	0.1587E-00
4.00	0.2230	0.04648	0.26029E 01	2	0.0006712	0.5038E 00	0.2311E-01
0.2549	0.94849E-01		0.3470	0.15681	0.3721	0.5046E 00	0.1549E-00
6.00	0.2203	0.04476	0.25475E 01	2	0.0006747	0.4955E-00	0.2290E-01
0.2508	0.92497E-01		0.3406	0.15485	0.3688	0.4943E-00	0.1510E-00
98.00	0.0193	0.00003	0.10998E-01	6	0.0017543	0.2194E-01	0.5639E-02
0.0078	0.70973E-03		0.0084	0.01356	0.0908	0.2208E-01	0.1356E-01
98.50	0.0156	0.00002	0.76159E-02	8	0.0018628	0.1685E-01	0.5182E-02
0.0056	0.46391E-03		0.0059	0.01097	0.0835	0.1698E-01	0.1096E-01
99.00	0.0125	0.00001	0.39063E-02	11	0.0019930	0.1287E-01	0.4800E-02
0.0038	0.29626E-03		0.0041	0.00876	0.0773	0.1292E-01	0.8787E-02

TOTL VAP TIME# 99.500 TOTL HEAT # 0.14936695E 02
FINL RADUS#0.12465576E-01 FINL VOL#0.81138213E-05

*The computer output represents only a selected group of computed numbers. See next page for the identification of each individual item listed in the table. The numbers are printed in two lines as a group for one time increment computation.

Case Identification

TS	normal boiling point of liquid, °C
MOL WT	molecular weight of fluid, gm
TP	plate temperature, °C
VO	initial volume of droplet, ml

Number Identification

i. First line:

TIME	elapsed time since start of evaporation, $t_o + n\ \Delta t$, sec
RADIUS	instantaneous radius of droplet, cm
INS VOL	instantaneous volume, ml
INS RATE	instantaneous evaporation rate, ml/sec
J	number of iterations for finite difference convergence
DELTA	instantaneous distance from plate to bottom center of droplet, cm
SQRAD	instantaneous heat removal from droplet, cal/sec (WAQ1 + WAQ2)
AV DETA	mean value for conductive film thickness computed by equation (31), cm

ii. Second line:

COND Q	instantaneous heat transfer rate to droplet by conduction only, cal/sec
RAD Q	instantaneous transfer rate by radiation to bottom of droplet, cal/sec
WAQ1	heat removal by evaporation from the bottom surface of droplet, cal/sec
WAQ2	heat removal by diffusion from the upper surface of droplet, cal/sec
RADK	instantaneous ratio between radiative heat transfer to bottom of droplet and conductive heat transfer

Q1	instantaneous total heat transfer rate to droplet, cal/sec
QRAD2	modified value for heat removal by diffusion from upper surface

Final Message

TOTL VAP TIME	total evaporation time of droplet, sec
TOTL HEAT	total heat transferred from plate to droplet for complete vaporization of droplet, cal
FINL RADUS	radius of droplet corresponding to last finite time increment prior to disappearance, cm
FINL VOL	volume of droplet corresponding to FINL RADUS, ml

APPENDIX E

EMPIRICAL CORRELATIONAL GROUPS

TABLE E1

EMPIRICAL CORRELATIONAL GROUPS

Fluid	r_o cm	T_p °C	τ sec	X_1	$X_2 \times 10^3$	$Y_{obs} \times 10^2$ (gm/sec,	$Y_{cal} \times 10^2$ cm^2)	Deviation percent
Carbon tetra-chloride	0.129	188.6	24.0	0.549	0.553	0.769	0.775	- 0.76
		215.0	22.5	0.591	0.732	0.822	0.866	- 5.41
		255.5	19.7	0.645	1.050	0.935	1.005	- 7.58
		314.1	16.1	0.689	1.605	1.149	1.189	- 3.49
		451.36	12.2	0.784	3.431	1.509	1.735	- 14.97
	0.114	188.6	21.0	0.518	0.553	0.781	0.738	5.52
		215.0	19.5	0.557	0.732	0.840	0.826	1.65
		255.5	17.4	0.608	1.050	0.942	0.962	- 2.09
		314.5	14.4	0.650	1.610	1.142	1.144	- 0.17
		451.36	10.6	0.739	3.431	1.543	1.682	- 9.00
	0.101	188.6	18.3	0.488	0.554	0.796	0.703	11.76
		215.0	17.5	0.525	0.732	0.830	0.789	5.00
		255.5	14.5	0.573	1.050	0.999	0.921	7.88
		314.5	11.6	0.613	1.610	1.255	1.100	12.29
		451.36	9.3	0.699	3.431	1.570	1.635	- 4.10
Ethyl alcohol	0.152	188.6	43.9	0.188	0.129	0.255	0.251	1.71
		215.0	39.0	0.204	0.173	0.287	0.279	2.71
		314.1	26.5	0.245	0.388	0.423	0.379	10.60
		395.4	19.8	0.264	0.630	0.566	0.460	18.82
		451.36	17.7	0.274	0.835	0.633	0.520	17.88
	0.135	188.6	38.1	0.177	0.129	0.262	0.238	8.89
		215.0	33.6	0.192	0.173	0.297	0.266	10.36
		314.5	22.6	0.231	0.389	0.442	0.363	17.88
		395.4	17.5	0.249	0.630	0.569	0.442	22.37
		451.36	15.9	0.259	0.835	0.625	0.502	19.72

(Continued)

TABLE E1 (Continued)

Fluid	r_o cm	T_p °C	τ sec	X_1	$X_2 \times 10^3$	$Y_{obs} \times 10^2$ (gm/sec, cm^2)	$Y_{cal} \times 10^2$	Deviation percent
	0.116	188.6	31.9	0.164	0.130	0.268	0.224	16.73
		215.0	28.5	0.178	0.173	0.301	0.250	16.97
		314.5	19.1	0.214	0.389	0.449	0.343	23.55
		395.4	15.3	0.231	0.630	0.562	0.421	25.19
		451.36	13.3	0.240	0.835	0.646	0.480	25.74
Benzene	0.161	314.1	18.5	0.497	0.726	0.710	0.754	- 6.26
		395.4	14.6	0.543	1.126	0.902	0.903	- 0.18
		188.6	31.1	0.375	0.262	0.422	0.501	- 18.65
		255.5	23.5	0.452	0.487	0.560	0.644	- 15.14
		451.36	12.7	0.565	1.448	1.036	1.006	2.91
	0.144	395.4	12.6	0.514	1.126	0.933	0.871	6.70
		188.6	27.4	0.355	0.262	0.430	0.478	- 11.15
		255.5	19.8	0.428	0.487	0.597	0.617	- 3.44
		314.5	16.6	0.472	0.728	0.709	0.725	- 2.23
		451.36	11.1	0.536	1.448	1.064	0.972	8.68
	0.124	188.6	23.2	0.330	0.262	0.438	0.448	- 2.20
		255.5	17.1	0.397	0.487	0.594	0.581	2.24
		314.5	13.5	0.437	0.728	0.753	0.685	9.00
		395.4	10.4	0.477	1.126	0.973	0.827	15.02
		451.36	9.4	0.497	1.448	1.084	0.926	14.56
Water	0.140	451.36	50.1	0.117	0.406	0.268	0.234	12.78
		420.75	52.2	0.114	0.341	0.258	0.215	16.71
		395.40	54.4	0.111	0.293	0.247	0.200	19.01
		314.50	63.9	0.100	0.167	0.211	0.157	25.36

(Continued)

TABLE E1 (Continued)

Fluid	r_o cm	T_p °C	τ sec	X_1	$X_2 \times 10^3$	$Y_{obs} \times 10^2$ (gm/sec, cm^2)	$Y_{cal} \times 10^2$	Deviation percent
	0.168	451.36	60.5	0.128	0.406	0.267	0.247	7.39
		420.75	64.7	0.125	0.341	0.249	0.227	8.76
		395.40	66.0	0.122	0.293	0.244	0.213	12.97
		314.50	82.6	0.109	0.167	0.195	0.168	13.77
	0.199	451.36	72.3	0.139	0.406	0.264	0.260	1.50
		420.75	78.6	0.136	0.341	0.243	0.240	1.09
		395.40	81.7	0.133	0.293	0.234	0.225	3.75
		314.10	95.7	0.119	0.167	0.199	0.179	10.15
n-Octane	0.159	215.0	18.13	0.422	0.325	0.477	0.570	- 19.58
		255.5	16.5	0.474	0.482	0.525	0.670	- 27.65
		314.1	13.4	0.516	0.725	0.648	0.776	- 19.83
		395.4	10.1	0.554	1.101	0.858	0.911	- 6.20
		451.36	8.8	0.549	1.389	0.989	0.974	1.54
	0.144	215.0	16.20	0.402	0.324	0.485	0.548	- 12.85
		255.5	15.1	0.452	0.482	0.522	0.644	- 23.43
		314.5	12.1	0.492	0.727	0.651	0.749	- 15.15
		395.4	8.7	0.529	1.101	0.904	0.881	2.26
		451.36	7.7	0.524	1.389	1.025	0.944	7.88
	0.125	215.0	14.4	0.374	0.324	0.474	0.515	- 8.66
		255.5	13.2	0.421	0.482	0.516	0.607	- 17.68
		314.5	10.3	0.458	0.727	0.660	0.709	- 7.41
		395.4	7.6	0.492	1.101	0.893	0.838	6.12
		451.36	6.7	0.488	1.389	1.016	0.9018	11.30

APPENDIX F

EXPERIMENTAL DATA

TABLE F1

DROPLET EVAPORATION TIME, SECONDS

TC #	1	2	3	4	5	Avg.
TP, °C	145	144	144	143	143.5	144

Trial	13 Gage Needle					16 Gage Needle				
No.	CCl_4	EtOH	C_6H_6	H_2O	$n\text{-}C_8H_{18}$	CCl_4	EtOH	C_6H_6	H_2O	$n\text{-}C_8H_{18}$
	26.5°C	26.5°C	26.5°C	26.5°C	31°C	26.5°C	26.5°C	26.5°C	26.5°C	31°C
1	0.80	1.50	0.95	9.27	6.72	0.70	1.22	0.93	**8.62**	6.00
2	0.75	1.40	1.00	8.65	6.40	0.72	1.25	0.91	**7.60**	5.90
3	0.79	1.40	1.00	10.50	6.50	0.70	1.18	0.91	**7.05**	5.92
4	0.80	1.40	1.02	9.55	6.75	0.72	1.28	0.90	**9.50**	5.90
5	0.73	1.50	1.00	8.35	6.79	0.73	1.20	0.93	**7.45**	5.97
Avg.	0.77	1.44	1.00	9.06	6.63	0.71	1.23	0.92	**8.05**	5.94
	17 Gage Needle					21 Gage Needle				
1	0.71	1.22	0.88	8.02	5.79	0.55	0.90	0.75	**7.18**	3.67
2	0.65	1.20	0.82	7.45	5.77	0.52	1.00	0.80	**5.85**	3.91
3	0.69	1.17	0.90	6.62	5.67	0.58	0.93	0.70	**7.87**	3.91
4	0.65	1.20	0.87	7.45	5.83	0.52	0.95	0.75	**7.28**	3.87
5	0.68	1.22	0.90	7.65	5.55	0.57	0.90	0.78	**8.20**	3.75
Avg.	0.64	1.20	0.87	7.44	5.72	0.55	0.94	0.75	**7.28**	3.82

TABLE F1 (Continued)

TC #	1	2	3	4	5	Avg.
Tp, °C	171.0	170.5	170.5	168.3	170.5	170.0

Trial No.	13 Gage Needle					16 Gage Needle				
	CCl_4 33°C	EtOH 26°C	C_6H_6 26°C	H_2O 26°C	n-C_8H_{18} 32°C	CCl_4 33°C	EtOH 26°C	C_6H_6 26°C	H_2O 26°C	n-C_8H_{18} 32°C
1	25.50	1.35	1.00	4.44	1.30	23.17	1.12	0.83	3.95	1.26
2	25.56	1.37	1.00	4.15	1.36	22.59	1.05	0.84	3.43	1.30
3	24.62	1.33	0.92		1.41	22.43	1.05	0.87	3.40	1.20
4	23.96	1.31	0.95		1.29	20.62	1.03	0.82	3.55	1.28
5	25.00	1.39	0.92		1.33	20.29	1.12	0.90	3.56	1.20
Avg.	24.93	1.35	0.96	4.35	1.34	21.82	1.07	0.85	3.58	1.25
	17 Gage Needle					21 Gage Needle				
1	20.61	1.09	0.74	2.90	1.11	18.32	0.85	0.69	2.15	0.88
2	20.26	1.03	0.72	3.20	1.13	18.89	0.85	0.65	2.73	0.87
3	21.56	1.15	0.79	2.85	1.12	19.35	0.86	0.70	2.62	0.92
4	18.35	1.05	0.81	2.60	1.15	19.35	0.91	0.63	2.19	0.88
5	21.00	1.00	0.76	2.73	1.15	18.25	0.89	0.67	2.35	0.88
Avg.	20.36	1.06	0.76	2.84	1.13	18.83	0.87	0.67	2.41	0.89

TABLE F1 (Continued)

TC #	1	2	3	4	5	Avg.
Tp, °C	181.5	181.0	181.0	178.8	180.7	180.6

Trial	13 Gage Needle					16 Gage Needle				
No.	CCl_4	EtOH	C_6H_6	H_2O	n-C_8H_{18}	CCl_4	EtOH	C_6H_6	H_2O	n-C_8H_{18}
	27°C	29°C	28.5°C	32.5°C	31°C	27°C	29°C	28.5°C	32.5°C	31°C
1	23.55	44.13	28.80	1.53	0.92	21.20	40.51	24.95	1.40	0.82
2	23.47	44.02	28.56	1.86	0.87	22.00	40.91	24.20	1.41	0.86
3	23.75	44.51	28.00	1.52	0.87	20.90	40.25	24.83	1.36	0.83
4	23.10	44.58	26.85	1.67	0.90	22.10	40.36	24.70	1.37	0.82
5	23.40	44.59	27.00	1.52	0.89	22.00	40.42	24.65	1.37	0.83
Avg.	23.45	44.37	27.84	1.62	0.89	21.64	40.49	24.63	1.38	0.83
	17 Gage Needle					21 Gage Needle				
1	21.00	38.20	21.76	1.18	0.82	18.06	33.55	20.60	0.68	0.61
2	20.91	38.10	21.65	1.22	0.80	18.05	33.67	21.10	0.68	0.66
3	20.26	38.90	23.48	1.30	0.82	18.00	33.53	18.90	0.69	0.63
4	21.00	39.00	24.20	1.21	0.81	18.30	33.61	19.40	0.71	0.65
5	20.70	38.95	21.80	1.20	0.81	18.10	33.75	21.00	0.72	0.62
Avg.	20.77	38.63	22.58	1.22	0.81	18.10	33.62	20.20	0.70	0.63

TABLE F1 (Continued)

TC #	1	2	3	4	5	Avg.
Tp, °C	189.3	189.0	189.0	187.0	188.7	188.6

Trial	13 Gage Needle					16 Gage Needle				
No.	CCl_4	EtOH	C_6H_6	H_2O	n-C_8H_{18}	CCl_4	EtOH	C_6H_6	H_2O	n-C_8H_{18}
	28°C	28.5°C	28.5°C	31°C	30°C	28°C	28.5°C	28.5°C	31°C	30°C
1	23.74	43.92	30.80	1.15	0.80	21.95	38.90	28.29	1.10	0.72
2	24.06	43.85	31.10	1.18	0.82	21.90	38.90	28.92	1.09	0.73
3	24.00	44.40	30.82	1.35	0.80	21.46	39.79	28.52	0.95	0.72
4	24.10	43.90	31.69	1.21	0.80	21.95	39.26	28.63	1.00	0.72
5	24.10	43.50	31.10	1.23	0.85	21.63	39.39	28.89	1.02	0.75
Avg.	24.00	43.91	31.10	1.22	0.81	21.78	39.25	28.65	1.03	0.73
	17 Gage Needle					21 Gage Needle				
1	21.02	37.94	27.84	0.90	0.70	18.38	32.21	23.12	0.65	0.63
2	20.92	37.55	27.30	1.00	0.72	18.30	32.46	23.02	0.70	0.60
3	21.19	38.75	27.25	0.92	0.73	18.20	31.62	23.19	0.70	0.61
4	20.76	38.79	27.32	0.92	0.70	18.22	31.93	22.85	0.66	0.64
5	21.03	37.50	27.50	0.95	0.70	18.25	31.58	23.62	0.72	0.60
Avg.	21.00	38.11	27.44	0.94	0.71	18.27	31.96	23.16	0.69	0.62

TABLE F1 (Continued)

TC #	1	2	3	4	5	Avg.
Tp, °C	192.5	192.5	192.5	190.5	192.5	192.5

Trial	13 Gage Needle					16 Gage Needle				
No.	CCl_4	EtOH	C_6H_6	H_2O	n-C_8H_{18}	CCl_4	EtOH	C_6H_6	H_2O	n-C_8H_{18}
	29°C	29°C	29°C	29°C	29.5°C	29°C	29°C	29°C	29°C	29.5°C
1	23.85	42.86	30.35	2.00	0.87	21.65	38.38	28.12	0.95	0.70
2	23.92	43.30	30.48	3.40	0.87	21.50	38.32	28.19	0.85	0.75
3	24.00	42.95	30.69	1.80	0.89	22.29	38.35	28.41	0.85	0.72
4	23.72	42.38	31.05		0.84	21.77	38.45	28.00		0.71
5	23.90	42.73	30.67		0.86	22.40	38.41	28.15		0.70
Avg.	23.88	42.84	30.65	2.40	0.87	21.92	38.38	28.17	0.88	0.72
	17 Gage Needle					21 Gage Needle				
1	21.32	37.78	25.97	0.80	0.66	18.10	30.42	22.65	0.65	0.61
2	21.36	37.63	25.92	0.85	0.69	18.10	30.21	22.60	0.55	0.60
3	21.52	38.19	25.52	0.90	0.69	18.10	30.84	22.50	0.60	0.61
4	21.00	37.98	26.00		0.69	18.15	30.93	22.45		0.60
5	21.07	37.20	26.24		0.60	18.50	31.40	22.65		0.61
Avg.	21.25	37.76	25.93	0.85	0.67	18.19	30.76	22.57	0.60	0.61

TABLE F1 (Continued)

TC #	1	2	3	4	5	Avg.
Tp, °C	215.75	215.75	215.50	213.0	215.0	215

Trial	13 Gage Needle					16 Gage Needle				
No.	CCl_4	EtOH	C_6H_6	H_2O	$n\text{-}C_8H_{18}$	CCl_4	EtOH	C_6H_6	H_2O	$n\text{-}C_8H_{18}$
	26.5°C	26.5°C	26.5°C	26.5°C	33°C	26.5°C	26.5°C	26.5°C	26.5°C	33°C
1	22.42	39.43	28.10	0.90	18.12	20.82	34.45	26.25	1.40	16.90
2	22.37	38.73	28.12	1.42	18.26	20.51	34.66	26.45	1.30	17.04
3	22.52	39.18	28.39		17.93	20.71	34.00	26.12		16.99
4	22.40	38.73	27.79		18.00	20.62	34.70	26.05		16.70
5	22.57	39.00	28.27		18.35	20.15	35.10	26.19		17.03
Avg.	22.46	39.01	28.13	1.16*	18.13	20.56	34.58	26.21	1.35*	16.93
	17 Gage Needle					21 Gage Needle				
1	19.72	33.70	24.49	1.23	16.32	17.75	28.45	20.75	0.95	14.42
2	19.52	33.70	25.30	1.12	16.45	17.70	28.35	20.76	0.75	14.22
3	19.41	33.30	24.60		16.32	17.55	28.66	21.00		14.50
4	19.57	33.81	24.77		16.64	17.45	28.55	20.78		14.29
5	19.40	33.50	25.10		16.36	17.22	28.50	20.43		14.49
Avg.	19.52	33.60	24.85	1.18*	16.21	17.53	28.50	20.72	0.85*	14.38

* Transitional boiling

TABLE F1 (Continued)

TC #	1	2	3	4	5	Avg.
Tp, °C	255.5	255.5	255.5	253.3	255.5	255.5

Trial	13 Gage Needle					16 Gage Needle				
No.	CCl_4	EtOH	C_6H_6	H_2O	n-C_8H_{18}	CCl_4	EtOH	C_6H_6	H_2O	n-C_8H_{18}
	26°C	25.5°C	27°C	28°C	30°C	26°C	25.5°C	27°C	28°C	30°C
1	19.96	33.69	23.70	75.70	16.50	17.68	30.40	21.93	70.7	15.73
2	19.82	33.85	23.20	77.10	16.44	17.05	30.21	21.88	64.2	15.84
3	19.47	33.50	23.58	74.60	16.60	17.40	30.47	22.00	68.8	15.81
4	19.65	33.80	23.60	72.10	16.45	17.72	30.00	21.65	71.6	15.89
5	19.85	33.47	23.20	75.30	16.45	17.81	30.60	21.83	74.3	15.90
Avg.	19.75	33.66	23.46	74.96	16.49	17.53	30.34	21.86	69.9	15.83
	17 Gage Needle					21 Gage Needle				
1	17.31	29.50	20.12	65.25	15.15	14.43	25.43	17.05	59.0	13.25
2	17.37	29.10	19.40	71.30	14.99	14.86	25.25	17.00	51.5	13.06
3	17.45	29.55	20.02	70.40	15.14	14.28	25.66	17.26	62.3	13.14
4	17.35	29.19	19.42	70.45	15.20	14.60	25.50	17.13	56.8	13.28
5	17.56	29.42	22.00	61.90	14.90	14.65	25.60	17.00	53.2	13.30
Avg.	17.41	29.35	19.79	67.90	15.08	14.56	25.49	17.09	56.56	13.21

TABLE F1 (Continued)

TC #	1	2	3	4	5	Avg.
Tp, °C	314.5	314.5	314.8	312.3	314.75	314.1

Trial	13 Gage Needle					16 Gage Needle				
No.	CCl_4	EtOH	C_6H_6	H_2O	n-C_8H_{18}	CCl_4	EtOH	C_6H_6	H_2O	n-C_8H_{18}
	30.5°C	29°C	31°C	29°C	28°C	30.5°C	29°C	21°C	29°C	28°C
1	16.12	26.83	18.22	96.30	13.47	14.70	23.87	16.92	86.73	12.87
2	16.00	26.59	18.44	95.92	13.20	14.42	23.63	16.90	85.29	12.70
3	16.08	26.56	18.57	94.27	13.41	14.85	23.80	17.00	86.09	12.66
4	16.11	26.33	18.55	96.90	13.22	14.45	23.70	17.21	86.17	12.82
5	16.00	26.13	18.70	95.26	13.52	14.41	23.44	17.12	87.00	12.67
Avg.	16.06	26.49	18.50	95.73	13.36	14.57	23.69	17.03	86.26	12.74
	17 Gage Needle					21 Gage Needle				
1	14.38	22.36	16.70	81.91	12.13	11.48	18.86	13.32	62.80	10.21
2	14.20	22.37	16.71	82.36	12.14	11.55	18.92	13.53	63.05	10.50
3	14.33	22.79	16.55	84.00	12.02	11.80	19.40	13.62	65.00	10.34
4	14.50	22.41	16.85	83.13	12.10	11.69	19.35	13.55	63.72	10.40
5	14.40	23.00	16.42	81.87	12.10	11.50	19.00	13.42	64.86	10.22
Avg.	14.36	22.59	16.65	82.65	12.10	11.60	19.11	13.49	63.89	10.33

TABLE F1 (Continued)

TC #	1	2	3	4	5	Avg.
Tp, °C	396.0	396.25	396.25	392.5	396.0	395.4

Trial	13 Gage Needle					16 Gage Needle				
No.	CCl_4	EtOH	C_6H_6	H_2O	n-C_8H_{18}	CCl_4	EtOH	C_6H_6	H_2O	n-C_8H_{18}
	26°C	26°C	25°C	28°C	29°C	26°C	26°C	25°C	28°C	29°C
1	12.92	19.82	14.35	81.25	9.99	11.35	17.87	13.27	70.00	9.48
2	12.59	20.50	14.70	80.40	10.36	11.00	17.75	13.02	70.91	9.20
3	12.82	20.08	14.73	83.46	10.07	11.41	17.95	13.14	70.98	9.12
4	12.55	19.29	14.37	81.75	10.21	11.75	18.10	13.00	70.30	9.29
5	12.94	19.47	14.70	81.51	9.80	11.50	18.20	13.05	71.37	9.18
Avg.	12.76	19.83	14.57	81.67	10.09	11.40	18.00	13.10	70.71	9.25
	17 Gage Needle					21 Gage Needle				
1	11.00	17.50	12.68	66.22	8.85	9.55	15.02	10.51	54.74	7.59
2	11.06	17.42	12.70	65.27	8.65	9.30	15.10	10.30	54.12	7.52
3	11.15	17.50	12.72	65.48	8.75	9.51	15.16	10.41	55.21	7.51
4	10.75	17.49	12.70	66.82	8.63	9.47	15.40	10.47	55.47	7.76
5	11.20	17.78	12.52	66.52	8.60	9.70	15.61	10.49	54.50	7.80
Avg.	11.02	17.54	12.66	66.02	8.70	9.51	15.26	10.44	54.41	7.64

TABLE F1 (Continued)

TC #	1	2	3	4	5	Avg.
Tp, °C	420.0	420.0	421.75	420.0	422.0	420.75

Trial	13 Gage Needle					16 Gage Needle				
No.	CCl_4	EtOH	C_6H_6	H_2O	n-C_8H_{18}	CCl_4	EtOH	C_6H_6	H_2O	n-C_8H_{18}
	27°C	26°C	27.5°C	26.5°C	26°C	27°C	26°C	26.5°C	26.5°C	26°C
1	13.18	19.16	13.93	78.97	9.70	11.75	17.78	12.48	**68.16**	**8.60**
2	13.17	19.40	13.80	78.07	9.40	12.02	17.25	12.78	**67.00**	**8.80**
3	13.14	19.45	13.66	78.41	9.50	11.70	17.15	12.78	**66.86**	**8.85**
4	13.36	19.27	13.70	78.57	9.31	12.00	17.55	12.47	**66.86**	**8.90**
5	13.30	19.70	13.91	79.20	9.40	11.78	17.50	12.62	**68.16**	**8.50**
Avg.	13.22	19.40	13.80	78.64	9.46	11.85	17.45	12.63	**67.41**	**8.73**
	17 Gage Needle					21 Gage Needle				
1	11.20	17.46	12.29	64.95	8.50	10.06	14.80	10.32	**53.00**	**7.19**
2	11.32	17.10	12.48	64.72	8.15	9.88	15.15	10.40	**50.83**	**7.31**
3	11.20	17.00	12.15	64.60	8.16	10.00	15.25	10.32	**53.22**	**7.22**
4	11.50	17.75	12.60	64.95	8.21	10.10	14.92	10.31	**51.12**	**7.29**
5	11.47	17.19	12.20	64.27	8.19	10.10	14.95	10.40	**52.63**	**7.25**
Avg.	11.34	17.30	12.34	64.70	8.24	10.03	15.01	10.35	**52.16**	**7.25**

TABLE F1 (Continued)

TC #	1	2	3	4	5	Avg.
Tp, °C	450.8	450.6	452.25	450.4	452.75	451.4

Trial	13 Gage Needle					16 Gage Needle				
No.	CCl_4 27°C	EtOH 27.5°C	C_3H_6 27.5°C	H_2O 29°C	n-C_8H_{18} 27°C	CCl_4 27°C	EtOH 27.5°C	C_6H_6 27.5°C	H_2O 29°C	n-C_8H_{18} 27°C
1	12.35	17.91	13.00	73.83	8.52	11.25	16.27	11.82	63.30	7.96
2	12.08	17.70	12.70	71.16	8.87	11.21	16.62	11.35	64.10	7.80
3	12.07	17.85	12.52	71.56	8.77	11.40	16.41	11.42	62.70	7.72
4	12.30	17.60	12.48	72.60	8.59	11.18	16.26	11.73	64.51	7.80
5	12.33	17.56	12.71	72.35	8.98	11.38	16.18	11.51	63.20	7.76
Avg.	12.23	17.72	12.68	72.30	8.75	11.28	16.35	11.57	63.56	7.81
	17 Gage Needle					21 Gage Needle				
1	10.53	16.08	11.06	59.50	7.69	9.21	13.27	9.36	49.60	6.78
2	10.59	15.77	11.11	60.59	7.75	9.36	13.00	9.46	50.92	6.82
3	10.69	15.36	11.02	60.40	7.62	9.49	13.32	9.42	49.41	6.65
4	10.70	16.27	11.30	59.40	7.60	9.06	13.67	9.25	49.32	6.63
5	10.63	16.38	11.00	62.37	7.75	9.21	13.12	9.36	51.36	6.69
Avg.	10.63	15.97	11.10	60.45	7.68	9.27	13.28	9.37	50.12	6.71

TABLE F2

INSTANTANEOUS DROPLET RADIUS VERSUS TIME

Liquid	Time sec.	Average Radius of Droplet, cm	Evaporation Time, Sec. Obs'd	Cal'd
Water,	10	0.1729		
V_o = 0.3196 ml.	20	0.1759		
T_p^o = 411.6°C	30	0.1547		
	40	0.1161		
	50	0.0916		
	60	0.0665		
	70	0.0343	75.5	81.0
Water,	10	0.1572		
V_o = 0.0192 ml.	20	0.1392		
T_p^o = 416.08°C	30	0.1066		
	40	0.0796		
	50	0.0622	64.6	61.0
Water,	5	0.2415		
V_o = 0.0500 ml.	10	0.2176		
T_p^o = 350°C	20	0.2181		
	30	0.1835		
	40	0.1775		
	50	0.1565		
	60	0.1453		
	70	0.1227		
	80	0.0997		
	90	0.0733		
	100	0.0498	112.7	117.5
Water,	10	0.1960		
V_o = 0.03196 ml.	20	0.1771		
T_p^o = 315.0°C	30	0.1597		
	40	0.1503		
	50	0.1208		
	60	0.1086		
	70	0.0935		
	80	0.0700		
	90	0.0632	100.8	100.5

TABLE F2 (Continued)

Liquid	Time sec.	Average Radius of Droplet, cm	Evaporation Time, Sec. Ovs'd	Cal'd
Ethanol,	5	0.1580		
V_o = 0.01391 ml.	10	0.1447		
T_p^o = 279.4°C	15	0.1161		
	20	0.0953		
	25	0.0726	30.4	30.5
Ethanol,	5	0.1578		
V_o = 0.01391 ml.	10	0.1293		
T_p^o = 218.94	15	0.1068		
	20	0.0927		
	25	0.0641		
	30	0.0357	36.8	36.5
Benzene,	5	0.1631		
V_o = 0.01618 ml.	10	0.1201		
T_p^o = 282.4°C	15	0.0716		
	20	0.0338	22.4	23.5
Carbon	5	0.1056		
tetrachloride	10	0.0756		
V_o = 0.00803 ml.	15	0.0500		
T_p^o = 267.8°C			19.1	20.3

VITA

Chau Jen Lee

Candidate for the Degree of

Doctor of Philosophy

Thesis: A THEORETICAL AND EXPERIMENTAL INVESTIGATION OF THE LEIDENFROST PHENOMENON FOR SMALL DROPLETS

Major Field: Chemical Engineering

Biographical:

Personal Data: Born in Chia-Yi, Formasa, October 7, 1935, the son of Len-Ting and Gien-Heng Lee. Married to Huey-Li Liu, Chia-Yi, Formosa, in September, 1961.

Education: Attended public school in Chia-Yi, Formosa; graduated from Chia-Yi High School in 1953; received the Bachelor of Science degree in Chemical Engineering from National Taiwan University in 1957; received the Master of Science degree with a major in Chemical Engineering from Kansas State University, June, 1961; completed requirements for Doctor of Philosophy degree in May, 1965.

Professional Experience: Employed as a student engineer with Taiwan Sugar Company in the summer of 1956. Served as second lieutenant, CBR officer with Chinese ROTC, 1957 to 1959. Employed as a research assistant with Kansas State Experimental Station in 1960. Currently employed as a research engineer at Phillips Petroleum Company.